

THÈSE

Présentée pour l'obtention du grade de

Docteur de l'Université de Haute-Alsace

MATHÉMATIQUES, SCIENCES DE L'INFORMATION ET DE L'INGÉNIEUR

Discipline : Électronique, Électrotechnique et Automatique

par

Somar KARHEILY

SEMG TIME-FREQUENCY FEATURES FOR HAND MOVEMENTS CLASSIFICATION

Sous la direction du Prof. Djaffar OULD ABDESLAM

Soutenue publiquement le 8 décembre 2022 devant le jury composé de :

Mme FOSSATI, Professeur, Institut Fresnel – École centrale de Marseille	Rapporteur
M. MESTE, Professeur, I3S – Université Côte d'Azur	Rapporteur
Mme FRINDEL, Maître de conférences, CREATIS – INSA Lyon	Examinatrice
M. MOUKADEM, Maître de conférences, IRIMAS – UHA	Co-encadrant
M. COURBOT, Maître de conférences, IRIMAS – UHA	Co-encadrant
M. OULD ABDESLAM, Professeur, IRIMAS – UHA	Directeur
Mme MEILLIER, Maître de conférences, ICube – Université de Strasbourg	Invitée
M. DIETERLEN, Professeur, IRIMAS – UHA	Invité

ABSTRACT

Surface Electro-MyoGraphic (sEMG) signals recorded on the forearm can provide information about the hand movement, which can help to control a prosthetic implant for the disabled people. To do so, the sEMG signals must be accurately classified despite the signals' non-stationarity, different kind of noises, multiple involved muscles, and patient's peculiarities. This thesis deals with the classification of hand movements using sEMG signals, and focuses especially on the use and enhancing the time–frequency domain features and several linear and non-linear methods for the dimension reduction. In this thesis, different known time-frequency methods were applied and compared such as Short Time Frequency Transform (STFT), Stockwell Transform (ST), Continues Wavelet Transform (CWT), and the Discrete Orthonormal Stockwell Transform (DOST) which is applied for the first time on sEMG signals. These methods were combined with different linear and non-linear dimension reduction methods as PCA, Isomap, Diffusion Maps (DM) and Multidimensional Scaling (MDS) which is also applied for the first time on sEMG signals. An extensive comparison study was made on the combinations of all used methods, and the evaluation of the applied methods used classical classifiers and a public dataset. We proved the efficiency of using the TF features and potential of using the non-linear dimension reduction methods. We applied the generalized version of DOST (GDOST) and enhanced the similarity calculations in the MDS method to significantly improve our best results from 90.96% to 97.56% as accuracy rate of 17 hand movements. Then the experiments were extended on a data recorded on amputees where the clinical amputation characteristics affect the quality of sEMG signals. The results were compared based on these clinical characteristics. The number of movements was also increased to 40 movements and the accuracy score was 90.02%. Finally, we applied our methods on a different data source recorded by our partner team under a completely different acquisition protocol, and the achieved classification accuracy was 99.31% for 4 different movements.

Résumé en français

Les signaux électromyogrammes de surface (sEMG) enregistrés sur l'avant-bras peuvent fournir des informations sur le mouvement de la main, ce qui peut aider à contrôler

un implant prothétique pour les personnes handicapées. Pour ce faire, les signaux sEMG doivent être classés avec précision malgré la non-stationnarité des signaux, les différents types de bruits, les multiples muscles impliqués et les particularités du patient. Cette thèse traite de la classification des mouvements de la main à l'aide de signaux sEMG, et se concentre particulièrement sur l'utilisation et l'amélioration des caractéristiques du domaine temps-fréquence et sur plusieurs méthodes linéaires et non linéaires pour la réduction de la dimension. Dans cette thèse, différentes méthodes temps-fréquence connues ont été appliquées et comparées, telles que la transformée temps-fréquence courte (STFT), la transformée de Stockwell (ST), la transformée en ondelettes continue (CWT) et la transformée orthonormée discrète de Stockwell (DOST), qui est appliquée pour la première fois aux signaux sEMG. Ces méthodes ont été combinées avec différentes méthodes de réduction des dimensions linéaires et non linéaires telles que l'ACP, l'Isomap, les cartes de diffusion (DM) et l'échelle multidimensionnelle (MDS) qui est également appliquée pour la première fois aux signaux sEMG. Une étude comparative approfondie a été réalisée sur toutes les méthodes utilisées. Nous avons prouvé l'efficacité de l'utilisation des caractéristiques TF et le potentiel de l'utilisation des méthodes de réduction des dimensions non linéaires. Nous avons appliqué la version généralisée de DOST (GDOST) et amélioré les calculs de similarité dans la méthode MDS pour améliorer de manière significative nos meilleurs résultats de 90,96% à 97,56% pour un taux de précision de 17 mouvements de la main. Les expériences ont ensuite été étendues à des données enregistrées sur des personnes amputées, dont les caractéristiques cliniques affectent la qualité des signaux sEMG. Les résultats ont été comparés en fonction de ces caractéristiques cliniques. Le nombre de mouvements a également été augmenté à 40 mouvements et la précision a été de 90,02%. Enfin, nous avons appliqué nos méthodes sur des données enregistrées par notre équipe partenaire selon un protocole d'acquisition totalement différent, et la précision de classification obtenue a été de 99,31 % pour 4 mouvements différents.

Keywords: *sEMG signals, time-frequency transforms, hand movements classification, non-linear dimension reduction.*

TABLE OF CONTENTS

ABSTRACT	i
LIST OF FIGURES	vii
LIST OF TABLES	ix
LIST OF TERMS AND ABBREVIATIONS	x
1 Introduction	1
1.1 English Version	1
1.1.1 Background And Motivation	1
1.1.2 Upper Limb Prosthetic	2
1.1.3 sEMG Signals	2
1.1.4 Objectives	6
1.1.5 This Thesis	6
1.2 Version en Français	7
1.2.1 Contexte et motivation	7
1.2.2 Prothèse du membre supérieur	8
1.2.3 Signaux sEMG	9
1.2.4 Objectifs	11
1.2.5 Cette thèse	12
2 Literature Review	14
2.1 Commercially-Available Prosthesis	14
2.2 sEMG Classification Work Flow	16
2.3 sEMG Acquisition	16
2.4 Windowing	18
2.5 Feature Extraction	18
2.5.1 Time Domain	18
2.5.2 Frequency Domain	21

2.5.3	Time-Frequency Domain	21
2.6	Dimension Reduction	22
2.7	Classification	23
2.8	Deep Learning	23
2.9	Methods Overview	25
2.10	Literature Review Recap	29
3	Theoretical Background	30
3.1	sEMG Data Sources	31
3.1.1	Analytical Modelling of sEMG Signals	31
3.1.2	ZHAW School's Pilot sEMG Data	32
3.1.3	Public Database	33
3.2	Features Extraction	35
3.2.1	Short Time Fourier Transform	35
3.2.2	Continuous Wavelet Transform	39
3.2.3	Stockwell Transform	40
3.2.4	Discrete Orthonormal Stockwell Transform	43
3.3	Dimension Reduction	45
3.3.1	PCA	45
3.3.2	Manifold Learning	46
3.3.3	Isomap	47
3.3.4	Diffusion Maps	49
3.3.5	Multidimensional Scaling	50
3.4	Theoretical Background Recap	52
4	Algorithms and Results	53
4.1	Algorithmic Considerations	54
4.1.1	Main Work Flow	54
4.1.2	The Referenced Data	56
4.1.3	Feature's Sliding Window	57
4.1.4	Feature Extraction	57
4.1.5	Dimension Reduction	61
4.1.6	Classification	61

4.2	Methods Comparative Study	62
4.2.1	TF Methods Comparison	63
4.2.2	Dimension Reduction Methods Comparison	64
4.2.3	Classifiers Comparison	64
4.2.4	Deep Learning	65
4.2.5	Comparison Recap	65
4.3	Generalized DOST and its Similarity Measurements	67
4.3.1	Generalized DOST	67
4.3.2	Feature Extraction from GDOST	68
4.3.3	Similarity Measurements	69
4.3.4	Distance Synchronization	69
4.3.5	Experiments	70
4.3.6	Results	71
4.3.7	Confusion Matrix	72
4.3.8	Section Recap	73
4.4	Generalization on Different Datasets	74
4.4.1	Amputation Impact on Classification Accuracy	74
4.4.2	Number of Movements' Impact on Accuracy	76
4.4.3	Data from ZHAW School of Health Sciences	78
4.5	Algorithms and Results Recap	79
5	Conclusion and Perspectives	80
5.1	English Version	80
5.1.1	Thesis Overview	80
5.1.2	Experiments Conclusion	81
5.1.3	Main Findings	81
5.1.4	Future Works	82
5.2	Version en Français	84
5.2.1	Aperçu de la thèse	84
5.2.2	Conclusions des expériences	85
5.2.3	Principales conclusions	85
5.2.4	Perspectives	86

Appendices

Appendix A	sEMG Database from ZHAW School of Health Sciences in	
	Zurich (Switzerland)	89
A.1	Background Information	89
A.2	Tasks	89
	LIST OF PUBLICATIONS	93
	REFERENCES	95

LIST OF FIGURES

1.1	Prosthetic control system outlines.	3
1.2	Recorded sEMG signals of two hand movements.	5
2.1	Typical prosthetic parts.	15
2.2	Movement classification workflow.	17
3.1	sEMG generation from MUs model.	31
3.2	The movements in the ZHAW school's database.	32
3.3	Up/Down chirp signals with their FFT, STFT.	36
3.4	Effect of using different window types in STFT.	38
3.5	Effect of using different window widths in STFT with Hann window. . .	38
3.6	STFT transform using different σ values.	39
3.7	CWT for a sEMG signal.	41
3.8	Stockwell transform for a sEMG signal.	43
3.9	DOST transform for a sEMG signal.	44
3.10	PCA applied on Swiss Roll data points.	46
3.11	Sphere manifold distances compared to Euclidean distances.	47
3.12	Isomap applied on Swiss Roll data points.	48
3.13	Isomap with different neighbors number.	49
3.14	DM with different ρ values.	50
3.15	MDS with different distance functions.	51
4.1	The main work flow.	55
4.2	Visual depiction of the 17 hand gestures.	56
4.3	Example of recorded signals on channel 1 for the 17 movements.	58
4.4	Features extraction of a sEMG signal over 250ms window.	59
4.5	Different TF transforms examples.	60
4.6	Preserved variance by number of embedded features.	62
4.7	Classification accuracy by features number.	63

4.8	Classification accuracy by number of neighbours in Isomap algorithm. .	63
4.9	DOST and GDOST representation.	68
4.10	GDOST transform example for two different movements.	69
4.11	Distance between two observations with circle-shifting.	70
4.12	Confusion matrix of 17 hand gestures.	72
4.13	The responsible muscles of the fingers' movements.	73
4.14	Main algorithm overview of the selected methods.	74
4.15	The percentage of remaining forearm.	76
4.16	Visual depiction of the 40 hand gestures.	77
4.17	The confusion matrix of classification of the 40 hand gestures.	77
4.18	The confusion matrix of classification of the 4 hand gestures.	78

LIST OF TABLES

2.1	List of commercially-available prosthetic hands.	16
2.2	List of related studies ordered by features type.	26
3.1	List of Ninapro datasets with their specifications.	34
4.1	TF feature computation time on a window of one channel.	59
4.2	The classification results of all combinations in the comparative study. .	66
4.3	The classification accuracy with synchronized distances.	71
4.4	Classification accuracy of GDOST and enhanced MDS compared to other methods.	72
4.5	The number of movements' observations.	74
4.6	The classification accuracy of amputees' sEMG data.	75
A.1	The electrodes placement in ZHAW database.	91

LIST OF TERMS AND ABBREVIATIONS

ANN	Artificial Neural Network
ASDD	Absolute Standard Deviation of Difference
CNN	Convolutional Neural Networks
CNN-LSTM	CNN Long Short-Term Memory Networks
CWT	Continuous Wavelet Transform
DAMV	Difference Absolute Mean Value
DBN	Deep Belief Networks
DL	Deep Learning
DM	Diffusion Maps
DOFs	Degrees Of Freedom
DOST	Discrete Orthonormal Stockwell Transform
DR	Dimension Reduction
DWT	Discrete Wavelet Transform
FD	Frequency Domain
FFT	Fast Fourier Transform
GAFs	Gaussian Analytic Functions
GDOST	Generalized DOST
GRNN	General Regression Neural Network
HD	High Density
KNN	k-Nearest Neighbors
LCNN	Lookup-based Convolutional Neural Network
LD	Low Density
LDA	Linear Discriminant Analysis
LMNN	Large Margin Nearest Neighbor

MAS Median Amplitude Spectrum

MAV Mean Absolute Value

MDF Median Frequency

MNF Mean Frequency

MU Motor Unit

NinaPro Non-Invasive Adaptive Hand Prosthetics

NN Neural networks

PCA Principal Component Analysis

PR Pattern Recognition

RF Random Forest

RMS Root Mean Square

RNN Recurrent Neural Networks

sEMG Surface Electromyography

SSC Slope Sign Change

SSI Simple Squared Integration

ST Stockwell Transform

STFT Short Time Fourier Transform

SVD Singular Value Decomposition

SVM Support Vector Machine

SVM-RFE SVM Recursive Feature

TD Time Domain

TF Time-Frequency

TFD Time-Frequency Domain

TL Transfer Learning

UPNs Unsupervised Pre-Trained Networks

WAMP Willison Amplitude

WL Waveform Length

WT Wavelet Transform

ZC Zero Crossing

CHAPTER 1

INTRODUCTION

1.1 English Version

1.1.1 Background And Motivation

The loss of a limb reduces the ability to have a normal life and negatively affects the patient by preventing him from carrying out his daily activities. This disability has an impact on the person mobility, self-care, self-image, community and leisure involvement. According to National Limb Loss Resource Center [1], there are nearly 1.6 million people living with limb loss in the United States with approximately 185,000 amputations occurring each year; and around 70% of amputations due to trauma involve the upper limbs. In the United Kingdom, amputation of upper limb may reach 10,000 of 250,000 per year with an estimated 55,000 - 60,000 of amputees attending specialist rehabilitation service centers [2, 3].

Forearm amputations are a life-changing event, usually caused due to sudden, unexpected trauma, but the lost body part could be replaced by an artificial device, called a prosthetic. The prosthetic should mimic the functionality of the lost part as close as possible which helps the amputee in rehabilitation and to stay independent, especially when speaking about the upper limb.

Although the upper limb prostheses could replace some of these essential activities, still up to 25% of amputees do not use any kind of prostheses, and around 50% do not use electrical prostheses at all [4].

The reluctance of upper limb prosthetic for the amputees is likely to be 50% and higher with no significant change in this rate in the last decade [5]. A main reason of such abandonment is the need for more proficiency in the prosthetic which could involve wider range of movements including movements of fingers and joints [6, 7]. Limited

degrees of freedom (DOFs), accuracy rate, time required for training, weight and shape are all important concerns that play significant role in amputees acceptance. This means a lot of research is still needed in this area to improve accuracy, DOFs, required training time, response time, and so on. These important factors increase the acceptance and possibility of using prostheses.

1.1.2 Upper Limb Prosthetic

There are two main types of prosthetic control: intrusive and non-intrusive. The most common type of prosthetic control system is the non-intrusive myoelectric control system which uses the surface electromyography (sEMG) signals as input to identify the intention of the limb movement. The acquisition of the EMG signals is made by electrodes placed on the skin near the muscles. The electrical activities detected by these electrodes contain signals patterns which can be used to identify the movement intention. The advantage of the non-intrusive myoelectric control is that it is more natural and does not need a harness or surgical procedure [8]. Although the myoelectric-controlled prosthetic was proposed in the late 1960s, it was a simple on/off device triggered when the sEMG amplitude exceed a certain threshold. Recently, the pattern recognition (PR) based control made a significant improvement in the prosthetic technology and improved to be the most promising for the upper limb control [9]. This kind of control assumes that each hand movement contains specific sEMG signal pattern different from other movements. The PR-based control system gives a new solutions for the complexity of the upper limb movements and allows prosthetic to have more DOFs by ability to classify the movements using their sEMG patterns. Nevertheless, movements of the fingers or hand grip or any other hand gesture result from combinations of multiple muscles contractions in the forearm, and the resulting sEMG signals will contain significant similarities which make distinguishing and classification of these sEMG a difficult challenge [10].

Upper limb prosthetic contains in general electrodes to detect the sEMG signals on the surface of the skin. These signals will be amplified, filtered and then will be processed to extract meaningful features. A suitable machine learning model should be trained to find out the patterns in these sEMG signals and to make a decision about the movements intention. Figure 1.1 summarizes the process of prosthetic control systems including sEMG acquisition, movements' identification and control.

1.1.3 sEMG Signals

The EMG signals are the electrical activities of the muscles which are activated by physiological neural signals. The EMG signals reflect a potential movement intended to be performed by the skeletal muscles [11]. The muscles include long tubular cells

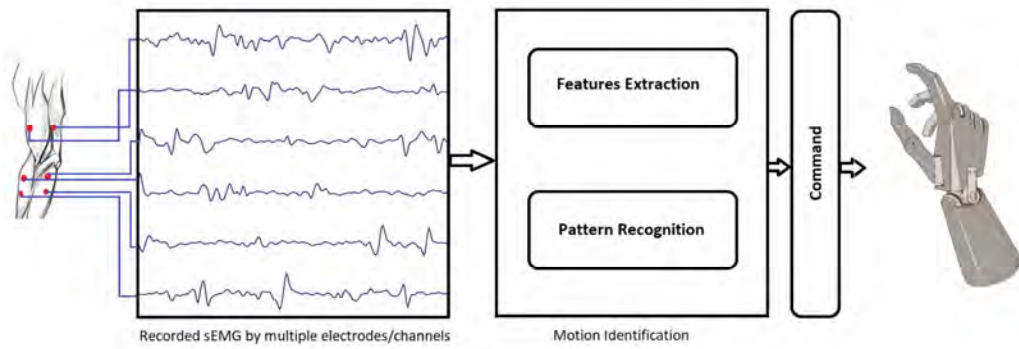


Fig. 1.1 Prosthetic control system outlines.

called fibers, and the EMG signal is the result of the signals from each of these muscle cells which by their turn affected by the person's physiology. The EMG signals are used widely in the medical area in clinical and rehabilitation devices as prostheses, and also in the industry and entertainment for human-machine interfaces [12]. These signals are used as input for electromyographic control systems which is based on classifying EMG signals.

EMG signals are non-stationary signals whose amplitude generally ranges from 0.01mV to 10mV. Their main energy is concentrated between 0Hz and 500Hz frequency band, and the most significant spectrum is 50-150Hz [13]. The acquisition of EMG signals can be invasive or non-invasive. The non-invasive is the preferred method as the invasive acquisition is painful as it needs surgical operation, besides to their limited use when activities from several muscles need to be monitored simultaneously [14, 15]. The signals recorded using non-invasive acquisition are called surface EMG (sEMG) signals. sEMG signals are usually recorded using electrodes placed on the surface of the skin near to the target muscles. Different studies were made on the placement of the electrodes [16] and different strategies were investigated to enhance these signals acquisition over the past decades. Some researchers study the use of multi-channel electrode arrays or high-density EMG strategy [17], while others explore the precise anatomical positioning approach [18].

1.1.3.1 sEMG Signal Origin

The movement starts by a nervous signal by the central nervous system (CNS) that activates the muscle and triggers the fiber contraction. The depolarized zones of the fibers of each recruited motor unit (MU) give rise to an electrical field and generate voltage contributions that add up on the skin to form a voltage distribution. The generated elec-

trical activity on the skin is impacted by the distances between the skin and each source, which gives the superficial MUs more contribution than the deep MUs. These generated electrical signals could be recorded using typically two electrodes for each muscle [19].

1.1.3.2 sEMG Noise Types

Despite the development in the acquisition technology, the sEMG signals are always accompanied with different types of noises due to the presence of electronic equipment and physiological factors [12]:

- Inherent noise in the electrodes: All types of electronic equipment generate this type of electrical noise. In order to reduce this noise in recording sEMG, the electrodes made of silver/silver chloride (10×1 mm) have been found to give adequate signal-to-noise ratio and are electrically very steady. For this reason, they are widely used as surface electrodes [20].
- Movement artifact: The EMG signals are recorded while movements are performed. The skin and the length of the muscle will change during this movement and that will cause some movement artifacts on the electrodes. This noise has a frequency range between 1-10 Hz with amplitude comparable to the recorded EMG, but it could be removed significantly using recessed electrodes, in which a conductive gel layer is used between the skin surface and the electrode interface.
- Ambient noise: Electromagnetic radiation is the source of this type of noise. The surfaces of our bodies are constantly inundated with electro-magnetic radiation and it is virtually impossible to avoid exposure to it on the surface of Earth. The dominant concern for the ambient noise arises from the power-line interference. This is caused by differences in the electrode impedance and in stray currents through the patient and the cables.
- Cross Talk: This type of noise comes from EMG signals that are generated by unrelated muscles, which are not involved in the movement under monitoring. Some possibilities to minimize this noise is by using smaller size electrodes and choosing best placement for the electrodes [21].
- Internal Noise: The quality of the recorded EMG signals are affected by the anatomical, biochemical and physiological factors. This comes from the fact that the EMG are generated on low level of muscle fibers, so the number, depth and location of the active fibers will affect the quality of EMG. Moreover, the characteristics of EMG signals can differ from a person to another for the same reason.

These different kind of noises make analyzing and classifying the sEMG signals more difficult challenge and increase the need of more accurate sEMG signal acquisition in both hardware and software.

1.1.3.3 sEMG States

The sEMG signals have two states: the first is the transient state which happens when the muscle is triggered to start contraction, then comes the steady state where the muscle maintains the contraction [22]. The transient state contains bursts of firing electrical activities that starts the muscles contraction, while the steady state contains a constant firing rate that keeps the position of contraction [23]. The sEMG features in general could be extracted and classified in both states. Although the steady-state data exhibits distinct superiority to the transient data and leads to better classification [24]. It has been observed in clinical applications that combining the transient and the steady-state EMG signals together for training the classifier can increase the recognition system's usability. Although using the combination of these two states might reduce the overall classification accuracy, it will improve the classification during the dynamic stages of the movements (start and end), which increases the usability by getting rid of the miss-classification in these stages and reducing the response time [25].

The fact that sEMG signals are non-stationary and can be contaminated by a wide variety of noises, besides to the complicated motions' patterns and many degrees of freedoms in the upper limb, makes the movements pattern recognition a very difficult task [26]. In figure 1.2, we can see example of recorded sEMG signals of the forearm when performing two different hand movements using one electrode.

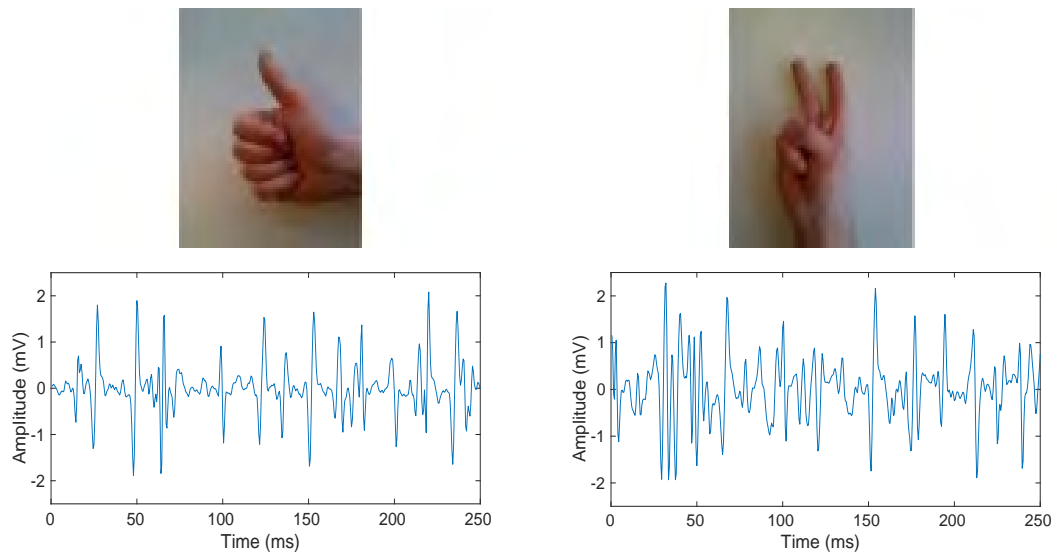


Fig. 1.2 Recorded sEMG signals of two hand movements [27].

1.1.4 Objectives

In this thesis, we aim to improve sEMG pattern recognition by applying advanced signal processing and machine learning methods. More precisely, the contribution of this thesis is focused on the features extraction and dimension reduction fields. The non-stationary nature of the sEMG signals promotes the time-frequency transforms, which in turn produces a high dimensional features space. These high-dimensional feature spaces require efficient dimension reduction methods that improve classification performance. The main objectives can be summarized as:

- Comparing the known feature extraction methods in the literature in the field of hand gesture recognition.
- Extending the state of the art Time Frequency (TF) transforms used in this area by introducing new methods.
- Extending the study on the non-linear Dimension Reduction (DR) methods, by comparing used ones and applying new methods in the field.
- Enhancing the non-linear DR methods by finding better similarity measurements, and improving their performance.
- Applying and comparing all of these methods combinations on same sEMG dataset. Give overall overview for different combination with a fair comparison in a helpful way for researchers in this field.
- Applying state of the art deep learning network with the TF features and compare with the other combinations.

1.1.5 This Thesis

In this thesis, we will follow the following structure:

- In chapter 2, we will give an overview about the state of the art regarding sEMG classification for hand movements, the known methods in feature extraction, dimension reduction and classification, besides the available industry solutions for the prosthesis.
- Chapter 3 contains a theoretical background of the used methods in both time-frequency features extraction and linear/non-linear dimension reduction methods. Some of these methods are used in the literature and others are newly applied in this area.

- Chapter 4 explains the process of applying list of methods' combinations seen in chapter 3, starting from the data used ending with the classification results using these methods combinations with extended comparison. Then we go through our improvements on the state of the art in this field. We explain the new methods we used and the improvements we added to these methods in both feature extraction and dimension reduction stages. Then we make experiments on different types of datasets. We test our methods on amputees' sEMG data, then we increase the number of movements in our experiment. Finally, we test our methods on sEMG signals recorded locally by our partner's team.
- Chapter 5 contains the final conclusion, the outlines of the research and the proposed future work.

The work in this thesis allowed to publish a journal paper in Expert Systems with Applications (2022)[28]. In this paper, several combinations of sEMG Time-Frequency (TF) features extraction and Dimension Reduction (DR) methods were compared. Methods as the Discrete Orthonormal Stockwell Transform (DOST) and Multidimensional Scaling (MDS) are applied for the first time on sEMG signals with promising results by DOST and significant reduction of the computational burden. The results of this journal paper are reported in section 4.2.

Two conference papers were also published, first one in BIOSIGNALS (2020) [29], which was a preliminary work for the previous journal paper. The second paper was published in the 30th European Signal Processing Conference (EUSIPCO) [30], in which we proposed the generalized version of DOST (GDOST) with an enhanced Multi-Dimensional Scaling (MDS) method. These results also appeared in the French signal processing conference (GRETSI) [31], and are reported in section 4.3.

1.2 Version en Français

1.2.1 Contexte et motivation

La perte d'un membre réduit la capacité à mener une vie normale et affecte négativement le patient en l'empêchant de mener à bien ses activités quotidiennes. Cet handicap a un impact sur la mobilité de la personne, ses capacités à prendre soin d'elle-même, son image de soi, sa participation à la vie de la communauté et aux loisirs. Selon le National Limb Loss Resource Center [1], près de 1,6 million de personnes vivent avec une perte de membre aux États-Unis, avec environ 185 000 amputations par an ; environ 70 % des amputations dues à un traumatisme concernent les membres supérieurs. Au Royaume-Uni, l'amputation des membres supérieurs peut atteindre 10 000 à 250 000 personnes par an, et on estime que 55 000 à 60 000 amputés fréquentent des centres

de rééducation spécialisés [2, 3]. Les amputations de l'avant-bras sont un bouleversement de la vie, généralement dû à un traumatisme soudain et inattendu, mais la partie du corps perdue peut être remplacée par un dispositif artificiel, appelé prothèse. La prothèse doit reproduire le plus fidèlement possible la fonctionnalité de la partie perdue, ce qui aide l'amputé à se réadapter et à rester indépendant, en particulier lorsqu'il s'agit du membre supérieur. Bien que les prothèses des membres supérieurs puissent remplacer certaines de leurs activités essentielles, jusqu'à 25 % des amputés n'utilisent aucun type de prothèse, et environ 50 % n'utilisent pas du tout de prothèses électriques [4]. La réticence des amputés à l'égard des prothèses des membres supérieurs est probablement de 50 % et plus, sans changement significatif de ce taux au cours de la dernière décennie [5]. L'une des principales raisons de cet abandon est la nécessité d'une plus grande maîtrise de la prothèse, qui pourrait impliquer une plus large gamme de mouvements, y compris les mouvements des doigts et des articulations [6, 7]. Les degrés de liberté limités, le taux de précision, le temps nécessaire à la familiarisation, le poids et la forme sont autant de facteurs qui jouent un rôle important dans l'acceptation de la prothèse par les amputés. Cela signifie que de nombreuses recherches sont encore nécessaires dans ce domaine pour améliorer la précision, les degrés de liberté, le temps de d'apprentissage nécessaire, le temps de réponse, etc. Ces éléments importants renforcent l'acceptation et la possibilité d'utiliser des prothèses.

1.2.2 Prothèse du membre supérieur

Il existe deux types principaux de commande prothétique : intrusive et non intrusive. Le type le plus courant de commande prothétique est le système de commande myoélectrique non intrusif, qui utilise les signaux d'électromyographie de surface (sEMG) pour identifier l'intention du mouvement du membre. L'acquisition des signaux EMG est réalisée par des électrodes placées sur la peau à proximité des muscles. Les activités électriques détectées par ces électrodes contiennent des signaux qui peuvent être utilisés pour identifier l'intention du mouvement. L'avantage de la commande myoélectrique non intrusive est qu'elle est plus naturelle et ne nécessite pas de harnais ou de chirurgie [8]. Bien que la prothèse à commande myoélectrique ait été proposée à la fin des années 1960, il s'agissait d'un simple dispositif marche/arrêt déclenché lorsque l'amplitude du sEMG dépassait un certain seuil. Récemment, la commande basée sur la reconnaissance des formes (PR) a apporté une amélioration significative à la technologie prothétique et s'est révélée être la plus prometteuse pour la commande des membres supérieurs [9]. Ce type de commande suppose que chaque mouvement de la main contient un signal sEMG spécifique différent des autres mouvements. Le système de commande basé sur le PR apporte de nouvelles solutions à la complexité des mouvements des membres supérieurs et permet aux prothèses d'avoir plus de DOF grâce à la capacité de classi-

fier les mouvements à l'aide de leurs signaux sEMG. Néanmoins, les mouvements des doigts, la préhension de la main ou tout autre geste de la main résultent de la combinaison de plusieurs contractions musculaires dans l'avant-bras, et les signaux sEMG qui en résultent contiennent des similitudes significatives qui rendent la distinction et la classification de ces sEMG difficiles à réaliser [10]. Les prothèses de membres supérieurs contiennent en général des électrodes pour détecter les signaux sEMG à la surface de la peau. Ces signaux sont amplifiés, filtrés puis traités pour en extraire des caractéristiques significatives. Un modèle d'apprentissage automatique approprié doit être entraîné pour trouver les modèles dans ces signaux sEMG et prendre une décision sur l'intention des mouvements. La figure 1.1 résume le processus des systèmes de contrôle prothétique, y compris l'acquisition des signaux sEMG, l'identification des mouvements et le contrôle.

1.2.3 Signaux sEMG

Les signaux EMG sont les activités électriques des muscles qui sont activés par des signaux physiologiques neuronaux. Les signaux EMG reflètent un mouvement potentiel destiné à être exécuté par les muscles squelettiques [11]. Les muscles comprennent de longues cellules tubulaires appelées fibres, et le signal EMG est le résultat des signaux provenant de chacune de ces cellules musculaires qui, à leur tour, sont affectées par la physiologie de la personne. Les signaux EMG sont largement utilisés dans le domaine médical, dans les appareils cliniques et de rééducation comme les prothèses, ainsi que dans l'industrie et les loisirs pour les interfaces homme-machine [12]. Ces signaux sont utilisés comme données d'entrée pour les systèmes de contrôle électromyographique qui sont basés sur la classification des signaux EMG. Les signaux EMG sont des signaux non stationnaires dont l'amplitude varie généralement entre 0,01mV et 10mV. Leur énergie principale est concentrée entre la bande de fréquence 0Hz et 500Hz, et le spectre le plus significatif est 50-150Hz [13]. L'acquisition des signaux EMG peut être invasive ou non invasive. La méthode non invasive est privilégiée car l'acquisition invasive est douloureuse et nécessite une opération chirurgicale, sans compter que son utilisation est limitée lorsque l'activité de plusieurs muscles doit être mesurée simultanément [14, 15]. Les signaux enregistrés à l'aide de l'acquisition non invasive sont appelés signaux EMG de surface (sEMG). Les signaux sEMG sont généralement enregistrés à l'aide d'électrodes placées à la surface de la peau, à proximité des muscles cibles. Différentes études ont été réalisées sur l'emplacement des électrodes [16] et différentes stratégies ont été étudiées pour améliorer l'acquisition de ces signaux au cours des dernières décennies. Certains chercheurs étudient l'utilisation de réseaux d'électrodes multicanaux ou d'une stratégie EMG à haute densité [17], tandis que d'autres explorent l'approche du positionnement anatomique précis [18].

1.2.3.1 Origine du signal sEMG

Le mouvement commence par un signal nerveux du système nerveux central (SNC) qui active le muscle et déclenche la contraction des fibres. Les zones dépolarisées des fibres de chaque unité motrice (UM) activée donnent naissance à un champ électrique et génèrent des variations de tension qui s'additionnent sur la peau pour former une distribution de tension. L'activité électrique générée sur la peau est influencée par les distances entre la peau et chaque source, ce qui donne aux UM superficielles une contribution plus importante que les UM profondes. Ces signaux électriques générés peuvent être enregistrés à l'aide de deux électrodes pour chaque muscle [19].

1.2.3.2 Les types de bruit sEMG

Malgré le développement des technologies d'acquisition, les signaux sEMG sont toujours accompagnés de différents types de bruits dus à la présence d'équipements électroniques et de facteurs physiologiques [12] :

- **Bruit inhérent aux électrodes** : Tous les types d'équipements électroniques génèrent ce type de bruit électrique. Afin de réduire ce bruit lors de l'enregistrement du sEMG, les électrodes en argent/chlorure d'argent (10×1 mm) offrent un rapport signal/bruit adéquat et sont électriquement très stables. C'est pourquoi elles sont largement utilisées comme électrodes de surface [20].
- **Artéfact de mouvement** : les signaux EMG sont enregistrés pendant que des mouvements sont effectués. La peau et la longueur du muscle changent au cours de ce mouvement, ce qui provoque des artefacts de mouvement sur les électrodes. Ce bruit a une fréquence comprise entre 1 et 10 Hz et une amplitude comparable à celle de l'EMG enregistré, mais il peut être éliminé de manière significative en utilisant des électrodes encastrées, dans lesquelles une couche de gel conducteur est utilisée entre la surface de la peau et l'interface de l'électrode.
- **Bruit ambiant** : Le rayonnement électromagnétique est la source de ce type de bruit. Les surfaces de notre corps sont constamment inondées de rayonnements électromagnétiques et il est pratiquement impossible d'éviter d'y être exposé à la surface de la Terre. Le principal problème lié au bruit ambiant provient de l'interférence des lignes électriques. Elles sont causées par les différences d'impédance des électrodes et par les courants parasites qui traversent le patient et les câbles.
- **Bruit croisé (Cross Talk)** : Ce type de bruit provient des signaux EMG générés par des muscles non apparentés, qui ne sont pas impliqués dans le mouvement à

surveiller. Il est possible de réduire ce bruit en utilisant des électrodes plus petites et en choisissant le meilleur emplacement pour les électrodes [21].

- **Bruit interne** : La qualité des signaux EMG enregistrés est affectée par des facteurs anatomiques, biochimiques et physiologiques. Cela est dû au fait que l'EMG est généré au niveau inférieur des fibres musculaires, de sorte que le nombre, la profondeur et l'emplacement des fibres actives affectent la qualité de l'EMG. En outre, les caractéristiques des signaux EMG peuvent varier d'une personne à l'autre pour la même raison.

Ces différents types de bruits rendent l'analyse et la classification des signaux sEMG plus difficiles et augmentent la nécessité d'une acquisition plus précise des signaux sEMG, tant au niveau du matériel que du logiciel.

1.2.3.3 États des signaux sEMG

Les signaux sEMG ont deux états : le premier est l'état transitoire qui se produit lorsque le muscle est déclenché pour commencer la contraction, puis vient l'état stable où le muscle maintient la contraction [22]. L'état transitoire contient des salves d'activités électriques qui déclenchent la contraction musculaire, tandis que l'état stable contient un niveau d'activité constant qui maintient la position de la contraction [23]. Les caractéristiques sEMG peuvent généralement être extraites et classées dans les deux états. Toutefois, les données à l'état stable présentent une nette supériorité par rapport aux données transitoires et permettent une meilleure classification [24]. Il a été observé dans les applications cliniques que la combinaison des signaux EMG transitoires et à l'état stable pour l'entraînement du classificateur peut améliorer la capacité d'utilisation du système de détection. Bien que l'utilisation de la combinaison de ces deux états puisse réduire la précision globale de la classification, elle améliore la classification pendant les phases dynamiques des mouvements (début et fin), ce qui augmente la fonctionnalité en éliminant les erreurs de classification pendant ces phases et en réduisant le temps de réponse [25]. Le fait que les signaux sEMG soient non stationnaires et puissent être perturbés par une grande variété de bruits, en plus des mouvements compliqués et des nombreux degrés de liberté du membre supérieur, fait de la reconnaissance des mouvements une tâche très difficile [26]. La figure 1.2 montre un exemple de signaux sEMG enregistrés sur l'avant-bras lors de l'exécution de deux mouvements différents de la main à l'aide d'une électrode.

1.2.4 Objectifs

Dans cette thèse, nous visons à améliorer la reconnaissance des signaux sEMG en appliquant des méthodes avancées de traitement du signal et d'apprentissage automa-

tique. Plus précisément, la contribution de cette thèse se focalise sur les domaines de l'extraction des caractéristiques et de la réduction de la dimension. La nature non stationnaire des signaux sEMG favorise les transformations temps-fréquence, qui produisent à leur tour un espace de caractéristiques à haute dimension. Ces espaces de caractéristiques à haute dimension requièrent des méthodes de réduction de dimension efficaces qui améliorent les performances de classification. Les principaux objectifs peuvent être résumés comme suit :

- Comparer les méthodes d'extraction de caractéristiques connues dans la littérature dans le domaine de la reconnaissance des gestes de la main.
- Étendre l'état de l'art des transformées temps-fréquence (TF) utilisées dans ce domaine en introduisant de nouvelles méthodes.
- Étendre l'étude sur les méthodes non linéaires de réduction de dimension (DR), en comparant les méthodes utilisées et en appliquant de nouvelles méthodes dans ce domaine.
- Améliorer les méthodes non linéaires de réduction de dimension en trouvant de meilleures mesures de similarité et en améliorant leurs performances.
- Appliquer et comparer toutes ces combinaisons de méthodes sur le même ensemble de données sEMG. Donner une vue d'ensemble des différentes combinaisons avec une comparaison équitable afin d'aider les chercheurs dans ce secteur.
- Application d'un réseau d'apprentissage profond de haute performance avec les caractéristiques de la TF et comparer avec les autres combinaisons.

1.2.5 Cette thèse

Dans cette thèse, nous suivrons la structure suivante :

- Dans le chapitre 2, nous donnerons un aperçu de l'état de l'art concernant la classification sEMG pour les mouvements de la main, les méthodes connues d'extraction de caractéristiques, de réduction de dimension et de classification, ainsi que les solutions industrielles disponibles pour la prothèse.
- Le chapitre 3 présente le contexte théorique des méthodes utilisées pour l'extraction des caractéristiques temps-fréquence et les méthodes de réduction des dimensions linéaires/non linéaires. Certaines de ces méthodes sont utilisées dans la littérature et d'autres sont nouvellement appliquées dans ce domaine.

- Le chapitre 4 explique le processus d'application de la combinaison des méthodes présentées au chapitre 3, en commençant par les données utilisées et en terminant par les résultats de classification obtenus à l'aide de ces combinaisons de méthodes et d'une comparaison approfondie. Nous présentons ensuite les améliorations que nous avons apportées à l'état de l'art dans ce domaine. Nous expliquons les nouvelles méthodes que nous avons utilisées et les améliorations que nous avons apportées à ces méthodes aux stades de l'extraction des caractéristiques et de la réduction des dimensions. Nous procédons ensuite à des expérimentations sur différents types de bases de données. Nous testons nos méthodes sur des données sEMG d'amputés, puis nous augmentons le nombre de mouvements dans notre expérimentation. Enfin, nous testons nos méthodes sur des signaux sEMG enregistrés localement par notre équipe partenaire.
- Le chapitre 5 présente la conclusion finale, les grandes lignes de la recherche et les travaux futurs proposés.

Les travaux de cette thèse ont permis de publier un article dans le journal "Expert Systems with Applications (2022)" [28]. Dans cet article, plusieurs combinaisons de méthodes d'extraction de caractéristiques temps-fréquence (TF) et de réduction de dimension (DR) ont été comparées. Des méthodes telles que la transformée orthonormée discrète de Stockwell (DOST) et l'échelle multidimensionnelle (MDS) sont appliquées pour la première fois aux signaux sEMG, avec des résultats prometteurs pour la DOST et une réduction significative de la charge de calcul. Les résultats de cet article de revue sont présentés dans la section 4.2. Deux articles de conférence ont également été publiés, le premier dans BIOSIGNALS (2020) [29], qui était un travail préliminaire pour l'article précédent. Le second article a été publié lors de la 30e conférence européenne sur le traitement du signal (EUSIPCO) [30], dans lequel nous avons proposé la version généralisée de DOST (GDOST) avec une méthode améliorée de mise à l'échelle multidimensionnelle (MDS). Ces résultats ont également été publiés lors de la conférence française sur le traitement du signal (GRETSI) [31] et sont présentés dans la section 4.3.

CHAPTER 2

LITERATURE REVIEW

This chapter starts with a summary of some existing prosthetic industry solutions. Then it provides an overview of the relevant literature with state of the art and the well-known methods in sEMG signal processing and classification. First, we introduce the general workflow for sEMG classification, then for each step, we introduce the methods used. We start from the sEMG acquisition, windowing, then the key parts of feature engineering and dimension reduction where we cover the used methods with their results based on recent studies in the field. We gathered the referenced studies with key information in the table 2.2 to give the reader a clear overview about the related studies. Then, we go through the deep learning approaches, which is also applied in this area, and explore some studies to get an overall image of the studies' main approaches.

2.1 Commercially-Available Prosthesis

The human hand has the ability to physically interact with the surrounding environment. It allows the person to perform a lot of various tasks both that need power or precision, besides to the different kind of sensing in the hand as pressure and heat which provide the feedback and feeling of this interaction. The sophisticated control and movement comes from the number of 21 DOFs for the hand and 6 for the wrist and the paramount role played by thumb opposition [32].

There were big steps done in the prosthetic technology recently, but the upper limb prostheses still have unsolved limitations. One of the main engineering challenges in the development of prosthetic devices is to embed actuators, sensors and electronic components into a prosthesis of the same size and weight of the replaced hand or limb. In the same time, the prosthesis should be improved to be able to perform more functionality. Another limitation that affects users' acceptance is the extensive amount of the required

training [32]. In figure 2.1, we can see a standard design of the hand prosthetic with the main parts. The main requirements of the prosthetic are the real time response, learning required time, accuracy, robust and simultaneous control of multiple DOFs in a natural and intuitive manner and bidirectional communication with the peripheral nervous system.

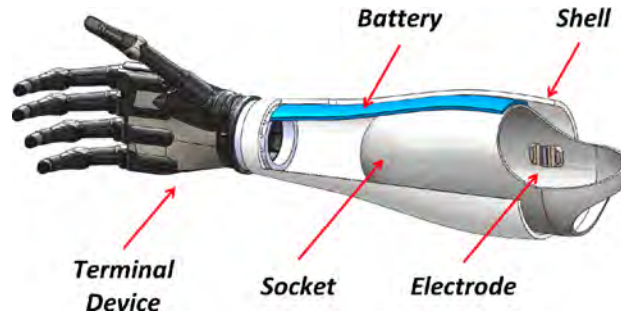


Fig. 2.1 Typical prosthetic parts [33].

The development of prosthesis produced some high-performance anthropomorphic prosthetic hands, with a high DOFs number, which can allow more functionalities and a higher potential if controlled by a pattern-recognition-based system. The high-end commercial myoelectric hands are the following: Bebionic, Hero Arm, i-limb ultra revolution, LUKE Arm (radial configuration), Michelangelo Hand, TASKA Hand, and VINCENT evolution 3 [34].

In 2007, the i-LIMB series developed by the UK-based company Touch Bionics introduced the first bionic hand with commercial value in the world. In 2013, the German company Ottobock developed the Bebionic prosthetic hand, which is based on the skeleton of the human hand and can support 14 different precise grasping movements. In 2009, a “revolutionary prosthesis” project jointly conducted by Johns Hopkins University and more than 30 other scientific research institutions successfully developed the Modular Prosthetic Limb (MPL) prosthetic hand. In 2013, this prosthetic hand was applied to a volunteer who had lost both arms by means of targeted muscle reinnervation, and 30 kinds of upper limb movements completely controlled by the volunteer’s mind were successfully realized [35]. At present, research on robotic exoskeleton systems for rehabilitation is still in the exploratory stage, but some basic functions for assisting human movement have already been achieved [35]. In table 2.1, we show most well-known companies with their state of the art prosthetic products seen from their commercial websites.

Table 2.1 List of commercially-available prosthetic hands.

Product Name	Manufacturer	DOF	Number of Grips Patterns
Bebionic	Ottobock	6	14
Hero Arm	Open Bionics	6	6
i-limb ultra revolution	Össur	6	18
LUKE Arm (Radial Configuration)	Mobius Bionics	6	6
Michelangelo Hand with Axon Rotation	Ottobock	4	7
TASKA Hand	TASKA Prosthetics	8	23
VINCENT Evolution 3	Vincent Systems	6	14

The industry shows the need of prostheses improvements regarding the ability to identify more movements with maintaining the accuracy and robustness, which requires more improvements in the sEMG pattern recognition.

2.2 sEMG Classification Work Flow

The sEMG classification follows the known approach of most machine learning algorithms by performing features extraction, dimension reduction and classification. Dealing with special kind of electrical signals as sEMG will add more steps regarding the acquisition of these biological signals in a way that reduces the noises and contains more informative patterns about the movements. In addition to that, the limitation of the response time in prosthetic applications requires a proper windowing that allows the system to classify the intended movements in a certain time range. The use of sEMG signals in controlling the prosthesis could be divided into four main steps as depicted in figure 2.2:

- Acquisition: The process of recording the sEMG signals.
- Windowing: Dividing the collected signals into windows.
- Feature Engineering: The process of extracting features and reducing the dimension of feature space if needed.
- Classification: Feeding the final features into a classifier to select the related class.

The workflow is common between all sEMG-based prosthetic control system, but the methods and tools used in each step vary a lot as we will see in the literature overview.

2.3 sEMG Acquisition

The sEMG signals are recorded in a non-invasive technique using special electrodes which are placed on the surface of the skin. These electrodes measure the electrical



Fig. 2.2 Movement classification workflow.

activity of the muscles by forming a chemical equilibrium between the detecting surface and the skin of the body through electrolytic conduction, so that current can flow into the electrode [36]. The non-invasive EMG measurement provides a simple way to record with no need for needles as in the invasive way of measurement, but placing all electrodes on the skin leads to crosstalk noise coming from other muscles. To overcome this problem, the subjects usually are asked to take a comfortable stable position which minimize the possibility of moving other muscles during the acquisition. The protocol of recording differs a lot between type of recorded movements, number of repetition, time of muscle contraction, time of the rest, the acquisition kit used, and so on [12]. The sEMG acquisition system contains four steps:

- **Signal recording:** The challenge in sEMG signals recording is to choose the best placement of the electrodes in a way that targets the muscles which participate in the movements without picking signals from irrelevant muscles [37]. The electrical view is highly dependent on where the electrode is overlying the muscle of interest, which is based on the movements themselves. Since electrode placement determines the electrical view of a muscle, then it is important in EMG measurements to be consistent in the placement of the electrodes for a subject over consecutive recording sessions and between different subjects [38]. Another research [39] showed the relation between the type of hand movements and the recommended electrodes placement, where they grouped the movements by the muscles involved. The used electrodes could be one of two types, gelled or dry. The gel is used to minimize the electrical noise but they need skin preparation as skin cleaning and hair removal. The dry electrodes on the other hand have direct contact with the skin and usually contain integrated amplification and filtering to improve the signal quality.

The number of the electrodes can follow two strategies:

- **Low Density (LD):** by placing more than two electrodes on the arm, and usually they are placed as a ring on the arm and the number of electrodes could be between 2 and 16 [27, 40, 41].
- **High density (HD):** this uses array of closely placed sEMG electrodes [17]. This could be useful for recognition of complex movements but creates a complexity in dealing with a large number of sEMG signals.

The LD strategy is usually sufficient for a successful movements' pattern recognition. Some studies showed that increasing the number of electrodes will increase the accuracy until a certain point and starts to decrease again [42, 43].

- Signal amplification: The EMG signals are usually amplified by factor 1000 for better interacting with common electronic instrumentation [44]
- Signal filtering: Filters are important to overcome the noise in sEMG signals, and usually a low pass filter of 500 Hz and a high pass filter of 20 Hz are used to reduce the motion artifacts [45]. Another used filter is the notch filter with 50 Hz center frequency to remove the distortion common noise that comes from the tissue and skin electrodes resistance [46].
- Analog-to-digital converting: The frequency band of sEMG signals could be up to 500 Hz, that requires a sampling rate at least 1000 Hz following Nyquist Theorem [44].

2.4 Windowing

The windowing is the process of dividing the signal stream into windows in fixed length before starting to extract features of these windows. In order to get real-time feeling response, a constraint should be set on the window length. The studies show that to keep the feeling of real time response in the prosthetic, the movement should be executed within 300 ms [22]. This time constraint includes the window length and the time required to identify the movement. A trade-off between the accuracy and the response time should be made in choosing the window length. A bigger window means less bias and variance of features but more delay in prosthetic response.

2.5 Feature Extraction

The success of any pattern recognition system is entirely based on the features that represents each observation. Feature extraction involves transforming raw sEMG data into a feature vector that is used to represent specific movement. Several features extractions methods were studied in this area which can be divided into three major domains: time domain, frequency domain, and time-frequency domain.

2.5.1 Time Domain

The Time Domain (TD) features are calculated directly from the time series values. These features are simple to calculate and convenient in their results, which makes them very popular in sEMG pattern recognition. Nevertheless, they are very sensible to

the noise and artifacts, besides to their dependency on the signals amplitude which is also highly affected by physical attributes of the muscles [47]. Let us consider a signal $x \in \mathbb{R}^N$, there are several well-known TD features which are used for sEMG signal pattern recognition such as Mean Absolute Value (MAV):

$$MAV(x) = \frac{1}{N} \sum_{n=1}^N |x_n| \quad (2.1)$$

Besides to the MAV, one of the common used attribute for the stochastic signal is the Variance (VAR), which is the measure of the sEMG signal's power:

$$VAR(x) = \frac{1}{N-1} \sum_{n=1}^N (x_n - \bar{x})^2 \quad (2.2)$$

Where \bar{x} is the mean of x .

Another TD attribute is the Simple Squared Integration (SSI) which describes the energy of sEMG, and calculated as a summation of the square of values of the signal:

$$SSI(x) = \sum_{n=1}^N x_n^2 \quad (2.3)$$

The Root Mean Squared value (RMS) is another important TD feature which correlates to the force applied in the muscle:

$$RMS(x) = \sqrt{\frac{1}{N} \sum_{n=1}^N x_n^2} \quad (2.4)$$

The number of times that the signal cross zero value is called zero-crossing feature. This count is usually combined with a threshold to consider only the activity that is triggered by the muscle [48]:

$$ZC = \sum_{n=1}^{N-1} f_{ZC}(x_n, x_{n+1}), \quad f_{ZC}(x_n, x_{n+1}) = \begin{cases} 1, & x_n \times x_{n+1} < 0 \\ 0, & \text{otherwise} \end{cases} \quad (2.5)$$

The wavelength (WL) is the distance between consecutive corresponding points of the same phase on the wave, such as two adjacent samples:

$$WL = \sum_{n=1}^{N-1} |x_{n+1} - x_n| \quad (2.6)$$

The Slope Sign Change (SSC) is the number of times the slope of the signal changes

its sign. This attribute is related to the frequency of the signal and a threshold is added to its calculation to reduce the effect of the noise in the signal [49]:

$$SSC = \sum_{n=2}^{N-1} f((x_n - x_{n-1}) \times (x_n - x_{n+1})), \quad f(x) = \begin{cases} 1, & x > threshold \\ 0, & otherwise \end{cases} \quad (2.7)$$

The number of times that the signal exceeds a threshold is called the Willison Amplitude (WAMP). This feature is an indicator to the quantity of the motor unit action potential [49]:

$$WAMP = \frac{1}{N} \sum_{n=1}^N f(|x_n|), \quad f(x) = \begin{cases} 1, & x > threshold \\ 0, & otherwise \end{cases} \quad (2.8)$$

The most common combinations are found in Hudgin's feature vector [50], which consists of the MAV, the WL, ZC, and SSC. Hudgin's feature vector yields a relatively high classification accuracy, and is not very dependent on the chosen length of the segment, besides to the advantages of stability in results and low computation time [50, 51]. In [52], Hudgin's feature vector was used and fed to a Support Vector Machine (SVM) classifier (5 classes and 4 channels) and the resulting accuracy was 96%. Note that in this case, the high classification accuracy must be tempered by the relatively low number of classes.

In a different study [53], features of the sixth-order autoregressive model was added to Hudgin's feature vector, with a Linear Discriminant Analysis (LDA) as a classifier. In this study sEMG signals were recorded on 15 channels, the results of using these features were varied based on the number of classes (movements), where it was 81.0% for 29 classes, and 88.8% for 17 classes, up to 97% for 9 classes. Another study [54] used high-density sEMG signals, by recording sEMG signals of the forearm using an array of 192 electrodes. RMS values were used as a feature for each signal, and an average of 95% of classification rate for 9 classes is reached with a SVM classifier. In a recent study [55], the most popular time domain features were tested with different classifiers, these features are: RMS, VAR, MAV, SSC, ZC, WL. These features were taken for 10 hand gestures recorded by 3 channels and tested on four different classifiers: Artificial Neural Network (ANN), SVM with Radial Basis Function (RBF) kernel, Random Forest (RF) and Logistic Regression (LR). These traditional TD features showed better accuracy when used with ANN classifier with 94% accuracy, and 87% for SVM. Despite the fact that TD features are simple to compute and could perform well for prosthetic with a few degrees of freedom (i.e. less classes), the nature of sEMG signals and its non-stationary characteristic make the TD features limited to capture the intrinsic features of the sEMG signals.

2.5.2 Frequency Domain

Frequency Domain (FD) features could be used to measure the tiredness in the muscle, force and changes in muscle activation patterns [47]. Using FD features alone in movement pattern recognition has not given good results compared to TD features which outperformed the frequency features and were more stable [47]. In [56] FD features alone were tested, which are Mean Frequency (MNF), Median Frequency (MDF), 1st, 2nd and 3rd spectral moments and frequency ratio. In this study, the FD features classification accuracy was between 75-85% where most of the used TD features accuracy was more than 85% for the classification of six upper limb movements applied on the same dataset. However, combining FD features with TD features could lead to more robust classification than TD features. Two studies [57, 58] appended the mean and median frequency to TD features, which increased the robustness of the classification. Different sets of features in noisy environment were tested in [58] and it was approved that by appending these two FD features, the error rate decreased from 20% to 5-10% for six upper limb motions. Another successful usage of TD features with FD features was in [59], where the following TD features were used: MAV, WAMP, VAR, and WL together with FD features: MDF and MNF. These mixed set of features were tested on 6 different hand gestures recorded on 4 channels, and the result was 97% accuracy using k-Nearest Neighbors (KNN) as classifier. Different set of TD and FD features were used together in another study [60], the features were RMS, WL and sample entropy as TD, besides to Median Amplitude Spectrum (MAS) as FD feature. The accuracy of the classification was 95% for 9 hand gestures recorded on 9 channels, where in this study a General Regression Neural Network (GRNN) classifier were used. The combined TD and FD features are giving better results than TD features although they are extracted separately without looking to their potential relation, which leads to next type of features time-frequency domain features.

2.5.3 Time-Frequency Domain

Time-Frequency Domain (TFD) features contains the combination of temporal and frequency information. They present the sEMG signals more accurately because they lies in a time-frequency plane; therefore they could show how the frequency of the signal varies in time. This advantage is very useful in non-stationary signals as sEMG.

Several time-frequency methods were used in the state of the art. Short Time Fourier Transform (STFT) [61] is a widely used time-frequency method. The signal is divided into time segments by a fixed-size window, then these segments are converted into spectral ranges. STFT was successfully used to extract intrinsic features of the movement identification, and led to high classification rate in case of large training data. In [62], STFT was used with Principal Component Analysis (PCA) as a linear dimension re-

duction method and Diffusion Maps (DM) as non-linear. The average accuracy of classification of six hand motions was of 94.8% for PCA and 88.0% for the DM. However, the STFT may be limited as time-frequency resolution for some non-stationary signals, where we need to adapt the resolution of the analyzing window over the frequency of the signal.

The Wavelet Transform (WT) overcomes the shortcoming of the frequency-invariant window in the STFT. The WT changes as the frequency varies by scaling the mother wavelet. When the frequency in the signal increases, the WT increases the resolution by narrowing the used wavelet. In [63] Myo armband was used to collect sEMG signals, these signals were filtered and sampled, then Continuous WT (CWT) was selected to obtain the signal spectrum, and the neural network model was applied to classify the spectrum to achieve gesture recognition. This study compared CWT with the TD features in [64] and proved that CWT outperforms TD features by testing on different datasets. In [65] Discrete WT (DWT) was proven to provide sufficient information about the signal, with big improvement in the calculation time compared to STFT. Another study [66] used Ternary Pattern DWT with 2-layered feature selection method and conventional classifiers. The methods were tested on different force levels of sEMG signals: low, medium and high. By applying these methods on sEMG signals containing six grip patterns; they achieved 92.96%, 93.33%, 97.41% and 99.14% classification accuracy for high, medium, low and all force levels respectively.

The Stockwell Transform (ST) is a time-frequency analysis method which is a kind of multi-resolution version of the STFT form. This method uses Gaussian window as a kernel window that changes its standard deviation by frequency [67]. Unlike the WT, the ST holds the information about the signal phase as in the Fourier transform. A recent study [68] shows that ST features overcomes wavelet packet transform features for sEMG classification. This study used the symmlet mother wavelet of order five as the wavelet packet basis function and the number of the wavelet decomposition levels was three. The ST achieved 98.12% of average accuracy for six hand motions while wavelet packet transform achieved 97.61% [68].

Time-frequency features were proved to have essential information about the sEMG signals [69, 62], but on the other hand they produce a high-dimensional feature vector. Hence using all the features would be numerically intractable and weakly relevant to the classification; therefore, it is mandatory to perform a dimension reduction on these features.

2.6 Dimension Reduction

The dimensionality reduction methods aim to represent the feature space into a lower-dimensional space while keeping most meaningful characteristics of the original data

points of the space.

The dimension reduction becomes an essential part when dealing with TF features because of their high-dimensional space. Usually, the discriminant characteristics of the signals could be presented in lower dimensional space. This dimensional reduction makes it easier and faster to operate classification and more importantly, it helps avoiding over-fitting.

A widely-used dimension reduction technique is PCA [70] as a linear dimension reduction method. In [71] PCA was applied to reduce dimension of the wavelet packet transform features, and the final classification accuracy result was 96% accuracy on 9 different classes. Dimension reduction has been notably generalized since the introduction of non-linear techniques, which do not assume the low-dimensional space to be Euclidean. The study [62] compared PCA and Diffusion Maps (DM), when applied on STFT features. This study concluded that DM outperforms PCA when less training data is available. This point is important, as the training effort is one of the challenges that faces prostheses development. Another study [72] shows how the features' dimension reduction process can improve the classification of sEMG in armband acquisition approach. The following dimensional reduction techniques were used on a set of TD and FD features: PCA, LDA, Isomap, Manifold Charting, Autoencoder, t-distributed Stochastic Neighbor Embedding, and Large Margin Nearest Neighbor (LMNN). This study found that, with respect to several other dimension reduction techniques, the best results in this study were obtained by using LMNN and a SVM classifier with 94% accuracy for six wrist movements acquired from an 8-channel armband.

2.7 Classification

Regarding the classification step, several methods were used to classify sEMG signals as k-Nearest Neighbors (k-NN) [73, 74], LDA [53, 74], SVM [52, 54] and Neural networks (NN) [75, 76]. A study [77] made a comparison between k-NN and SVM when applied on the TF features of sEMG signals. Both methods performed well on these kind of features with better accuracy score for k-NN. For 15 fingers' motions, k-NN with PCA had average accuracy of 93.76% while SVM with PCA had 88.88%.

2.8 Deep Learning

Although the classic approach of feature engineering and searching for the best features that carry intrinsic properties of the movements is dominant in sEMG pattern recognition, the feature learning as exemplified by deep learning started to be applied successfully in this area. In Deep Learning (DL), the machine learning system automatically discovers and extract the features needed by the classifier. Deep learning algorithms

started only recently to be applied for sEMG due to the need of a large dataset for training. The deep learning machine learning systems consists of networks which have many hidden connected layers inside with many neurons forming elementary units. This kind of neural networks structures have millions of parameters to be adjusted in order to get good pattern recognition performance. This creates another kind of challenges considering the computation issues that require GPU-based implementation and optimized deep learning models, besides to the need of large training sEMG data [78]. The application of deep learning in sEMG is relatively new, the main types of deep learning models are already used, namely: Unsupervised Pre-Trained Networks (UPNs), Convolutional Neural Networks (CNN), and Recurrent Neural Networks (RNN) [78].

Deep Belief Networks (DBN) as kind of UPNs is already used in sEMG pattern recognition. In [79] a DBN was used to classify 5 wrist movements recorded by two channels, the input of this deep learning system was 5 time-domain features, namely: Difference Absolute Mean Value (DAMV), Absolute Standard Deviation of Difference (ASDD), MAV, ZC. The results showed that the DBN accuracy was 88.60%, which was 7.55% higher than LDA and 2.89% higher than SVM. In another study [80], the ST transform was used to calculate the spectrogram of four channels raw sEMG signals, then the eigenvalues of these spectrograms were calculated using Singular Value Decomposition (SVD). These eigenvalues were used as features for 9 hand gesture features and fed into the DBN for classification. The overall classification accuracy using this method was 93.33%.

Another kind of deep learning is the CNN (or ConvNet), which is relatively widely used for sEMG pattern recognition compared to other models. CNN are quite similar to ordinary neural networks but make an assumption that the inputs are image-based. This assumption adds constraints to the model as the neurons should be arranged in three dimensions [78]. In [81], sEMG signals of 3 hand gestures were recorded using 8 channels with 1000 Hz sampling rate. A window of 8-channels sEMG raw data was used as an input for CNN as 128x8 input data. The final average accuracy was 94.6%. A different study [82] used a convolutional network with three parts, segmentation, feature extraction and classifier, and evaluated their architecture on DB2 from the Non-Invasive Adaptive Hand Prosthetics (NinaPro) database on 17 different hand gestures. The accuracy of their classification was 83%, which showed improvements when compared to classical classifiers SVM and RF with four TD features (MAV, WL, ZC, and HIST) and one feature (mDWT) from time-frequency domain. CNN is used in another work [83], where Hilbert fractal curve is employed to transform multi-channel sEMG signals into 2D image representations. In this study the authors applied their methods on Ninapro DB1 [84] by taking 52 movements recorded on 10 channels by sampling rate 2 KHz. The study applied different structures of CNN and proposed a

multi-scale Hilbert network, which achieved 78% average accuracy rate with the optimal values for the hyper-parameters. In [63], different deep learning CNN models were applied. The methods were applied on Ninapro DB5 dataset [85] with 23 different movements (including neutral) recorded by two Myo armbands with 200 Hz sampling rate. Both CNN Long Short-Term Memory Networks (CNN-LSTM), Lookup-based Convolutional Neural Network (LCNN) models were used with raw sEMG data as direct input and scored 61%, 66% respectively, while CWT transform was used as input proposed EMGNet model which has CNN architecture consisting of four convolutional layers and a max pooling layer with a compact structure and fewer parameters. That method increased the accuracy to 69.6%.

RNNs have connections that feed back into prior layers, giving ability to have information from the previous input. LSTM units and gated recurrent Units (GRUs) are two of the prevailing RNN architectures. In [86] authors combined LSTM network with multi-layer perceptron so they combine both the dynamic and static information of the sEMG signals in feature learning. This approach was evaluated on Ninapro database including 52 hand motions and achieved accuracy of 75% on 400ms segment window and 73% on 200ms segment window.

Time domain and time-frequency domain was used as input in [87] with proposing to use the Transfer Learning (TL) algorithm which aggregate the data of multiple individuals instead of recording thousands of windows from a single subject. The TL is important in the case of deep learning because of the large amount of the needed training data. the authors used two different ConvNet: one for the raw sEMG data as input and another for CWT. Both ConvNet models were tested on Ninapro DB5 (18 hand/wrist gestures) and using transfer learning. The augmented TL-ConvNet model with raw sEMG as input has the highest accuracy of 68.98%.

Although the Deep learning technology yields promising results, it still needs an equivalent development in the embedded devices that make it possible to run it in a prosthetic, besides to the lack of big sEMG database that is enough to build and train robust deep learning based model [78].

2.9 Methods Overview

We can get an overall overview about the methods combinations in the literature by looking at the table 2.2. We see in general that the TF features perform better than the TD features especially with the increment of the movement number, where also the deep learning combined with the TF features gives a promising results. A lot of possible combinations are used and evaluated with different number of movements and channels, different sampling frequency and different classifiers. This big variety makes it impossible to compare these methods and get a clear conclusion about their perfor-

mance when applied under the same conditions. In our work, we aim to do an extensive comparison and research in the TF features and the ways to improve both feature extraction and dimensional reduction methods.

Table 2.2: List of related studies ordered by features type. DB: database used in the corresponding study, SR: sampling rate of the sEMG signals.

Ref	Year	Features	DB	SR (Hz)	Key Points
[52]	2008	TD	Own	1000	<ul style="list-style-type: none"> - gestures: 5 limb motions - channels: 4 - features: MAV + WL + ZC + SSC - classifier: SVM - accuracy: 96%
[54]	2011	TD	Own	2000	<ul style="list-style-type: none"> - gestures: 9 - channels: (HD) 192 - features: RMS - classifier: SVM - accuracy: 95%
[53]	2014	TD	Own	1000	<ul style="list-style-type: none"> - gestures: 29 / 17 / 9 - channels: 15 - features: 6AR + MAV + WL + ZC + SSC - classifier: LDA - accuracy: 81% / 89% / 97%
[55]	2022	TD	Own	2000	<ul style="list-style-type: none"> - gestures: 10 - channels: 3 - features: RMS, VAR, MAV, SSC, ZC, WL - classifier: LDA - accuracy: 94% / 87%
[56]	2012	FD	Own	1000	<ul style="list-style-type: none"> - gestures: 6 - channels: 5 - features: MDF / SM1 / MNF - classifier: ANN / SVM - accuracy: 70% / 80% / 75%

Continued on next page

Table 2.2: List of related studies ordered by features type. DB: database used in the corresponding study, SR: sampling rate of the sEMG signals. (Continued)

Ref	Year	Features	DB	SR (Hz)	Key Points
[59]	2020	TD + FD	Own	2000	<ul style="list-style-type: none"> - gestures: 6 - channels: 4 - features: (MAV, WAMP, VAR, WL) + (MDF, MNF) - classifier: KNN - accuracy: 97%
[60]	2020	TD + FD	Own	1000	<ul style="list-style-type: none"> - gestures: 9 - channels: 16 - features: (RMS, WL, sampleEN) + (MAS) - classifier: GRNN NN - accuracy: 95%
[68]	2019	TFD	Own	1000	<ul style="list-style-type: none"> - gestures: 6 - channels: 2 - features: ST / wavelet packet transform - classifier: ANN - accuracy: 98% / 97%
[62]	2020	TFD	UCI [88]	500	<ul style="list-style-type: none"> - gestures: 6 - channels: 2 - features: STFT - classifier: KNN - dimension reduction: PCA / DM - accuracy: 95% / 88%
[63]	2020	TFD	Own	200	<ul style="list-style-type: none"> - gestures: 5 - channels: 8 - features: CWT - classifier: CNN - accuracy: 98%

Continued on next page

Table 2.2: List of related studies ordered by features type. DB: database used in the corresponding study, SR: sampling rate of the sEMG signals. (Continued)

Ref	Year	Features	DB	SR (Hz)	Key Points
[66]	2020	TFD	Own	2000	<ul style="list-style-type: none"> - gestures: 6 (high / moderate force) - channels: 8 - features: TP-DWT - classifier: KNN - accuracy: 93% / 99%
[79]	2015	Learned	Own	2000	<ul style="list-style-type: none"> - gestures: 5 - channels: 2 - input: (DAMV, DASDV, MAV, ZC) - model: DBN - accuracy: 88.60%
[81]	2018	Learned	Own	1000	<ul style="list-style-type: none"> - gestures: 3 - channels: 8 - input: raw sEMG - model: CNN - accuracy: 94.6%
[82]	2018	Learned	Ninapro DB2 [27]	2000	<ul style="list-style-type: none"> - gestures: 17 - channels: 12 - input: raw sEMG - model: CNN - accuracy: 83%
[86]	2018	Learned	Ninapro DB1 [84]	2000	<ul style="list-style-type: none"> - gestures: 52 - channels: 10 - input: raw sEMG - model: LSTM + MLP - accuracy: 75%
[87]	2019	Learned	Ninapro DB5 [85]	200	<ul style="list-style-type: none"> - gestures: 18 - channels: 8 (one Myo armband) - input: raw sEMG - model: ConvNet - accuracy: 69%

Continued on next page

Table 2.2: List of related studies ordered by features type. DB: database used in the corresponding study, SR: sampling rate of the sEMG signals. (Continued)

Ref	Year	Features	DB	SR (Hz)	Key Points
[63]	2020	Learned	Ninapro DB5 [85]	200	<ul style="list-style-type: none"> - gestures: 23 - channels: 16 - input: raw sEMG / CWT - model: LCNN - accuracy: 66% / 69.6%
[83]	2021	Learned	Ninapro DB1 [84]	2000	<ul style="list-style-type: none"> - gestures: 52 - channels: 10 - input: Hilbert fractal curve - model: CNN - accuracy: 78%
[80]	2021	Learned	Own	2000	<ul style="list-style-type: none"> - gestures: 9 - channels: 4 - input: ST - model: DBN - accuracy: 93.33%

2.10 Literature Review Recap

The literature overview shows that the prosthetic control systems still lack a lot of development to be accepted widely by people who need it. Although this development include all phases such as the sensors, sEMG acquisition, prosthetic design, natural movement and so on, the core challenge is still in the ability of the device to identify the intended movement from the sEMG signals. The literature shows that the TF features are superior features that could describe the characteristics of the sEMG signal due to its nature, but that would arise another problem of the needed real-time response and extensive training needed, which are both essential requirements in the prosthetic acceptance for the users. We focus in our research on extending the studies made on the TF features and improving the state of the art in both features extraction and dimension reduction methods with the aim to solve the related challenges of accuracy, training size, computation time problems.

In the next chapter we will explain the existing methods in the literature that we adapted and perform an extended comparison between them with multiple combinations of feature extraction, dimension reduction and classification methods.

CHAPTER 3

THEORETICAL BACKGROUND

We saw in the related work that Time-Frequency (TF) features and dimension reduction play an essential part in sEMG classification. The most promising features are the TF features; nevertheless, they still have challenges to be solved like accuracy improvement, computation time and training size. The promising results achieved by using TF features comes from the non-stationary nature of the sEMG signals, which promotes the change in frequency over the time as an informative characteristics. The ability of these features to properly describe the patterns and distinguish between sEMG signals encouraged us to extend this research area. So far, the performance of different TF methods with different dimension reduction techniques and different classifiers have not been tested properly under the same conditions in the literature. The importance of these features motivated us to do an extended comparison between a wide range of combinations in different classification stages, and to improve the methods themselves in order to gain better accuracy.

The usage of TF features leads also to extended research in the DR methods as these feature extraction methods would create high-dimension features space, and this dimension should be effectively reduced in order to obtain a better classification.

The starting point of any ML system is the data source which could provide sufficient data for training and evaluating. Next in this chapter, we will describe some of the available databases to evaluate our methods, after that, we will explain the methods we used in the sEMG features extraction, then we will explain the dimension reduction techniques that we applied in our research.

3.1 sEMG Data Sources

3.1.1 Analytical Modelling of sEMG Signals

The simulation models of signals could be very helpful for testing the performance of new developed systems before experimenting on real data. The simulation is however very complicated for signals as sEMG which depend on a large number of anatomical and physiological parameters. EMG signals are the summation of individual action potentials generated from Motor Units (MUs) as shown in figure 3.1. Each muscle contains a lot of fibers which acts as motor units. The overall generated EMG signal is the summation of contributions from many motor units inside the muscle, and even using electrodes on the surface of the skin will collect these motor activities from multiple muscles [89]. There are several variables that are used to describe the state of the muscle such as the intensity and power spectrum, the RMS, MDF, MNF of the power spectral density [90]. These variables are used in sEMG modeling to make simulated stochastic process related to the underlying physiological and anatomical parameters in the muscle.

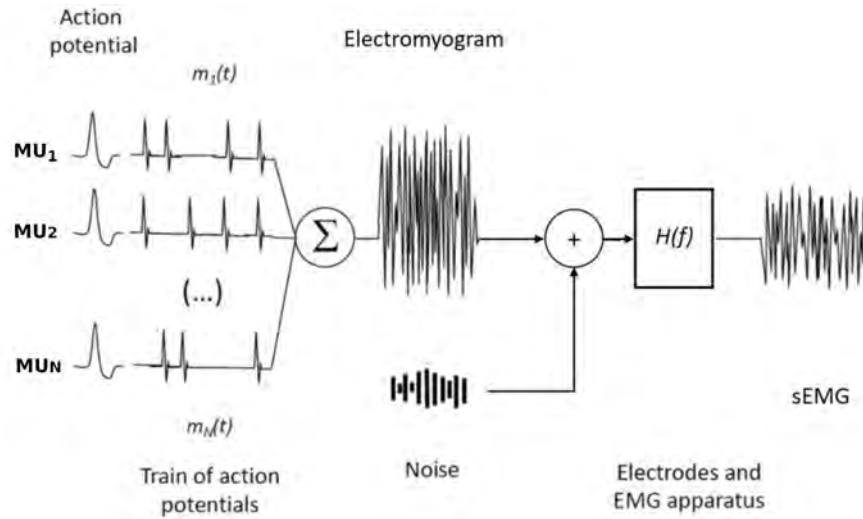


Fig. 3.1 sEMG generation from MUs model [89].

Many sEMG simulation methods modelled the stochastic properties of EMG signals following a Gaussian distribution [91, 92]. The EMG signals do not follow a steady Gaussian distribution as some studies declared [93, 94], and another study showed that sEMG probability distribution falls between a Gaussian and a Laplacian distribution [95]. The sEMG models are very useful in many applications, but these mod-

els are still under research to improve the acceptance, precision and ability to reflect more anatomical or physiological parameters more than muscle-fibre conduction velocity [90].

3.1.2 ZHAW School's Pilot sEMG Data

A partner team from ZHAW School of Health Sciences in Zurich (Switzerland) started to create a new sEMG database. They made the first pilot data, and we used our methods to make initial evaluation for this recorded signals. This dataset consists of movements that are performed by two hands, and the electrodes were places on both arms. The participant of the pilot was right-handed, the number of movements was 4 and the channels number was 16. The signals were sampled with sampling frequency 1200Hz. The movements performed are shown in figure 3.2:

1. Open a bottle.
2. Pour water from a jug into a glass.
3. Cut bread.
4. Cut meat.

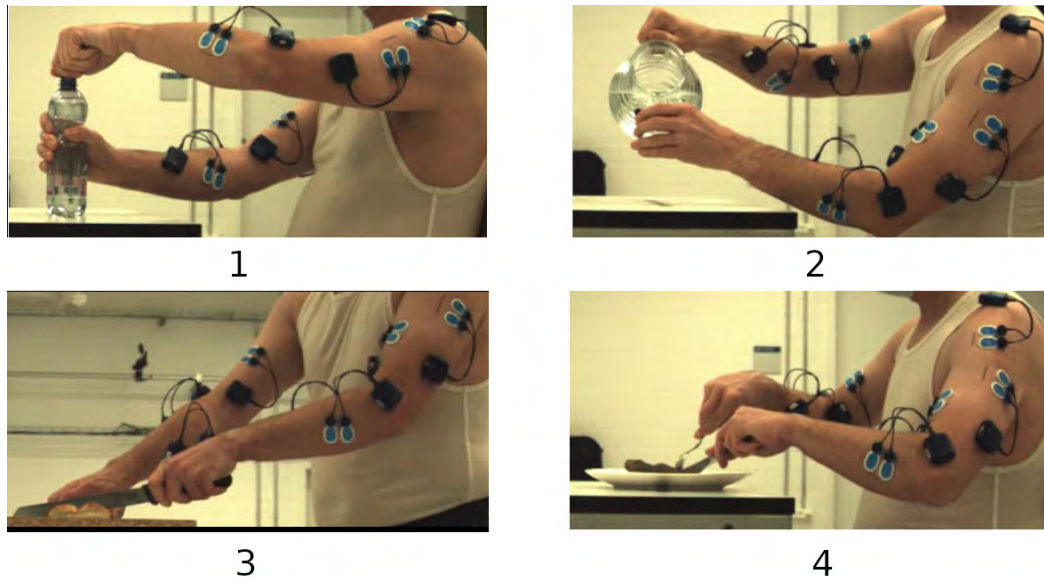


Fig. 3.2 The movements in the ZHAW school's database.

The movements were repeated by the subject 15 times. Each repetition lasts for 10s. More details about the protocol of acquisition are shown in the appendix A. We will use this pilot dataset to extend our numerical experiments in chapter 4 on different

data sources, which improves our concept and used methods, besides to providing a feedback for our partner team to proceed with their database creation.

3.1.3 Public Database

There are different publicly available databases that enable researchers to evaluate their methods on sEMG signals. One of the biggest and well-known sEMG database is Ninapro [96]. This database contains well annotated signals is open for public use, which made it widely used in this kind of researches. The Ninapro project first dataset was available for public in 2014 [96]. Currently, the Ninapro database includes 8 datasets containing surface EMG signals from the forearm and upper arm using 10–16 EMG channels together, in addition to 2 datasets contain kinematic data of the upper arm. In chapter 4, in our numerical experiments, we will use Ninapro database to test our methods. We will use both intact and amputees subjects and different number of movements taken from this database.

The Ninapro database contains more than 60 movements for hand and fingers. These movements data were recorded on 142 intact people and 15 amputees, with all related data as weight, age, left or right handed, height. The sEMG signals in Ninapro are recorded using different kind of sensors with different sampling rates. In table 3.1, we can see the list of the available data sets in Ninapro and the properties of each one of them.

Table 3.1 List of Ninapro datasets with their specifications.

N°	Channels	Sampling rate	Moves	Subjects	Information
1	10	100 Hz	52	27 intact	<ul style="list-style-type: none"> - Each movement repetition lasts 5s followed by 3s of rest - 10 repetition for each movement - Otto Bock MyoBock 13E200 electrodes
2	12	2 kHz	49	40 intact	<ul style="list-style-type: none"> - Each movement repetition lasts 5s followed by 3s of rest - 6 repetitions for each movement - Wireless electrodes from a Delsys Trigno Wireless EMG system
3	12	2 kHz	49	11 amputee	<ul style="list-style-type: none"> - Each movement repetition lasts 5s followed by 3s of rest - 6 repetitions for each movement - Wireless electrodes from a Delsys Trigno Wireless EMG system
4	12	2 kHz	52	10 intact	<ul style="list-style-type: none"> - Each movement repetition lasts 5s followed by 3s of rest - 6 repetitions for each movement - Wireless electrodes from a Cometa
5	16	200 Hz	52	10 intact	<ul style="list-style-type: none"> - Each movement repetition lasts 5s followed by 3s of rest - 6 repetitions for each movement - 2 Thalmic Myo armbands
6	14	2 kHz	7	9 intact	<ul style="list-style-type: none"> - Each movement repetition lasts 4s followed by 4s of rest - 12 repetitions for each movement - Wireless electrodes from a Delsys Trigno Wireless EMG system
7	12	2 kHz	40	20 intact 2 amputee	<ul style="list-style-type: none"> - Each movement repetition lasts 5s followed by 3s of rest - 6 repetitions for each movement - Wireless electrodes from a Delsys Trigno Wireless EMG system
8	16	2 kHz	9	10 intact 2 amputee	<ul style="list-style-type: none"> - Each movement repetition lasts 6s to 9s followed by 3s of rest - 10 repetitions for each movement - Wireless electrodes from a Delsys Trigno Wireless EMG system

3.2 Features Extraction

As seen in the literature overview in chapter 2, the main types of features extraction for sEMG signals could be divided into three main parts: TD, FD and TFD features. Although the TD features are the most used features for sEMG signals due to their simplicity and low computation time, they do not preserve the frequency intrinsic characteristics. In the other hand, the Fourier transform of the signal cannot depict how the frequency of the signal changes over the time, which is a very important description for the non-stationary signals. TF analysis summarizes analysis techniques that quantify the temporal evolution of spectral properties of signals; therefore the time-frequency domain provides a temporal description of the frequency component as a function of time.

In order to understand the importance of preserving the frequency change over the time, we look on an example of two linear chirp signals (up-chirp and down-chirp) shown in figure 3.3a, we see two different kind of chirp signals. In the first signal (the up-chirp), we have linear increment in the frequency from 0 to 40Hz, while the frequency decreases in the another signal (the down-chirp) from 40 to 0Hz. Although these two signals are different signals but the modulus of the Fast Fourier Transform (FFT) is identical for both as we see in figure 3.3b. This comes from the fact that Fourier analysis does not preserve the information about the frequency changes over the time (increment vs decrement in our example). In the other hand, if we look on the modulus of one of the typical time-frequency transforms as STFT 3.3c, we see clearly how the frequency varies by time for each signal. This kind of information can carry distinctive features for each signal.

In this thesis, we applied different time-frequency methods to study the best features that describe the sEMG signals and lead to a better classification accuracy. The following sections will explain in details these methods and the differences between them. We will enrich the theoretical explanation by applying these methods on chosen signals, and in all chapters in this thesis, the modulus of the TF coefficients will be used to show the TF representations.

3.2.1 Short Time Fourier Transform

Short Time Fourier Transform (STFT) divides the signal into smaller segments, in which we assume that the signal is stationary inside this window. Then we calculates the Fourier transform on each of them, which shows how the frequency varies in the time. Let the original signal be $x(t) \in L^2(\mathbb{R})$, the segmentation is done using a sliding window $g(t) \in L^2(\mathbb{C})$ where the Fourier transform is applied in order to obtain the local

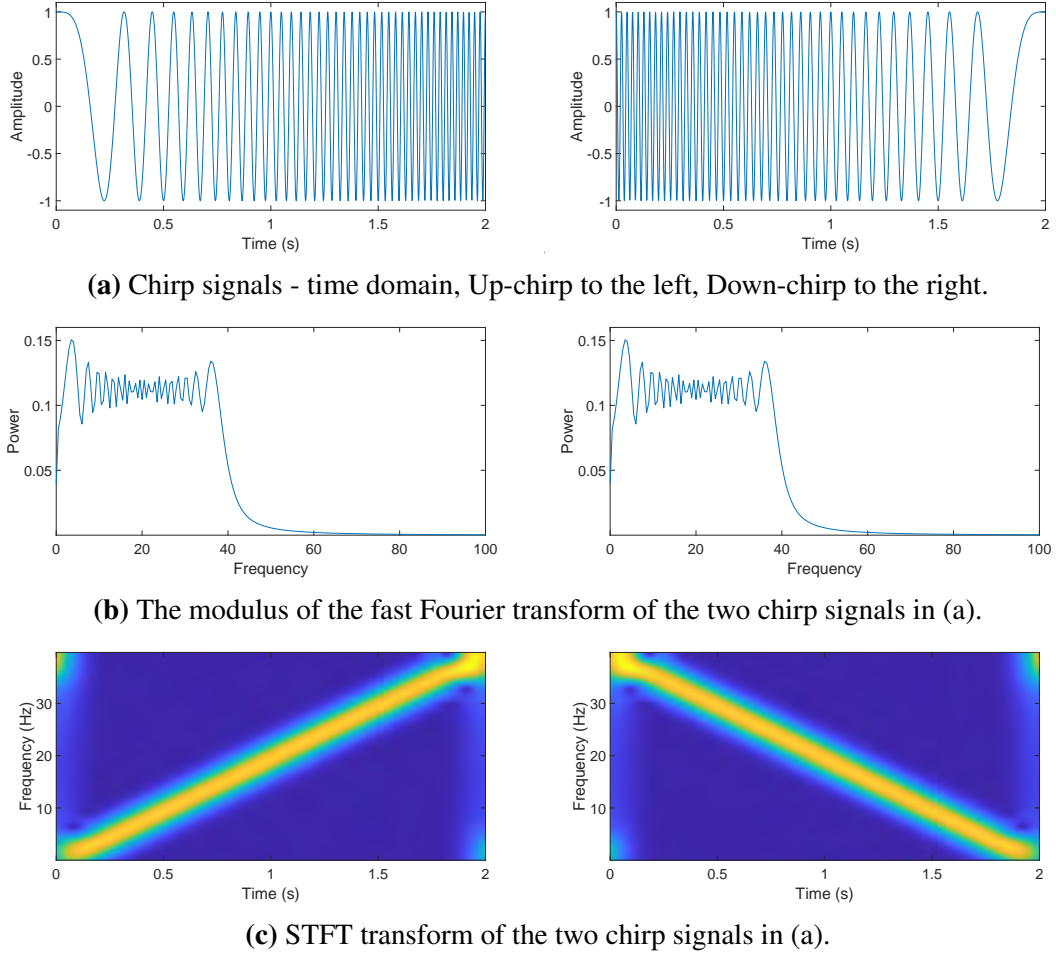


Fig. 3.3 Up-Chirp and Down-Chirp signals with their FFT and STFT transforms.

spectrum [97] as follows:

$$V_g(\tau, f) = \int_{-\infty}^{+\infty} x(t) \overline{g(t - \tau)} e^{-i2\pi ft} dt \quad (3.1)$$

Where $\tau \in \mathbb{R}$ refers to time and $f \in \mathbb{R}^*$ is the frequency.

The STFT formula can also be written as an inner product:

$$V_g(\tau, f) = \langle x(t), g(t - \tau) e^{-i2\pi ft} \rangle \quad (3.2)$$

The length of the chosen window will determine the trade-off between frequency and time resolution. The use of narrow window length in time domain will give us a good temporal resolution but with more blurring in the frequency domain. In the opposite, using a wider window length will lead to a worse temporal resolution and sharper frequency resolution [98]. In order to understand behaviour and limitation of the STFT

transform, let us consider a signal x_1 which changes its frequency sharply when $t = 1$:

$$x_1(t) = \begin{cases} \cos(2\pi f_1 t) & : t \leq 1 \\ \cos(2\pi f_2 t) & : t > 1 \end{cases} \quad (3.3)$$

Where $f_1 = \frac{100}{2\pi}$, and $f_2 = \frac{400}{2\pi}$.

3.2.1.1 Window type and size

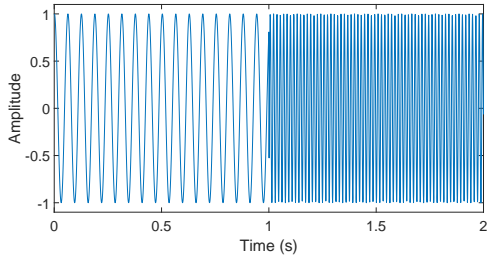
In figure 3.4a, we can see the signal x_1 in time domain, where it shows how the signal changes its frequency sharply at some point in the time (at 1s). The type and size of the chosen window in STFT play an important role in the quality of the spectrograms energy concentration, i.e., the spread of the energy around instantaneous frequency. In figure 3.4b, we can see a manual drawing of the ideal representation of the TF, while if we look on figure 3.4c, we can see two different windows used in STFT which are the rectangle (to the left) and Hann windows¹ (to the right). Note that the windows introduce some smearing of frequencies in the Fourier domain as well as additional artifacts, which explains the weaker lines that appears around the main energy line. These weaker stripes correspond to the ripples occurring in the Fourier transform of the window function. One can observe that the ripple artifacts are stronger when using a rectangular window instead of a Hann window. In general, it is not easy to distinguish the characteristics of the signal and the effects introduced by the window function.

The size of the used window also has an effect on the energy concentration, so a wide time-domain window implies good localization in the frequency domain for low frequencies, while a narrow window provides good localization in the time domain for higher frequencies. If we change the width of Hann window in STFT transform, we can see the effect on the STFT transform of signal x_1 as shown in figure 3.5, where we see that for narrower window width, we get better time resolution but wider (less concentrated) frequency values, while using wider window will give better frequency resolution but with cost of the time resolution and we can see in the figure the sharp jump in the frequency values (i.e. happens in small time interval) will be blurred with bigger window width.

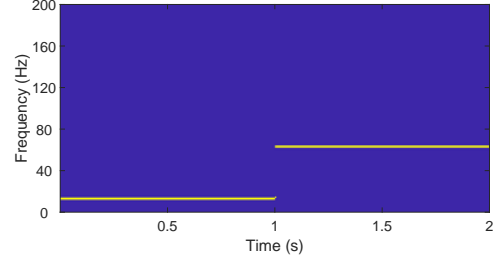
3.2.1.2 STFT limitation

The main limitation of the STFT is that it has a fixed temporal resolution. In order to obtain good concentration at higher frequencies, a narrow window in the time domain should be used for the STFT. However, the narrow window in the time domain significantly diminishes the concentration of the lower frequencies contents of the signal. This

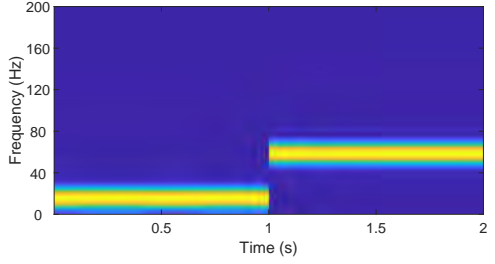
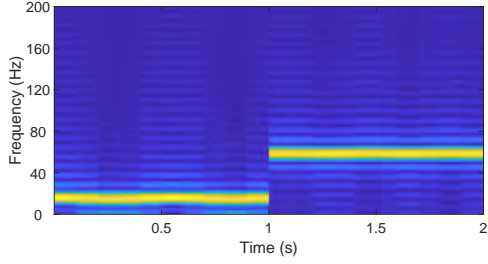
¹Hann window is defined as: $\frac{1}{2}[1 - \cos(2\pi t/T)]$, $t \in [0, T]$



(a) Signal x_1 in time domain.



(b) The manual drawing of the ideal TF representation of the signal x_1 .



(c) STFT for signal x_1 when using two different windows, rectangular window to the left, Hann window to the right.

Fig. 3.4 Effect of using different window types in STFT.

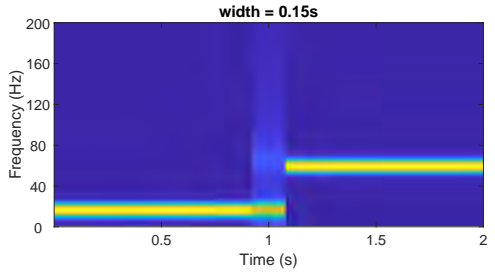
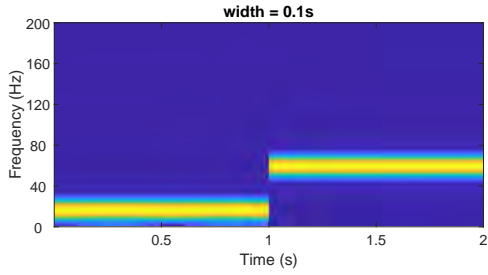


Fig. 3.5 Effect of using different window widths in STFT with Hann window.

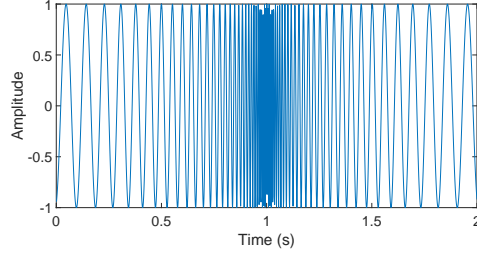
limitation appears in the signals where the frequency changes sharply in high and low values. To give an example of such signal, we look at signal x_2 , which is shown in 3.6a:

$$x_2(t) = \begin{cases} \cos[-20\pi \ln(-20(t-1)+1)] : 0 \leq t < 1 \\ \cos[+20\pi \ln(+20(t-1)+1)] : t > 1 \end{cases} \quad (3.4)$$

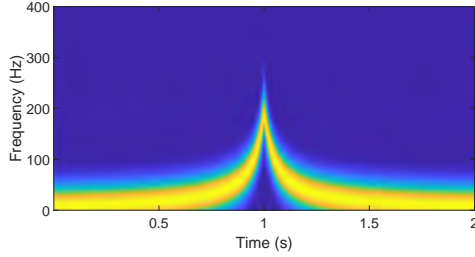
We apply the STFT transform on this signal using a real Gaussian window with standard deviation σ :

$$g(t) = \frac{1}{\sigma\sqrt{2\pi}} e^{-\frac{t^2}{2\sigma^2}} \quad (3.5)$$

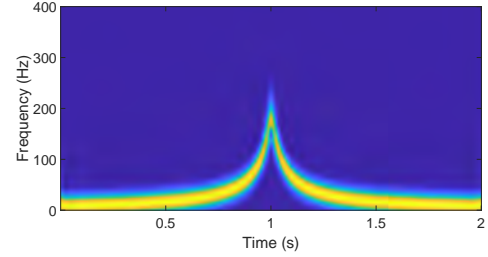
The figures 3.6(b,c,d,e) show different STFT representations when using different σ values, and we can see that there is no width value could result in good concentration in the spectrogram. The fixed window size could be chosen to be suitable for either high values or low values of frequency, and there is no way in the previous example to compensate the width to get a better results in both.



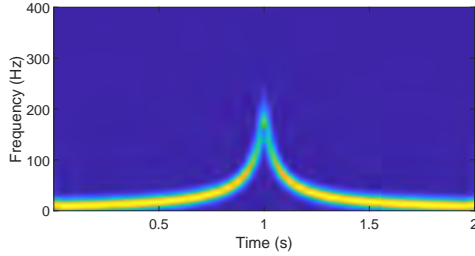
(a) The signal x_2 in the time domain.



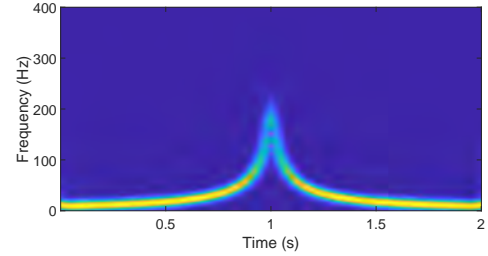
(b) STFT of x_2 with $\sigma = 0.002$.



(c) STFT of x_2 with $\sigma = 0.004$.



(d) STFT of x_2 with $\sigma = 0.006$.



(e) STFT of x_2 with $\sigma = 0.008$.

Fig. 3.6 STFT transform for the signal x_2 using different σ values in STFT Gaussian window.

The intuitive way to overcome this limitation is to use different window sizes in STFT calculation, which is called multi-resolution analysis. The desirable way would be to decompose our signal in a way that high frequency components are analyzed with high temporal resolution (since they vary rapidly in time), and low frequency components are analyzed with low temporal resolution.

3.2.2 Continuous Wavelet Transform

The main approach proposed in the Continuous Wavelet Transform (CWT) was to add a scaling operation to the mother window in STFT. This transform was introduced to overcome the limitation of the fixed window size in STFT which we discussed in the previous section. Morlet and Grossman modified the Gabor transform to produce the continuous wavelet transform by making the width of the window changes according to the frequency [99].

The CWT uses the inner products to measure the similarity between the signal and analyzing function, as in the Fourier transform where the analyzing function is $e^{i\omega t}$ or in

the STFT where the analyzing function is $g(t)e^{iwt}$. In the CWT, the analyzing function is a wavelet Ψ . The CWT compares the signal to shifted and compressed or stretched versions of a wavelet. Stretching or compressing a function is collectively referred to as dilation or scaling and corresponds to the physical notion of scale.

The CWT of a signal $x(t) \in L^2(\mathbb{R})$ is defined at each time τ and scale a for an admissible mother wavelet Ψ as follows:

$$W_\Psi(\tau, a) = \frac{1}{\sqrt{|a|}} \int_{-\infty}^{+\infty} x(t) \overline{\Psi\left(\frac{t-\tau}{a}\right)} dt \quad (3.6)$$

where $\Psi(t)$ and its Fourier transform $\hat{\Psi}(f)$ are satisfying the admissibility condition of the mother wavelet :

$$C_\Psi = \int_{-\infty}^{+\infty} \frac{|\hat{\Psi}(f)|^2}{f} df < \infty \quad (3.7)$$

By defining the scale $a = \frac{\sqrt{2\pi}}{f}$, Eq. 3.6 can be expressed as a time-frequency transform as follows :

$$W_\Psi(\tau, f) = \frac{\sqrt{|f|}}{2\pi^{1/4}} \int_{-\infty}^{+\infty} x(t) \overline{\Psi\left(\frac{f}{\sqrt{2\pi}}(t-\tau)\right)} dt \quad (3.8)$$

In order to have a better comparison with the STFT with a Gaussian window, the CWT and the ST (presented in the next section), we use a Morlet wavelet. The Morlet wavelet is defined as [100]:

$$\Psi(t) = \frac{\pi^{-1/4}}{\sqrt{\sigma}} e^{\frac{-t^2}{2\sigma^2}} e^{i\sqrt{2\pi}t} \quad (3.9)$$

where σ plays the role of time-spread parameter. By introducing Eq. 3.9 in Eq. 3.6 we obtain the definition of the Morlet wavelet transform of the signal s denoted MW_Ψ .

The variable window width in CWT improves the time-frequency representation considering the limitation in STFT. The CWT provides good time resolution and relatively poor frequency resolution at high frequencies while good frequency resolution and relatively poor time resolution at low frequencies. If we look to the signal x_2 where we show the blurred spectrum when we apply STFT and we compare it to the spectrum in figure 3.7, we can already see that improved representation when using variable window size.

3.2.3 Stockwell Transform

The Stockwell transform is a generalized version of the STFT. The ST uses a Gaussian window with standard variation that varies with the frequency [101], so the ST formula is same as in STFT 3.1 where the window g is Gaussian and related to σ :

$$S_g(\tau, f) = \int_{-\infty}^{+\infty} x(t) \overline{g_\sigma(t-\tau)} e^{-i2\pi ft} dt \quad (3.10)$$

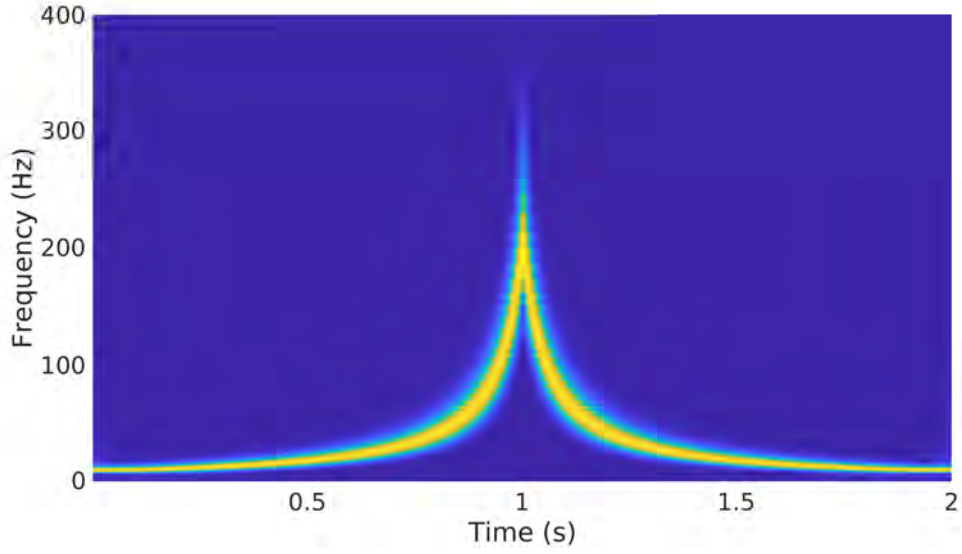


Fig. 3.7 CWT for the x_2 signal shown in figure 3.6a.

This formula could also be written as an inner product as:

$$S_g(\tau, f) = \langle x(t), g_\sigma(t - \tau)e^{-i2\pi ft} \rangle \quad (3.11)$$

For the ST transform, the value of σ in the Gaussian window (Eq 3.5) is replaced with $1/|f|$, and its formula will be:

$$g(t) = \frac{|f|}{\sqrt{2\pi}} e^{-\frac{t^2 f^2}{2}} \quad (3.12)$$

The ST formula is then written as:

$$S_g(\tau, f) = \int_{-\infty}^{+\infty} x(t) \frac{|f|}{\sqrt{2\pi}} e^{-\frac{(t-\tau)^2 f^2}{2}} e^{-i2\pi ft} dt \quad (3.13)$$

If we write the ST as a convolution product between as follows:

$$\begin{aligned} S_g(\tau, f) &= \int_{-\infty}^{+\infty} p(t, f) g(\tau - t, f) dt \\ &= p(\tau, f) * g(\tau, f) \end{aligned}$$

where $p(\tau, f) = x(\tau) e^{-i2\pi f\tau}$ and $g(\tau, f) = \frac{|f|}{\sqrt{2\pi}} e^{-\frac{\tau^2 f^2}{2}}$. Using the convolution theorem in the Fourier space (operator F), we can write ST as a function of the Fourier

transform $X(f)$ of $x(t)$:

$$F_{\tau \rightarrow \alpha} \{S_g(\tau, f)\} = P(\alpha, f) G(\alpha, f) \quad (3.14)$$

$$= X(\alpha + f) e^{\frac{-2\pi^2 \alpha^2}{f^2}} \quad (3.15)$$

Then by applying the inverse Fourier transform we obtain:

$$S_g(\tau, f) = \int_{-\infty}^{+\infty} X(\alpha + f) e^{\frac{-2(\pi)^2(\alpha)^2}{f^2}} e^{i2\pi\alpha\tau} d\alpha \quad f \neq 0 \quad (3.16)$$

The implementation of the ST will be based on the equation 3.16 since it establishes a direct link with the Fourier transform of the signal and therefore can benefit from the efficiency of the FFT algorithm.

Discrete ST Implementation: Let us consider the discrete presentation of $x(t)$ as $x[kT] \in L^2(\mathbb{R})$ with $k = 0, 1, \dots, N-1$ where T is the sampling interval. Then the discrete Fourier transform of x will be:

$$X\left[\frac{n}{NT}\right] = \frac{1}{N} \sum_{k=0}^{N-1} x[kT] e^{\frac{-i2\pi nk}{N}} \quad (3.17)$$

where $n = 0, 1, \dots, N-1$.

By setting $f = \frac{n}{NT}$ and $\tau = jT$ in Eq(3.16), we can get a direct link between the discrete ST and the discrete Fourier transform of both S and the Gaussian window $e^{\frac{-2\pi^2 m^2 \alpha^2}{n^2}}$ as follows [102]:

$$S[jT, \frac{n}{NT}] = \sum_{m=0}^{N-1} X\left[\frac{m+n}{NT}\right] e^{\frac{-2\pi^2 m^2 \alpha^2}{n^2}} e^{\frac{i2\pi mj}{N}} \quad (3.18)$$

which is optimized for implementation with respect to Eq. (3.17), because of its relation to FFT.

The ST replaces the fixed value of σ in the STFT transform, with a function of frequency $1/|f|$. This overcomes the limitation that we explained about the STFT by finding a way to decompose a signal with high spatial resolution in high frequency (narrow window), and low spatial resolution for the low frequency values (wide window). If we look to the same signal x_2 for which we were not able to choose window width in STFT that gives us a good TF representation. We see a good TF representation for this signal as shown in figure 3.8. In this figure we notice how ST transform led to very good energy concentration in the spectrogram in both high and low frequency values.

The discrete ST is a projection of the time series $x[kT]$ onto a spanning set of vectors. These spanning vectors are not orthogonal, and the elements of the ST are not independent. Each basis vector (of the Fourier transform) is divided into N localized

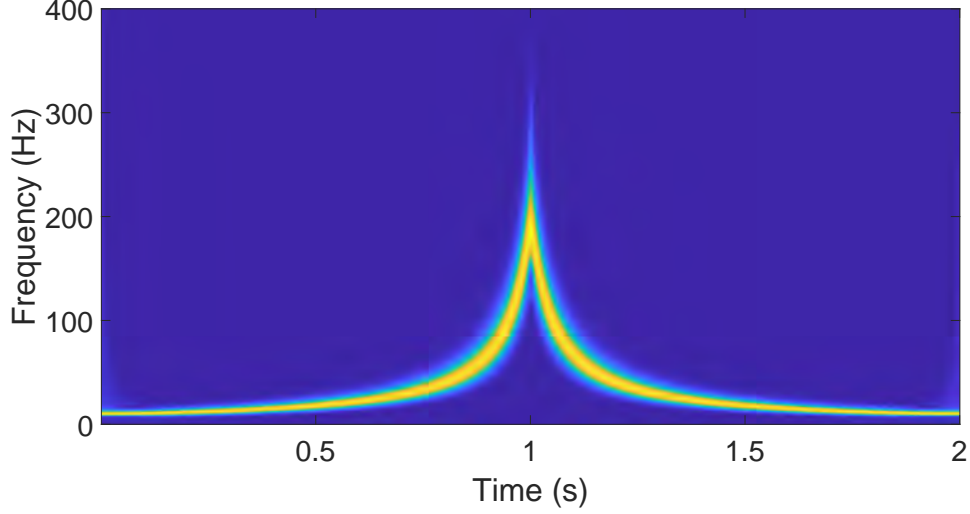


Fig. 3.8 Stockwell transform for the x_2 signal shown in figure 3.6a.

vectors by element-wise product. With the N shifted Gaussian, the sum of these N localized vectors is the original basis vector [102].

The projection on the non-orthogonal functions (Eq 3.18), creates a redundancy in the previous transforms, together with the complexity of calculations increases the need of different kind of transforms which overcome these two important points.

3.2.4 Discrete Orthonormal Stockwell Transform

For a signal of length N , there are N^2 Stockwell coefficients, and their computation has a $\mathcal{O}(N)$ time complexity. Hence, the complexity of the ST will be $\mathcal{O}(N^3)$, which is very time-consuming for high-dimension space.

The Discrete Orthonormal Stockwell Transform (DOST) prunes the redundancy within the ST. Indeed, the DOST down-samples the low frequencies as they have wider window, while it keeps the high sampling rates for the high frequencies.

The DOST creates N orthogonal basis vectors, where each vectors targets a certain area in time-frequency [103, 104]. It can be performed as the inner products between a time series $x[kT]$ and the orthogonal basis functions defined as function of $[kT]$, with the parameters ν (a frequency variable locating the center of a frequency band), β (defining the frequency resolution), and τ (for time localization), so the ST formula in (3.18) will change in DOST to:

$$D_s(\tau T, \frac{\nu}{NT}) = \sum_{k=0}^{N-1} x[kT] C_{[\nu, \beta, \tau]}[kT]; \quad (3.19)$$

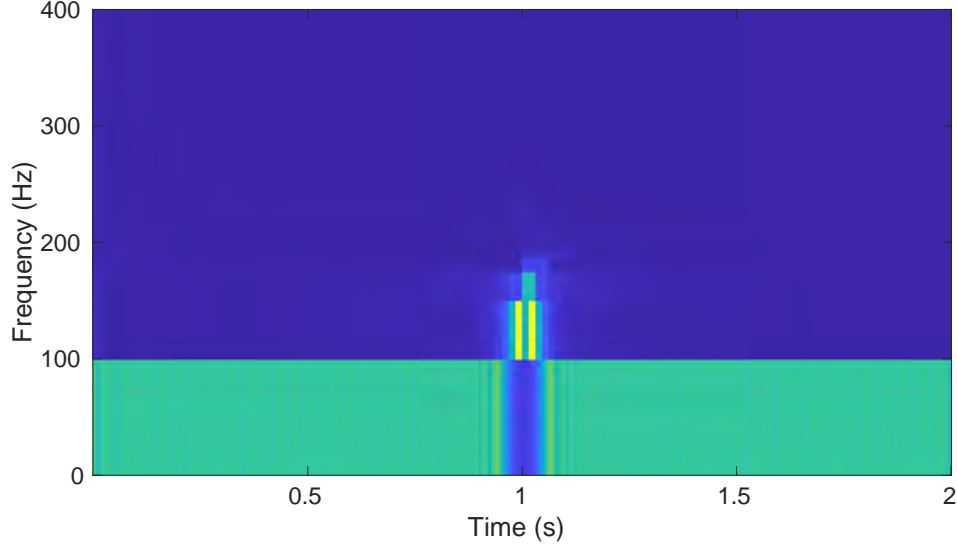


Fig. 3.9 DOST transform for the x_2 signal shown in figure 3.6a.

Where the $C_{[\nu, \beta, \tau]}$ are the orthogonal basis:

$$C_{[\nu, \beta, \tau]}[kT] = \frac{ie^{-i\pi\tau}}{\sqrt{\beta}} \frac{e^{-i2\pi(\frac{k}{N} - \frac{\tau}{\beta})(\nu - \frac{\beta}{2} - \frac{1}{2})} - e^{-i2\pi(\frac{k}{N} - \frac{\tau}{\beta})(\nu + \frac{\beta}{2} - \frac{1}{2})}}{2 \sin[\pi(\frac{k}{N} - \frac{\tau}{\beta})]}. \quad (3.20)$$

To ensure orthogonality, the sampling of TF domain should satisfy [104]:

- $\tau = 0, 1, \dots, \beta-1$.
- ν and β should be chosen such that each Fourier frequency sample is used only once.

If we apply the DOST on the signal x_2 (see figure 3.6a), we can notice how it looks in figure 3.9, and how the down-sampling in DOST clearly appears when rearranging the DOST coefficients in a TF representation.

Now that we have explained that STFT, CWT, ST are good candidates to be used to get TF representation of a signal, with special specification of each method. These methods contain redundancy and have a high complexity to be considered in applications that have time restrictions, while on the other hand, DOST is much less complex and remove the redundancy.

The question is still open about which one of these methods is more suitable for sEMG signals classifications from the perspective of complexity, time consumption and having enough intrinsic representation to be used in sEMG classification.

3.3 Dimension Reduction

Dimension reduction is a way to reduce the apparent complexity of data and to avoid over-fitting. This mapping from a high dimensional space into a low-dimensional space, while retaining meaningful properties, is a substantial step in many machine learning models especially when dealing with huge dimensional feature space. In this thesis, we apply both linear and nonlinear methods in order to study the best approach for sEMG classification. We will detail each used dimension reduction method, assuming that we have a dataset of observations $F \in \mathbb{R}^{N \times k}$ where N is the number of observations (i.e. data points), and k is the number of features in each data point. The purpose of any dimension reduction method is to reduce the features number from k dimensions to q dimensions where $q \ll k$.

3.3.1 PCA

The baseline method for the dimension reduction consists in Principal Component Analysis (PCA), which is a very popular and widely-used linear dimension reduction [70]. PCA is a linear projection-based method which transforms the data by projecting it onto a set of orthogonal axes, which are formed by the eigenvectors of the co-variance matrix of the original data. For a set of data points $F \in \mathbb{R}^{N \times k}$, the first step in PCA is to calculate the covariance matrix $A \in \mathbb{R}^{k \times k}$ of the dataset. The elements of A are the covariance between each pair of variables (features) x, y in the dataset:

$$cov_{x,y} = \frac{1}{N} \sum_{i=1}^N (x_i - \bar{x})(y_i - \bar{y}) \quad (3.21)$$

Where \bar{x} and \bar{y} are the mean of x and y respectively, N is the number of the data points. Next, we calculate the eigenvalues and eigenvectors of the covariance matrix:

$$A = U \lambda U^T \quad (3.22)$$

Where $U \in \mathbb{R}^{k \times k}$ is the matrix of corresponding eigenvectors, and λ is the diagonal matrix constructed from the eigenvalues of A . The eigenvectors correspond to eigenvalues which are sorted in descending order.

The last step in PCA is to select the largest $q < k$ eigenvalues and their corresponding eigenvectors, and the new embedded features matrix $Y \in \mathbb{R}^{N \times q}$ of the manifold F will be:

$$Y = F U_q \quad (3.23)$$

PCA projects the original data into lower dimensional space through combination of linear translations with maintaining most variance. This approach has a limitation when

the variance of the data points of the space are distributed on all dimensions and could not be projected without a big loss in variance. To understand this limitation, let us assume that we have 3-dimensional space whose data points approximately fit in a plane, the PCA method will be suitable for such space and will yield orthogonal direction within the plane. However, the "Swiss roll" example in figure 3.10, shows that PCA depends entirely on the nature of the data and their distributions in the original space. PCA will not work very well in this situation because it will look for a plane to project this data on it. In this example, there is no plane that can give a good representation of the data, where the manifold learning solves this problem very efficiently.

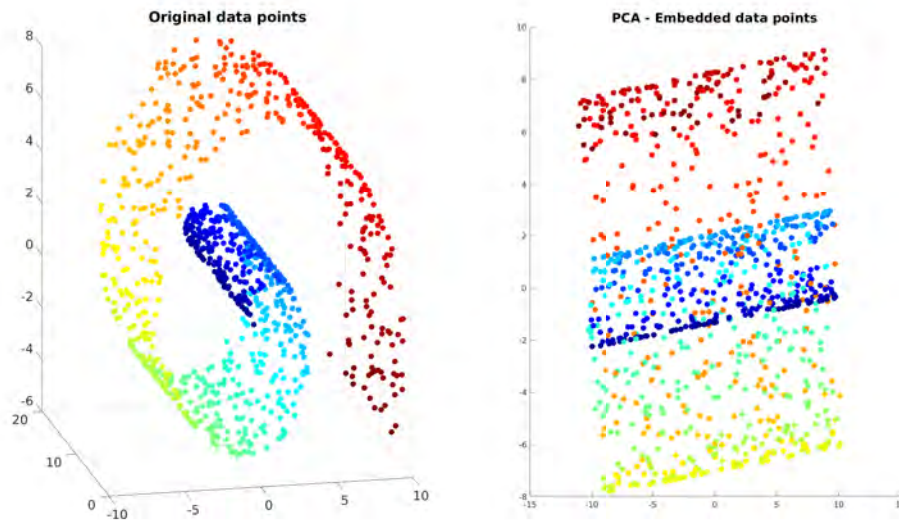


Fig. 3.10 PCA applied on Swiss Roll data points.

3.3.2 Manifold Learning

The manifold is a topological space that locally resembles Euclidean space. To get the intuition about the difference between the usual Euclidean space and a manifold, we can look at the two-dimensional manifolds which also called surfaces. Examples include the plane, the sphere, and the torus. If we look at the sphere example in figure 3.11, we can see the difference between calculating the distances in the Euclidean space compared to the manifold, here the distance from point a to b will be $2r$ where it is πr when calculating as a shortest path in the manifold (similar to moving from point a to point b on the Earth). This manifold distance calculations takes into consideration the geodesic properties of the manifold and preserves the neighborhood characteristics and relations to other data points in the space.

Manifold learning is an approach to non-linear dimensionality reduction. Unlike PCA which attempts to create several linear hyper-planes to represent dimensions, man-

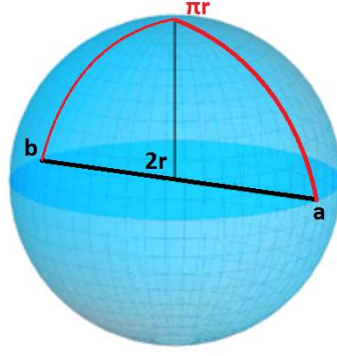


Fig. 3.11 Sphere manifold distances compared to Euclidean distances.

ifold learning attempts to describe the characteristics of the manifold that contains the data points. The Manifold learning is based on a more general approach in distance calculation than the Euclidean which is used in PCA. This generalization promotes this approach to be studied and evaluated empirically in the field of sEMG classification.

3.3.3 Isomap

Isomap [105] stands for "isometric mapping", and assumes that the data in the high-dimensional space lies on some manifold. Isomap is a non-linear dimension reduction method which aims at preserving the geodesic distances in the lower dimension. It constructs a graph that approximates the geodesic distances of the points in the manifold, then it considers this graph as an approximation of the manifold.

For a set of data points $F \in \mathbb{R}^{N \times k}$, the first step in Isomap is to compute the inter-point Euclidean distances matrix $D \in \mathbb{R}^{N \times N}$. The elements of D denoted d_{ij} are, $\forall i, j \in \{1, \dots, N\}$, d_{ij} will be the Euclidean distance between $F_i, F_j \in F$ as:

$$d_{ij} = \|F_i - F_j\|_2 \text{ where } F_i, F_j \in \mathbb{R}^k \quad (3.24)$$

Then, we define the initial paired-distance matrix $P \in \mathbb{R}_+^{N \times N}$ such that each element p_{ij} is, $\forall i, j \in \{1, \dots, N\}$:

$$p_{ij} = \begin{cases} p_{ij}, & \text{if } F_j \text{ belongs to the } u \text{ nearest neighbors of } F_i \\ \infty, & \text{otherwise} \end{cases} \quad (3.25)$$

P serves as an adjacency matrix in order to build a graph \mathcal{G} which approximates the manifold that contains data points F .

In its second step, Isomap calculates the geodesic distances between each pairs by computing the shortest path on \mathcal{G} using Dijkstra's algorithm. This yields a geodesic

distance matrix $D_G \in \mathbb{R}_+^{N \times N}$, which represents the new kernel of the initial manifold. Finally, we calculate the spectral decomposition of D_G :

$$D_G = \mathcal{V} \Lambda \mathcal{V}^T \quad (3.26)$$

where Λ is the diagonal matrix constructed from the eigenvalues of D_G , and \mathcal{V} is the matrix of corresponding eigenvectors. To get the embedded features in the q -dimensional space, we take the first q eigenvalues as Λ_q and first q eigenvectors as \mathcal{V}_q and the new embedded features matrix Y of the manifold F :

$$Y = \mathcal{V}_q \Lambda_q^{\frac{1}{2}} \quad (3.27)$$

Isomap is able to keep the geodesic properties of the space by preserving the local relations between the data points in a manifold. If we look at the Swiss roll example again and reduce its dimension from 3D to 2D as shown in figure 3.12 we can see how Isomap creates the graph of geodesic distances which preserves the inter-points distances of the space, and that leads to better discrimination when projecting the 3D space into 2D.

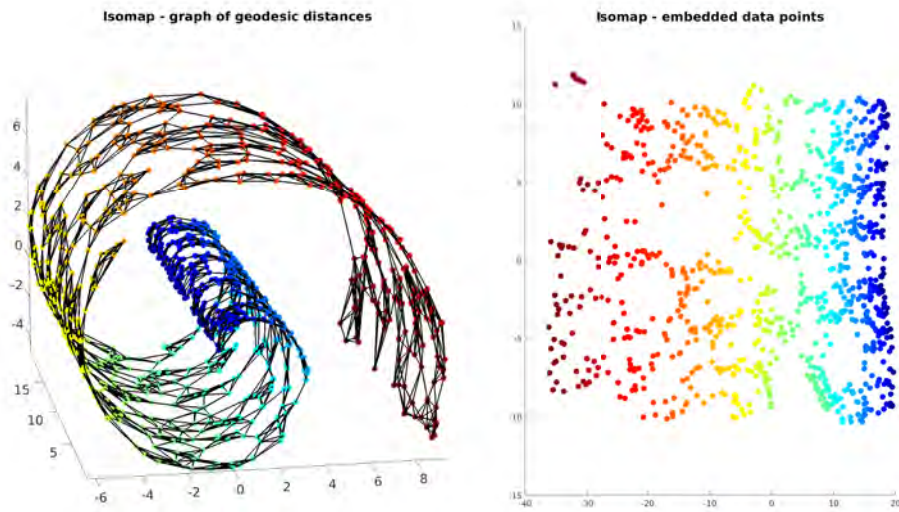


Fig. 3.12 Isomap applied on Swiss Roll data points.

The only parameters to be tuned in Isomap is the number of nearest neighbors u in equation (3.25). This parameter determines the area in which the points are considered to be neighbors and the distance between them will be calculated as Euclidean distance. If we look on the figure 3.13, we see that for the low value of u , less neighbors will be defined and as a result we will have less connecting points when calculating the shortest path, while increasing the number of neighbor will lead at its maximum to

the state where all data points are considered to be neighbors and the distances are calculated as Euclidean distances. We see that for value $u = 1000$ which is the number of all points, in this case, the distance calculations shown in equation 3.25 will be the Euclidean distance as the neighbors are all the points.

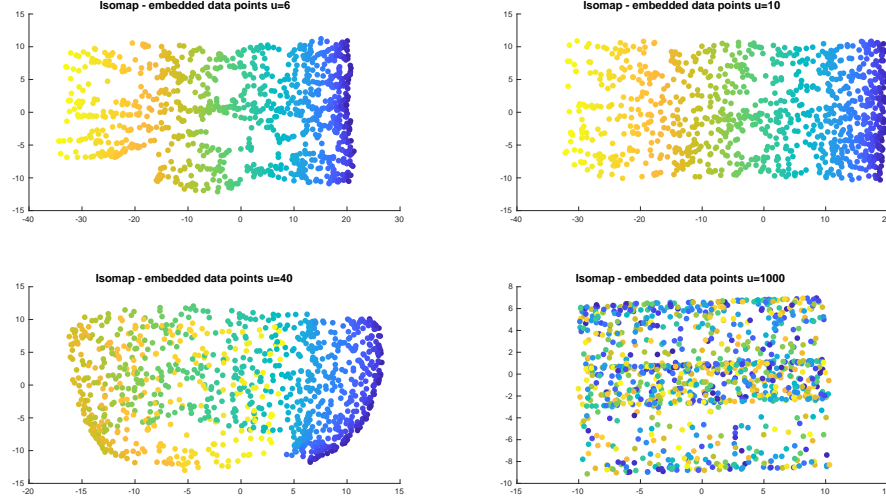


Fig. 3.13 Isomap applied on Swiss Roll data points with different neighbors number.

3.3.4 Diffusion Maps

Diffusion Maps (DM) aims to reduce the dimension of a high-dimensional dataset while preserving the geometrical properties [62]. The kernel in DM is Gaussian, and it defines the connectivity of each point with its neighbourhood. Using a Gaussian kernel has special characteristics:

- Values in the kernel decrease with distance and goes to zero for distant points which are more likely belong to different cluster or kind.
- It is bounded between zero and one, so it is less sensitive to abnormal observations, where zero means unconnected points.

The first step in this method is to calculate the positive weight matrix $W \in \mathbb{R}_{+*}^{N \times N}$ such that w_{ij} is, $\forall i, j \in \{1, \dots, N\}$:

$$w_{ij} = e^{-\frac{\|F_i - F_j\|_2^2}{2\rho}}. \quad (3.28)$$

This defines the local similarity measurement between i and j . This measurement could be tweaked by the kernel scale ρ , the choose of this scale is based on prior knowledge

of the structure and experiments on the data [106].

Next, a normalized kernel matrix $A \in \mathbb{R}_{+*}^{N \times N}$ is computed, $\forall i, j \in \{1, \dots, N\}$:

$$a_{ij} = \frac{w_{ij}}{\sum_{i=1}^N w_{ij} \times \sum_{j=1}^N w_{ij}} \quad (3.29)$$

After that we produce the Markov transition matrix $M \in [0, 1]^{N \times N}$ such that $\forall i, j \in \{1, \dots, N\}$:

$$m_{ij} = \frac{a_{ij}}{\sum_{i=1}^N a_{ij}} \quad (3.30)$$

M is a normalized version of A so that it is analog to a probability of moving from F_i to F_j .

The final step is similar to the final step in Isomap (3.26), as we calculate the spectral decomposition of the matrix M and the embedded features matrix Y .

We see in figure 3.14, how DM unfolds the Swiss roll data points into 2D space, and how this unfolding changes with the value of ρ .

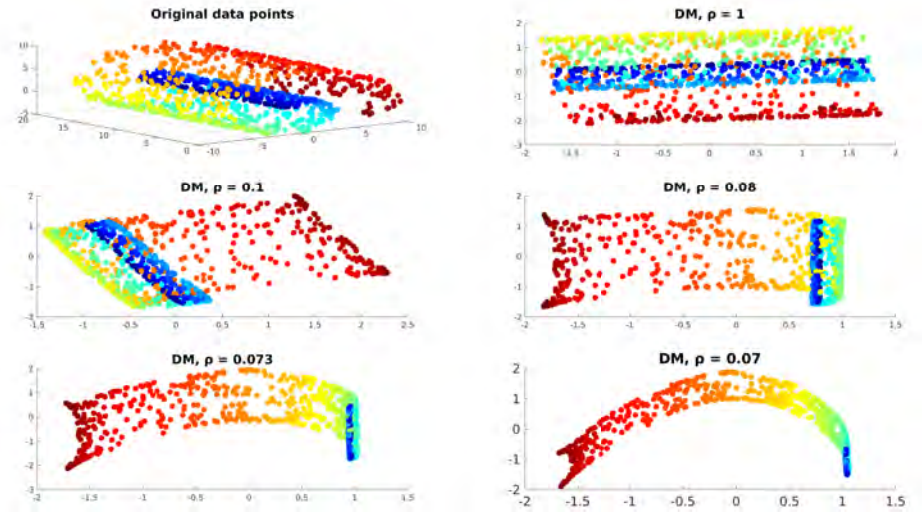


Fig. 3.14 DM applied on Swiss Roll data points with different ρ values.

3.3.5 Multidimensional Scaling

Multidimensional Scaling (MDS) [107] aims to reduce the dimension of the data by using only the dissimilarities measures between observations rather than using the data points. The idea is to find a lower-dimensional representation of the data that preserves the pairwise distances as well as possible [108]. The MDS creates a configuration of

points which have paired distances similar to the original ones. The steps of MDS are the following [109]:

- From the features matrix F , we calculate the inter-point distances matrix $D \in \mathbb{R}^{N \times N}$ as in equation (3.24).
- From D , we form the matrix V so that $\forall i, j \in \{1, \dots, N\}$:

$$v_{ij} = -\frac{1}{2}d_{ij}^2 \quad (3.31)$$

- Then we apply double centering:

$$B = HVH \quad (3.32)$$

where H is the centering matrix: $H = I - \frac{1}{N}1_N1_N^T$ with 1_N a vector of ones.

- As in Isomap and DM, in the last step we calculate the spectral decomposition of B which is explained in (3.26) and the new embedded features as in (3.27).

The new dimension q should be chosen so that features still preserve intrinsic characteristics of the observation, while removing weakly-relevant or redundant information. Choosing distance measurements method in MDS is very essential as it measures the dissimilarities between the data points. In figure 3.15, we notice how space unfolding changes with the change of the distance function in MDS, and that with a proper distance calculations, the MDS was able to unfold the space successfully.

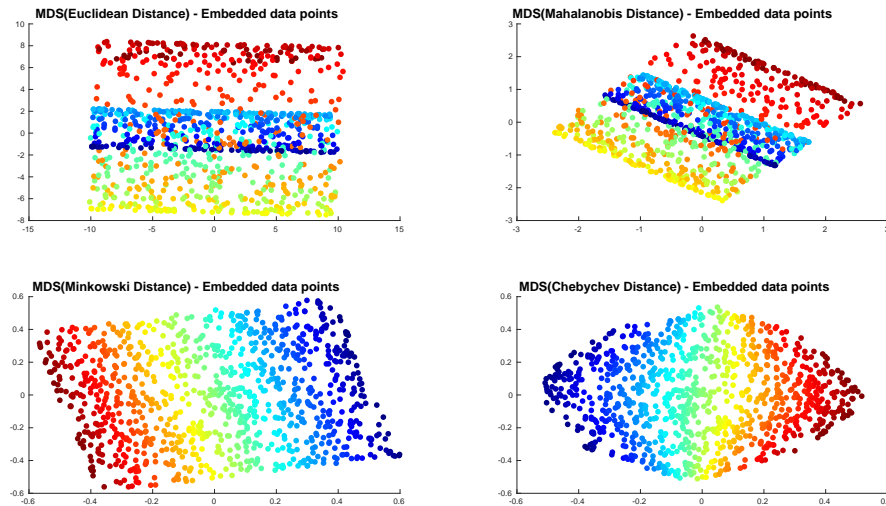


Fig. 3.15 MDS applied on Swiss Roll data points with different distance functions.

3.4 Theoretical Background Recap

In this chapter, we introduced the theory of some known TF methods that are used in sEMG classification; namely: STFT, CWT, ST and DOST. We showed some differences between these methods, advantages and disadvantages compared to each others. As the TF methods yields a high dimensional space, we introduced some of the dimension reduction methods that we will use in combination with the previous TF methods. These dimension reduction methods are: PCA, Isomap, DM and MDS.

The TF features of the sEMG signals are proven to be suitable in this area, but confidently using this kind of features requires answering questions as which method is more suitable to describe movements patterns in the sEMG signals, or the complexity of each methods considering the time limits in the prosthesis. The dimension reduction method is also very related to the features type and the data itself, and affects both the accuracy of classification and the training efficiency. In the next chapter, we apply all of these methods combinations; features extraction and dimension reduction with widely used classifiers in this area. Applying these combinations on the same database gives us the ability to fairly compare known methods in this field, besides to applying new methods. This comparison is further used to focus on improving the performance of the selected combinations.

CHAPTER 4

ALGORITHMS AND RESULTS

The TF methods we discussed in chapter 3 are good representatives for the sEMG signals, as they address their non-stationary properties of these signals and represent the intrinsic characteristics of them. We saw that the ST and CWT could be more suitable than STFT due to their adaptive window length, but all of these methods are time-consuming and this makes it difficult to be applied in real prosthetic application. The other factor is the number of the features they yield which is very high. These two criteria promote using DOST as it removes the redundancy in ST and has much less complexity in calculations. The number of features extracted in any of previous methods (including DOST), will be high and it is important to do the dimension reduction efficiently in order to keep the distinctive properties while decreasing the space into less dimensional space. The methods of dimension reductions could be linear or non-linear as we saw in previous chapter. The main concept of the non-linear methods is based on measuring the similarity/dissimilarity between the data points. The use of non-linear methods could improve the training by decreasing the size of the needed training set, and also better performance with cross-subjects features [62]. In our study, we at first do an extended comparison between different TF/DR methods combinations, then we improve both in features extraction and dimension reduction methods in the goal of increasing accuracy and efficiency of calculations.

In this chapter, in section 4.1, we will show the workflow of our algorithm, the reference data we use to compare methods combination, and how we apply these methods in each step of feature extraction, dimension reduction and classification. In section 4.2, we show the comparison results we got for each stage in our workflow besides to the results from a DL methods with TF features as an input. Based on this comparison, we then select the best combination for our algorithm. In section 4.3, we improve the selected methods combination by using a Generalized DOST (GDOST), then we pro-

pose an enhancement on the similarity measurements in MDS kernel calculations. We apply these improvements and show the results and discussions. Finally in section 4.4, We extend our tests on different datasets in NinaPro, where we apply our methods on sEMG data collected from amputees. We also test our methods on an increased number of movements. Finally in this section, we extend our tests on a different database built by the partner team.

The workflow of our research starts from the sEMG data, feature extraction, dimension reduction and finally the classification. In the next section, we will explain the main algorithm and how we applied our methods in each step.

4.1 Algorithmic Considerations

4.1.1 Main Work Flow

The workflow is divided into the following main parts:

- Data pre-processing: Starting from the raw sEMG, this step includes data normalization which is done by making the mean value is equal to 0 and the standard deviation is 1 on each channel. The normalized data is $S \in \mathbb{R}^{n \times m}$, where m is the number of channels and n is the total number of signal's samples on each channel, will be used in features extraction.
- Time-frequency features extraction: A time-frequency transform is applied on the normalized signals of each channel. Then for each observation, we combine the result into a single vector of length k . The resulting features matrix for all observation is $F \in \mathbb{R}^{N \times k}$ where N is the observations number (data points).
- Dimension reduction of the features space: we apply a dimension reduction method to transform the feature matrix $F \in \mathbb{R}^{N \times k}$ into a more compact $Y \in \mathbb{R}^{N \times q}$ where $q \ll k$.
- Classification: We evaluate the extracted features using group of widely-used classifiers for sEMG signals.

This algorithm is summarized in figure 4.1, in which we recall the main methods of interest in each step. In order to extend the comparative study we made, we also applied the Deep Learning (DL) method on the same data. The DL can merge stages of features extraction, dimension reduction and classification to be embedded inside the neural network. We followed a known approach of the DL applied in this area to provide a baseline of differences in performance between the DL and other approaches.

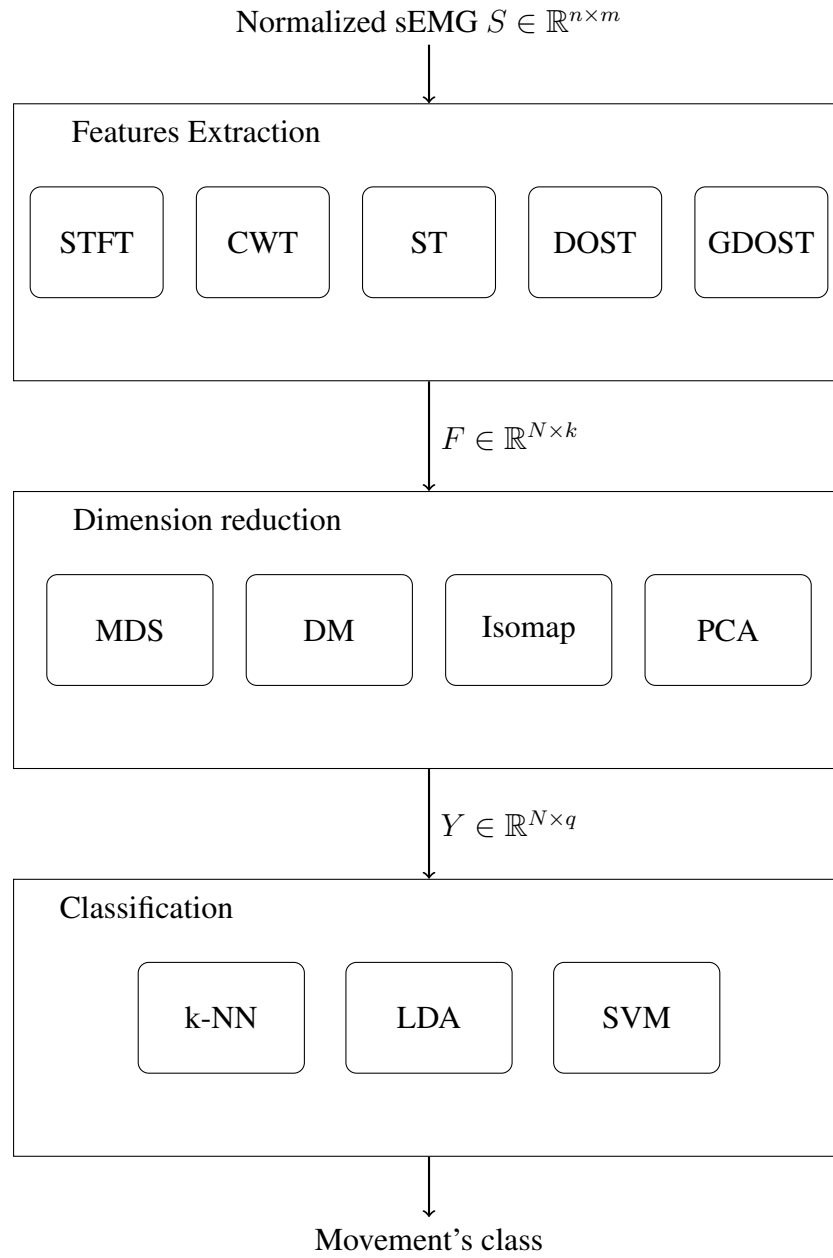


Fig. 4.1 The main work flow. It shows the data flow starting from the normalized sEMG signals; and how the data processed until the classification.

4.1.2 The Referenced Data

For evaluating the combinations of the chosen methods in our comparison study, we used the database we mentioned in section 3.1.3, and this database is provided by the NinaPro Project [27]. The advantages of this database is that it contains recorded data for a wide range of movements and for many subjects, which provides a good resource for training and testing. This database is recorded in a unified format which is useful when comparing our applied methods. For the experiments in section 4.2, we selected the dataset 2 and inside this dataset, we selected the movements group in the exercise 1. This group contains 17 basic movements performed by the wrist and fingers. In this exercise, subjects were asked to execute each movement 6 times with holding the position for 5 seconds followed by 3 seconds of resting. The raw sEMG signals were saved with their movements index. We also extended our tests to include exercise 2 from this dataset, which has 23 movements of grasping and functional movements, so the total number of movements with the previous exercise was 40 movements. Besides to dataset 2, we also used sEMG data from dataset 3, which contains sEMG collected from amputees. For these NinaPro datasets, the sampling rate is 2 kHz and the signals are recorded using $m = 12$ electrodes placed on subject's skin of the arm. The recorded sEMG data is saved into the matrix $E \in \mathbb{R}^{n \times m}$ where n is the number of recorded samples on one channel. Figure 4.2 shows the list of these basic hand moves.

In addition to the NinaPro, we applied one selected method combination on a completely different database, which we mentioned in section 3.1.2. This database is recorded by a partner team from ZHAW School of Health Sciences in Zurich (Switzerland), and contains 4 movements performed by the two hands, recorded on 16 channels with sampling rate 1200Hz. The purpose of this experiment was to show that our selected method could be generalized on other sEMG database and to help our partners to evaluate their acquisition protocol.



Fig. 4.2 Visual depiction of the 17 hand gestures considered in section 4.2, based on the NinaPro database [27].

4.1.3 Feature's Sliding Window

Identifying the movement that the person intends to perform should be done in a reasonable time frame, because this time will determine the delay between the intention and the movement decision which will be sent to the prosthetic. In order to keep the response time in acceptable range, a threshold of 300 ms should be respected as a response times [22], this includes the window length in addition to the computation time. However, the segment should be long enough to have sufficient features for classification. Therefore a trade-off in response time and accuracy should be considered when selecting the window length. In our experiments we chose the window length equal to 250 ms with 125 ms overlapping as it is used in studies with similar constraints [53, 42, 110]. The sampling frequency is 2 kHz, for each observation we get 12 windows (i.e. 12 electrodes) with 250 ms length. In figure 4.3 we can see an example of observation windows on one of the channels.

4.1.4 Feature Extraction

After segmentation, we get 12 windows for each single observation. We apply the TF method on each of them, and then we yield the resulting matrix into a vector. Finally we combine all these 12 vectors into one vector F_i which represents the TF features of this observation $F_i \in \mathbb{R}^k$ where k is the number of TF features of a single observation. For each observation in the dataset, we extract the features' vector in the same way, then we save it into the feature matrix $F \in \mathbb{R}^{N \times k}$ where N is the observations' number as shown in 4.4.

For the TF features, we use a frequency range between 1 and 200 Hz, which contains the main energy of the sEMG signals [13].

Given these values, the number of TF features k on a single observation is $k \simeq 3 \cdot 10^5$ for STFT, CWT and ST, while $k \simeq 6 \cdot 10^3$ for the DOST. We empirically choose the value $\sigma = 0.03$ in STFT (see Eq. (3.5)) because it permits a compromise between the resolutions of time and frequency. For the ST, we keep the original version where $\sigma = 1/|f|$ (see Eq. 3.12). Similarly, for the DOST, the original version proposed by [104] is applied in this paper (Eq. 3.19).

Figure 4.5 depicts an instance of STFT, ST, CWT, and DOST transforms applied on the same two samples of movements. The figure depicts some of the mathematical properties of each method: STFT has the same resolution along all the time-frequency plane, while we notice that CWT and ST have a variation in the resolution over the value of frequency. This will give better frequency resolution for low frequency and better time resolution for high frequency. In DOST, it shows visually less resolution because it removes the redundancy that exists in the other methods. Notably that will not significantly affect the accuracy result.

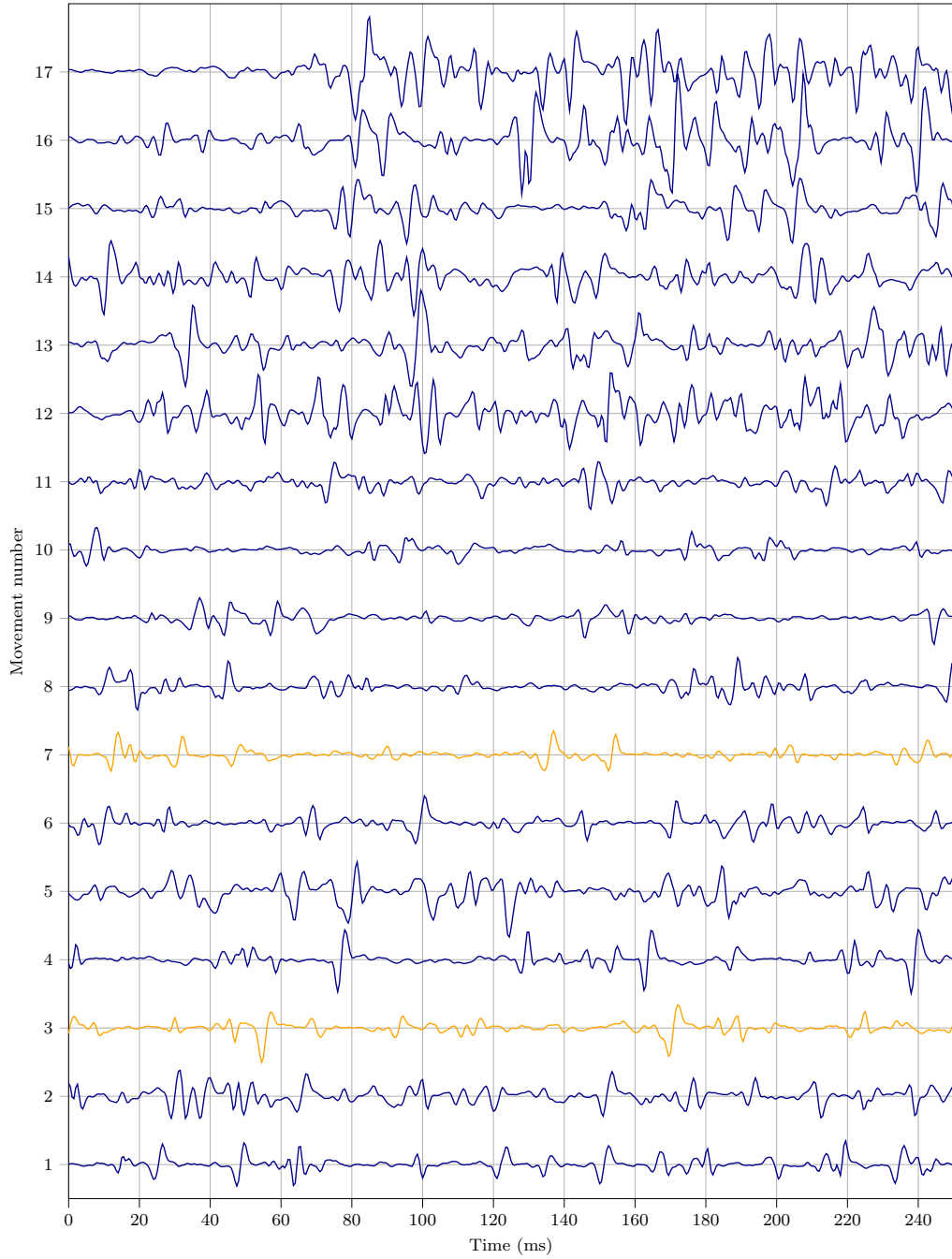


Fig. 4.3 Example of recorded signals on channel 1 for the 17 movements (see 4.2). TF transforms of the highlighted movements are shown in Fig.4.5.

In practice, we observe a significant drop in computation time when using the DOST, which takes around 8% of the required time for STFT or ST (Table 4.1), in addition to lying in a lower-dimensional space.

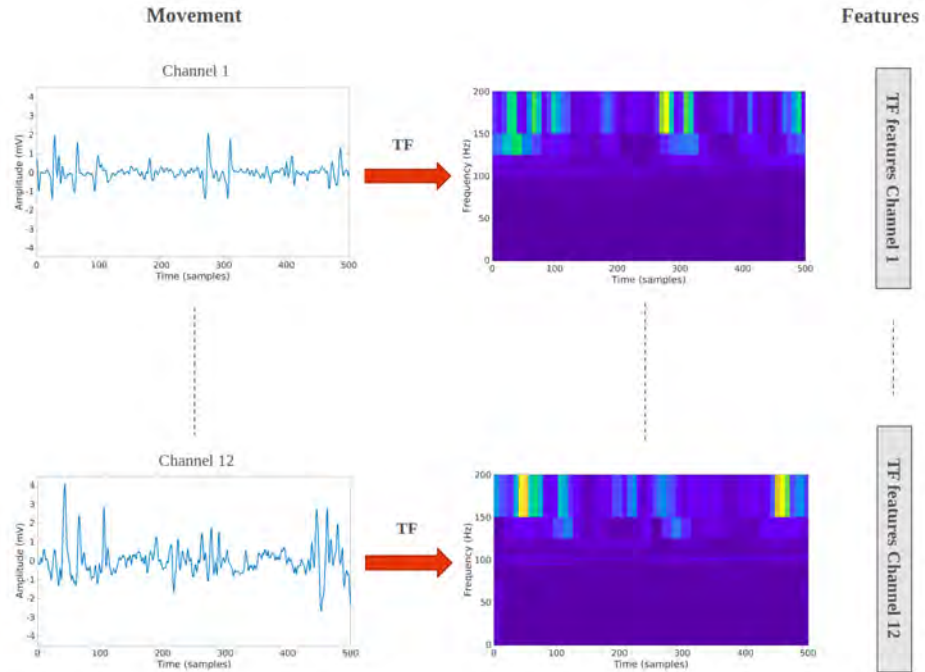
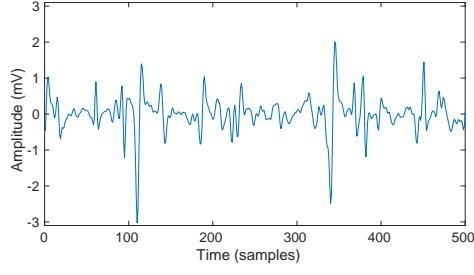


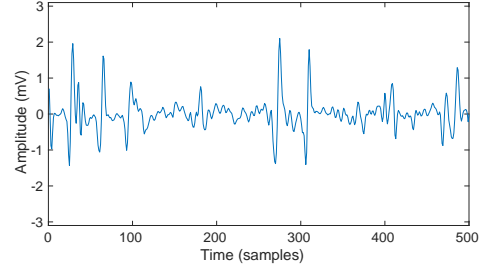
Fig. 4.4 Features extraction of a sEMG signal over 250ms window.

Method	Time(ms)
STFT	1.75
CWT	2.3
ST	1.60
DOST	0.13

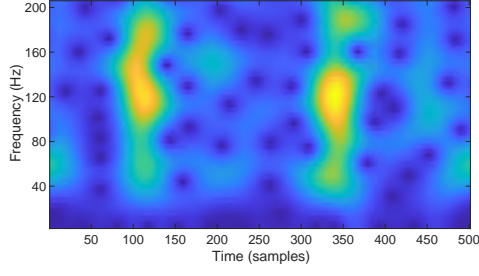
Table 4.1 TF feature computation time on a window of one channel, averaged over all 39360 samples windows in the dataset.



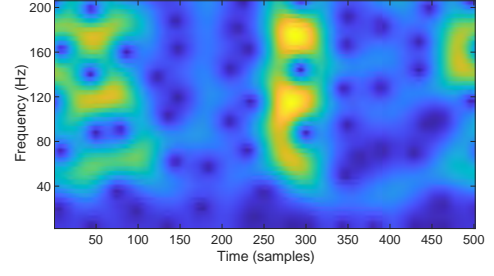
(a) Move 3, channel 1.



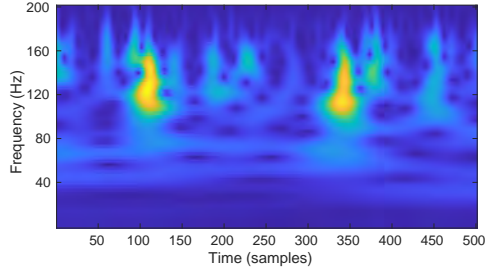
(b) Move 7, channel 1.



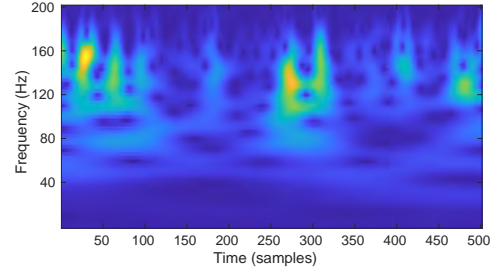
(c) STFT of move 3, channel 1.



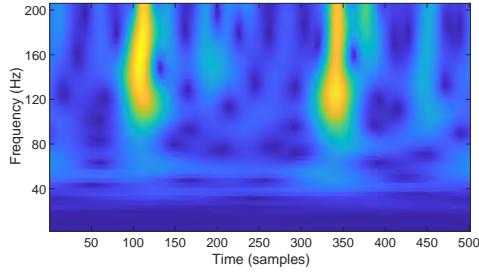
(d) STFT of move 7, channel 1.



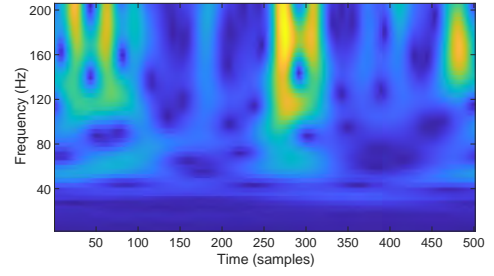
(e) CWT of move 3, channel 1.



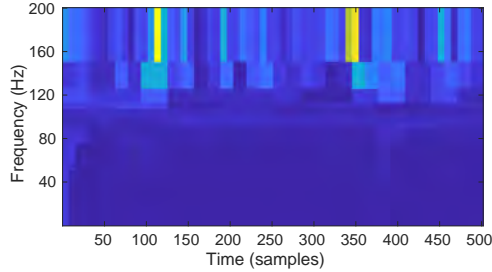
(f) CWT of move 7, channel 1.



(g) ST of move 3, channel 1.



(h) ST of move 7, channel 1.



(i) Rearranged DOST coefficient of move 3, (j) Rearranged DOST coefficient of move 7, channel 1.

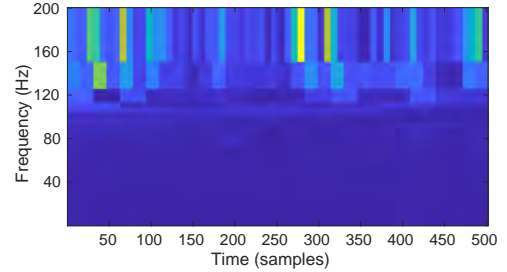


Fig. 4.5 TF transforms examples: left side is the movement 3 - channel 1, right side is the movement 7 - channel 1. The corresponding hand gestures are shown in figure 4.2.

4.1.5 Dimension Reduction

For all methods applied in dimension reduction, the input is the features matrix $F \in \mathbb{R}^{N \times k}$, with k depending on the method used in previous step. The number of the embedded features is important as selecting too many features will lead to over fitting in the classification and slower training, while in the other hand, selecting not enough features will lose valuable data in the features and in both cases the classification accuracy will be worse.

For PCA, the dimension of the new embedded space is decided based on the preserved variance from the original space. There will be a trade-off between the number of the features in the embedded space and the preserved variance. Based on our tests, we can see in Figure 4.6a the change of the preserved variance by the number of the embedded features and the slope which presents the changing rate of the preserved variance. We test different values of embedded features number in a range where preserved variance stop increasing rapidly (i.e. $Var_{k+1} - Var_k < \varepsilon$). Finally, we choose the value of q with the best accuracy (figure 4.7).

For the non-linear methods, the original space of the features matrix is replaced by a kernel of paired similarity/dissimilarity. Therefore, we use the variance of the new kernel as a factor for choosing the new dimensions.

First, we specify the range in which the preserved variance is changing significantly with the number of embedded features. In figures 4.6b, 4.6c, 4.6d we see the relation between the preserved variance and the number of the features in the embedded space for kernels of MDS, Isomap, DM respectively. Then, we test all possible values of the embedded features in this range to choose the one with best results. Figure 4.7 shows classification accuracy by number of embedded features for non-linear methods tested on a specific range of values.

Isomap requires the setting of an additional parameter, namely the value u in Eq 3.25 which is the number of neighbours to be considered when building the graph. In order to choose u , we run our tests for all u values $[10, 300]$. Choosing bigger values for u means that more data points will be considered as neighbors (Eq 3.25), which leads into converting to the Euclidean distances rather than the manifold distances. We chose $u = 220$ as it leads to the best accuracy based on this test as shown in figure 4.8.

4.1.6 Classification

For the k-NN classifier, we choose value of 3 nearest neighbors, as it gave better results on our data compared to bigger values, and for SVM, we choose the Gaussian kernel function and combine several one-versus-one of multiple binary SVMs. Each combination is evaluated based on K-fold Cross-Validation with value $K = 5$.

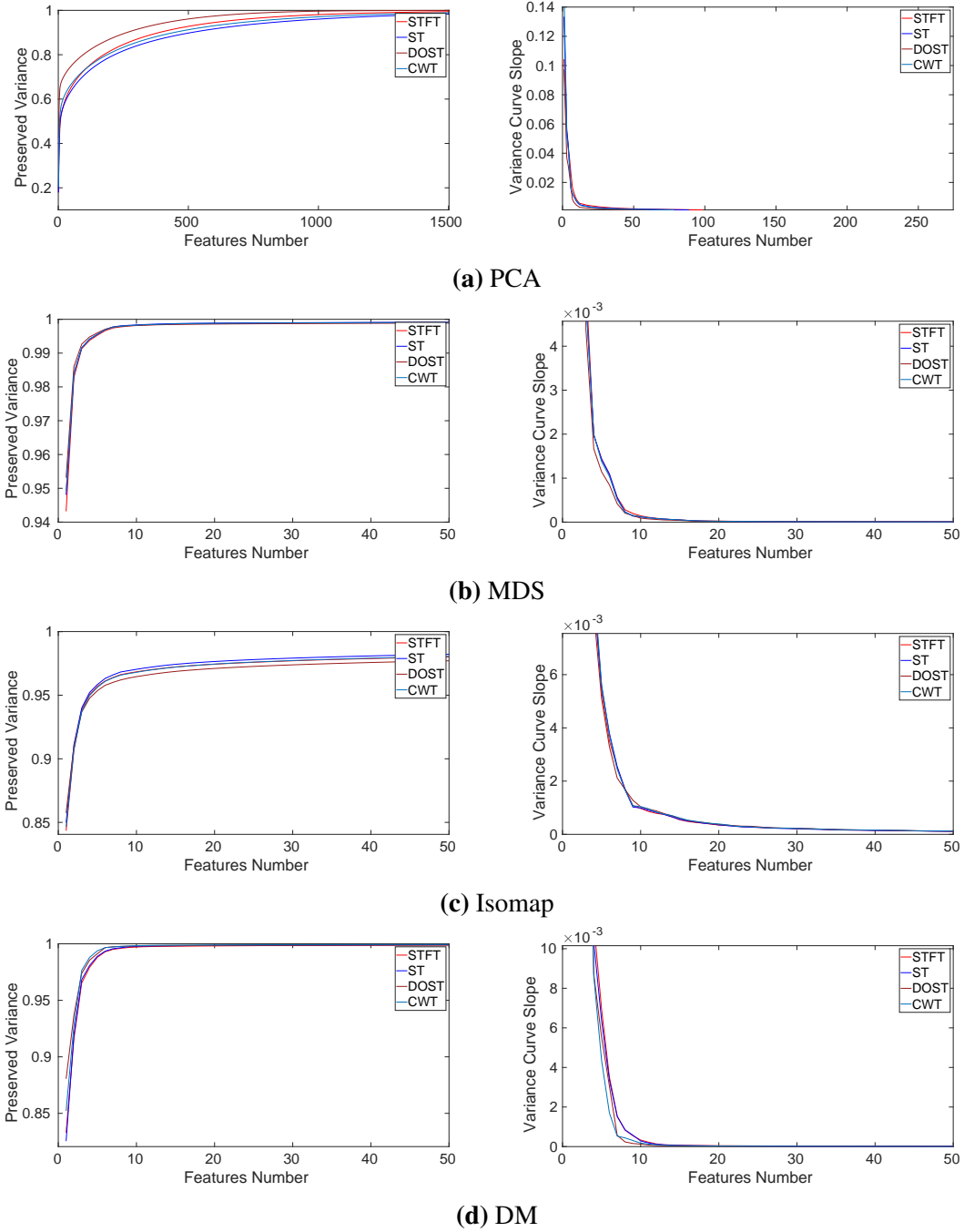


Fig. 4.6 Preserved variance by number of features in the embedded space.

4.2 Methods Comparative Study

The variety of the methods in each step of the movement identification increases the number of possible combinations. Some of these combination could be found in the literature, but it is still difficult to compare fairly as they are applied on different datasets with completely different experimental circumstances, such as the number of the movements under study, the number of the electrodes used when recording the sEMG signals, the sampling rate of the recorded signals... etc. These criteria play an essential role

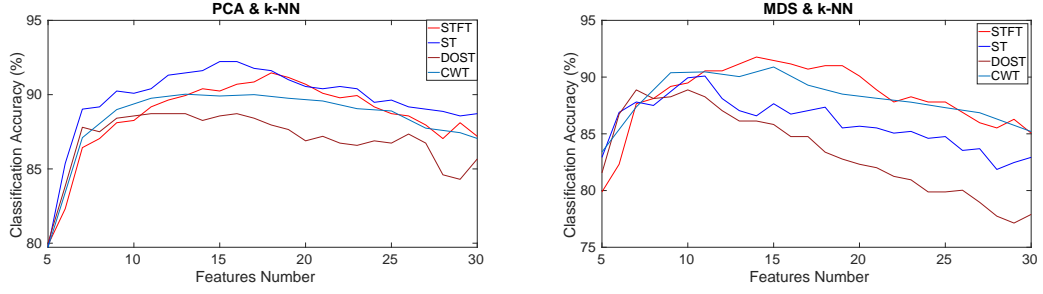


Fig. 4.7 Classification accuracy by features number.

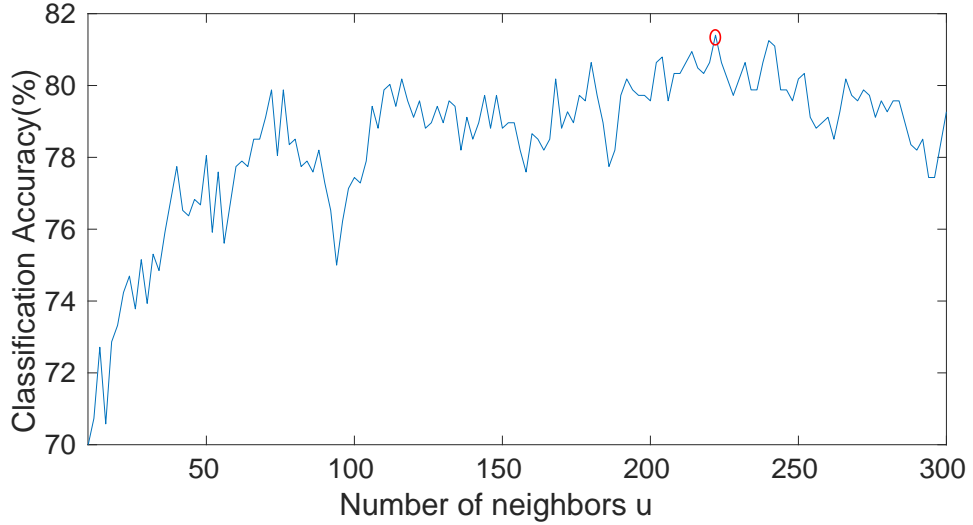


Fig. 4.8 Classification accuracy by number of neighbours in Isomap algorithm, with the selected values of 220 that gives best accuracy.

in the overall methods' evaluation; therefore, having a fair comparison between these methods' combination requires applying them on the same dataset under the same criteria. In order to achieve this goal, we applied all the methods combinations mentioned in chapter 2, and shown in Figure 4.1. The final numerical results are shown in Table 4.2.

4.2.1 TF Methods Comparison

As we see in Table 4.2, the methods STFT, CWT and ST are approximately giving the same performance with a slight advantage for the ST features.

The advantage of ST is due to its multi-resolution nature, also it adapts better to the variation of the frequency content of the sEMG signal comparing to the STFT, which can enhance the quality of the extracted features. Both CWT and ST adapt their resolution to the frequency change, but ST representation gave a slight advantage over the other methods.

The DOST gives less accuracy with no noticeable difference from both STFT and ST. The DOST preserves information in time-frequency domain in a non-redundant approach (due to the used orthogonal basis) and it has a $\mathcal{O}(N)$ time complexity (to be

compared to $\mathcal{O}(N^3)$ for other TF methods), which explains why the DOST was more than 10 times faster on our testing platform¹ (see Table 4.1). This criteria is an important advantage for the DOST as it makes it possible for real prosthetic application when processing time is a very critical factor and the processing power is limited. However, rigorously speaking, the DOST is not exactly the orthonormal version of the ST. As shown in [111], the classical DOST version applies the equivalent of a boxcar window, and not a Gaussian one as in the ST. This can explain in part the slightly decreasing performance for the classification rate for the DOST.

4.2.2 Dimension Reduction Methods Comparison

For the dimension reduction methods, PCA yields better results than non-linear dimension reduction methods, then comes MDS which outperformed Isomap and DM. The proposed method MDS performs less than PCA, but based on a study [62] which compared PCA with DM on STFT features; it was shown that non-linear dimension reduction outperforms PCA when less training data is used. Training data size is an important factor as it reflects the time and effort needed by the amputee to be able to use his prosthetic. Non-linear dimension reduction methods is based completely on the constructed kernel that describes similarity/dissimilarity between paired observations. The fact that they perform less than PCA could be because a better way is required to measure the similarity between observations. This point will be further explained in this chapter in section 4.3.

4.2.3 Classifiers Comparison

The k-NN classifier is giving the best classification accuracy. These results are consistent with some studies on sEMG signals classification. In [77] both k-NN and SVM were applied on TF features with PCA as dimension reduction method and k-NN outperformed SVM. Another study [74] did comparison between k-NN and LDA classifiers on sEMG signals of wrist motions and they concluded that k-NN has better average recognition rate.

For the purpose of comparing combinations of TF methods with DR methods, we observed that the methods combination that leads to better accuracy using k-NN classifier is also giving better accuracy than other methods combinations using LDA and SVM, which means, changing the classifier will not promote a different combination from the one with the other classifier.

¹Intel(R) Core(TM) i7-9750H CPU @ 2.60GHz - 64 GB Ram

4.2.4 Deep Learning

In the previous comparison, we did an extended comparison of a wide range of TF methods and dimension reduction methods. All of these methods are studied and chosen based on sEMG signals characteristics and experiments. Another popular approach in machine learning is deep learning, where the whole stage of feature engineering (including features extracting, selecting, dimension reduction) could be done automatically by deep structure of neural network, or could be used as an input for the DL neural network. In order to compare the performance of the previous combinations with DL, we choose the ST features as an input for a DL model, as these features gave best accuracy score in the combinations comparison. We chose to use the TF features instead of the raw sEMG data as an input for the DL model, because it is proven to perform better with deep learning, as shown in a different study [63].

For the deep learning model, we choose a classical model called GoogLeNet with a gradient descent algorithm to minimize the loss function and 20 epochs for training.

After applying deep learning under same condition for combinations in Table 4.2, the accuracy was 84.06% which is less than other methods combinations, which is explainable as any DL model will need relatively large amount of labeled data to be able to perform well.

4.2.5 Comparison Recap

The previous experiments showed the importance of using TF features even with automated feature engineering methods (DL) as these features are good representatives of the sEMG signals. The downside of known and widely used methods are their computation time, complexity, and the redundancy in their representation. Moreover, the large number of features they produce requires to apply a dimension reduction method before the classification phase. The essential role of the dimension reduction is not only minimizing the dimension of the features space, but also affecting the needed size of training set and generalizing the features across the subjects [62]. A preliminary version of this comparison was published as a conference paper [112], and the full comparative study were published as a journal paper in *Expert Systems with Applications* journal [28]. Looking to Table 4.2, we see that the combination of ST, PCA, k-NN achieved the best accuracy among all the other combinations, but considering the previous criteria, the DOST would be preferred due to its lower complexity and non-redundant representation. In the dimension reduction, PCA is slightly better than MDS; however, MDS will be preferred considering the training size and generalizing features MDS. The combination of DOST and MDS has advantages over the other combinations but has still a lower accuracy. This is the main motivation to extend our study in the next section.

TF	DR	q	Class.	Acc. (%)	Time(s)
STFT	PCA	18	k-NN	90.05	167
			LDA	81.78	167
			SVM	84.48	168
	MDS	14	k-NN	87.88	91
			LDA	77.76	91
			SVM	82.84	92
	Isomap	14	k-NN	79.17	688
			LDA	73.50	688
			SVM	75.03	689
	DM	14	k-NN	86.09	95
			LDA	79.42	95
			SVM	83.17	96
ST	PCA	15	k-NN	90.96	179
			LDA	83.62	180
			SVM	85.63	181
	MDS	11	k-NN	88.99	89
			LDA	77.60	89
			SVM	82.58	100
	Isomap	11	k-NN	81.10	695
			LDA	73.11	695
			SVM	75.11	696
	DM	11	k-NN	87.91	87
			LDA	82.17	88
			SVM	84.70	89
Deep Learning		GoogLeNet	84.06	9600	
CWT	PCA	13	k-NN	89.92	197
			LDA	82.41	198
			SVM	85.29	199
	MDS	15	k-NN	88.18	112
			LDA	79.38	113
			SVM	83.10	113
	Isomap	15	k-NN	79.88	715
			LDA	73.65	715
			SVM	76.48	716
	DM	15	k-NN	86.53	115
			LDA	81.35	116
			SVM	83.21	116
DOST	PCA	11	k-NN	88.08	15
			LDA	80.40	15
			SVM	82.31	16
	MDS	10	k-NN	87.13	28
			LDA	72.68	29
			SVM	75.74	29
	Isomap	10	k-NN	76.88	589
			LDA	70.23	589
			SVM	72.73	590
	DM	10	k-NN	85.22	13
			LDA	78.14	13
			SVM	81.60	14

Table 4.2 The final classification results of all combinations of the used methods with their computation time. The classification rate for each combination were calculated using cross-validation method and an average of accuracy for 5 subjects. We highlighted in bold the best results for each combination group, and the overall best results (accuracy and time) are highlighted with colors. TF: time-frequency method, DR: dimension reduction method, q : the number of features in the embedded space, Acc.: the classification accuracy, Time: the overall time for feature extraction, dimension reduction and training.

4.3 Generalized DOST and its Similarity Measurements

4.3.1 Generalized DOST

The promising results of DOST and MDS with their advantages over other methods motivated us to extend our study in this direction, and improve the performance of these methods. The DOST is the orthonormal version of the ST. It avoids redundancy in the time-frequency plane and paves the way to compute time-frequency representation in lower algorithmic complexity [104]. Let $x(t)$ be a signal $\in L^2([0, 1])$, p is the number of the frequency bands, ν indicate the center of a frequency band, β indicates the width of the frequency band and τ for the time localization. Let us recall the DOST coefficients $D_{p,\tau}$ calculations, which is an inner product between the signal $x(t)$ and the orthonormal basis functions $C_{p,\tau}$:

$$D_{\tau,p} = \langle x, C_{p,\tau} \rangle \quad (4.1)$$

where $C_{p,\tau}$ is given as [103]:

$$C_{p,\tau}(t) = \frac{1}{\sqrt{\beta(p)}} \sum_{f=\nu(p)-\beta(p)/2}^{\nu(p)+\beta(p)/2-1} e^{2\pi i f t} e^{-2\pi i f \tau / \beta(p)}, \quad t \in \mathbb{R} \quad (4.2)$$

The basis $C_{p,\tau}$ is not equivalent to the classical ST with Gaussian window. Indeed as R.G. Stockwell pointed in [104] this is equivalent to ST with boxcar window. In order to propose a generalized version of the DOST that allows to apply an admissible generalized window φ , authors in [111] propose the following basis for the Generalized DOST (GDOST):

$$E_{p,\tau}^{\varphi}(t) = \frac{1}{\sqrt{\beta(p)}} \sum_{j=0}^{\beta(p)-1} [c_{p,j}^{\varphi}(\nu(p))]^{-1} e^{2\pi i (\beta(p)+j)(t - \frac{\tau}{\beta(p)})} \quad (4.3)$$

For the special case of boxcar window, let $\varphi = \check{\chi} = F^{-1}\chi$ with F^{-1} is the inverse Fourier transform operator, then $\chi(\nu)$ can be expressed as follows:

$$\chi(\nu) = \begin{cases} 0 & \nu \in (-\infty, -\frac{1}{N}] \cup [\frac{1}{N}, +\infty) \\ 1 & \nu \in (-\frac{1}{N}, \frac{1}{N}) \end{cases} \quad (4.4)$$

where N is the length of the analyzing window. In this case, we have:

$$c_{p,j}^{\check{\chi}}(\nu(p)) = 1, \quad (4.5)$$

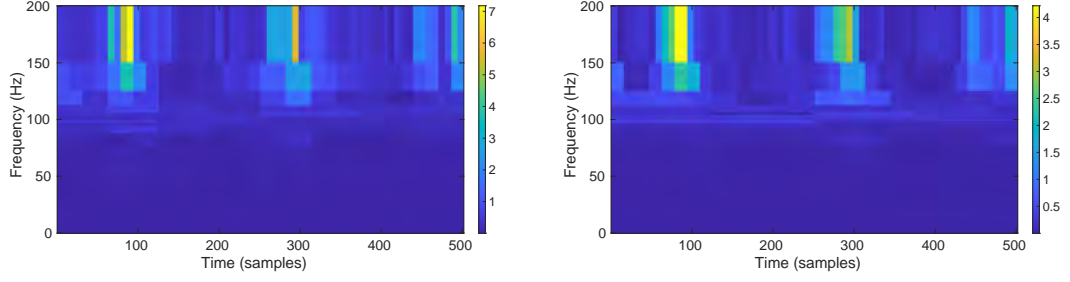


Fig. 4.9 DOST representation (left), and its GDOST counterpart of the same movement. Both are rearranged to yield a TF representation.

for all p and j . Hence, $E_{p,\tau}^{\check{x}}$ can be re-written as :

$$\begin{aligned}
 E_{p,\tau}^{\check{x}}(t) &= \frac{1}{\sqrt{\beta(p)}} \sum_{j=0}^{\beta(p)-1} [c_{p,j}^{\check{x}}(\nu(p))]^{-1} e^{2\pi i(\beta(p)+j)(t-\frac{\tau}{\beta(p)})} \\
 &= \frac{1}{\sqrt{\beta(p)}} \sum_{j=0}^{\beta(p)-1} e^{2\pi i(\beta(p)+j)(t-\frac{\tau}{\beta(p)})} \\
 &= C_{p,\tau}(t)
 \end{aligned} \tag{4.6}$$

In this thesis, we introduced the use of Gaussian window in DOST as originally used in the ST with $\sigma = 0.1$. In this case, $\varphi = g(t)$ which can be given as:

$$g(t) = \frac{1}{\sigma\sqrt{2\pi}} e^{-\frac{t^2}{2\sigma^2}}. \tag{4.7}$$

An example of DOST and GDOST on the same signal is given in Fig. 4.9.

4.3.2 Feature Extraction from GDOST

For an observation X recorded on m channels: $X = \{x_1, x_2, \dots, x_m\}$, the GDOST transform of this observation is represented as:

$$GDOST(X) = \{F_{x_1}, F_{x_2}, \dots, F_{x_m}\}, \tag{4.8}$$

where F_{x_i} is the GDOST transform of x_i .

The GDOST yields a number of features equals to the number of the samples in the signal, so that $\forall i \in \{1, \dots, m\}, F_{x_i} \in \mathbb{R}^a$. This means that the features number of observation X on all channels will be $k = m \times a$. We extract the GDOST features for every observation in the dataset, so that the features matrix of the all observations in the dataset is $F \in \mathbb{R}^{N \times k}$, where N is the overall existing observations in the dataset. In figure 4.10, we can see GDOST representations of two different movements.

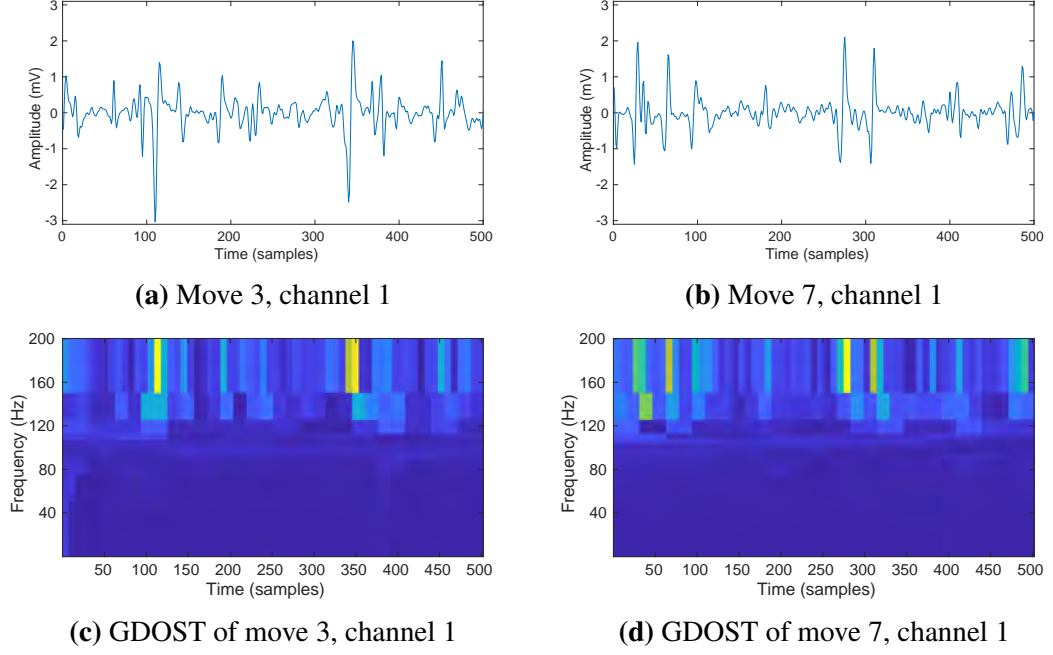


Fig. 4.10 GDOST transform example for two different movements (3 and 7, see Fig. 4.2) acquired on the same channel.

4.3.3 Similarity Measurements

We saw in chapter 3, how the non-linear dimension reduction methods as MDS are based on the similarity (distance) measurements between the data points. These methods replace the observations' features by a new set of features measuring the similarities between each pair of observations. The paired distances between two observations x, y is calculated as:

$$d_{xy} = \sum_{i=1}^m \|F_{x_i} - F_{y_i}\|_2 \quad (4.9)$$

The good distance measurement means that the values are relatively low when the observations belong to the same movement, and high when they belong to different movements.

4.3.4 Distance Synchronization

The Euclidean distances between the TF representations are sensitive to the time shift in GDOST features, which leads to erroneous similarity calculations (Eq. 4.9), while better similarity calculations should consider the relative positions of the energy in the time-frequency plane. To achieve that when calculating the distance between X and Y , we shift features of Y step-by-step and calculate the distance after each shifting.

Let the operator $\mathcal{T}^j F$ be the circular shift with step $j \in \mathbb{Z}$ on the sequence of features F . Then, the distance between X and Y is taken as the minimal distance between Y and shifted versions of X . The proposed operation can be expressed as

follow:

$$d_{xy} = \min_{j \in \{0, \dots, a-1\}} \sum_{i=1}^m \|(\mathcal{T}^j F_{x_i}) - F_{y_i}\|_2 \quad (4.10)$$

Where $\forall i \in \{1, \dots, m\}$, $F_{x_i} \in \mathbb{R}^a$. The final distance matrix is $D \in \mathbb{R}^{N \times N}$, will contains all paired distances d_{xy} .

Figure 4.11 shows GDOST representations of two different observations of the movement 9 recorded on channel 1. In Fig. 4.11a, and Fig. 4.11c we notice that calculating the distance directly between these two observations (Eq. 4.9) would lead to high dissimilarity as shown in Fig. 4.11b, while distance between GDOST in Fig. 4.11a and Fig. 4.11d will be the minimum value of distance (Eq. 4.10) between these observations and actually reflects the fact that they both represent the same movement. Fig. 4.11b shows how the distance between these two observations differs while performing circle-shift on the time resolution. We can notice that in this example, the minimum distance happens with shift value equal to 210 time-sample, as shown in Fig. 4.11b as a red point, and the corresponding GDOST shifted transform could be seen in Fig. 4.11d.

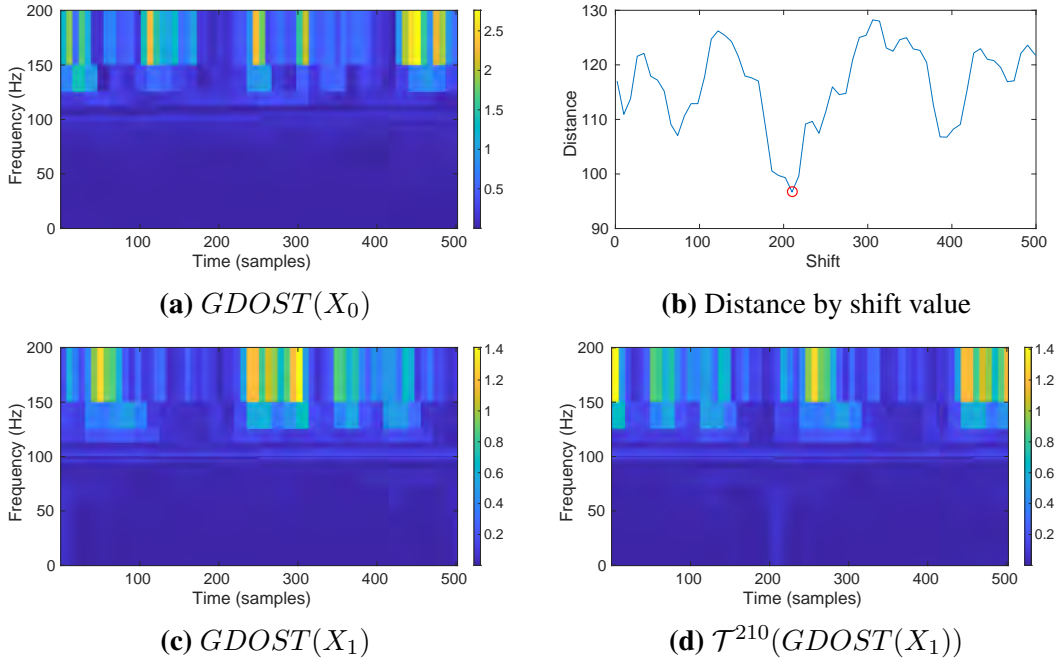


Fig. 4.11 GDOST of two different observations X_0 and X_1 that belong to a same movement. (d) shows $GDOST(X_1)$ with circle-shifting by value 210. (b) shows the distances between $GDOST(X_0)$ and $GDOST(X_1)$ while shifting X_1 .

4.3.5 Experiments

We choose the number of features q that yields the maximum classification accuracy on our database over the range $[10, 400]$, which is $q = 191$. The classification accuracy

Methods	Euclidean Distance	Synchronized Distance
GDOST, Isomap, k-NN	80.58%	90.26%
GDOST, DM, k-NN	88.38%	95.79%
GDOST, MDS, k-NN	88.91%	97.56%

Table 4.3 The classification accuracy GDOST with Isomap, DM and MDS using both Euclidean and synchronized distances.

will start to drop as adding more features will increase the classifier's over-fitting. The approach of the non-linear dimension reduction methods is based on the measurement of similarities between the observations, so we applied this enhancement on each non-linear dimension reduction methods, Isomap, DM and MDS.

For MDS, once the synchronized paired-distances between observations are computed, we get the kernel matrix of MDS, which contains the new features of each observation as a vector of distances from other observations. For Isomap, and DM the Euclidean distance calculations between observations will be replaced with new synchronized distance calculation (Eq 3.24 and Eq 3.28). In order to evaluate our features extraction methods and dimension reduction approach, we used kNN classifier with $k = 3$, with a 5-Fold cross-validation. The main work flow is shown in figure 4.14.

4.3.6 Results

We first show the improvement in classification accuracy with using the synchronized distances in the non-linear dimension reduction methods in Table 4.3. We notice a significant improvement when using the synchronized distances compared to usual Euclidean distances. We see that for the MDS which has the highest accuracy with 97.56%, the improvement on the classification accuracy was approximately by 9%. We also see that the accuracy increased from 80.58% to 90.26% for Isomap kernel, and from 88.38% to 95.79% for DM kernel.

The accuracy of MDS has a significant improvement when compared to the results in Table 4.2 which are applied on the same data. Table 4.4 summarize these results, compared with previous results shown in Table 4.2 and other studies made on the same database and with the same number of movements.

In 4.2, DOST with MDS gave 87.13% accuracy, which means by using enhanced MDS kernel and GDOST, we were able to increase the accuracy by 10%. Comparing with the best results obtained before; which was achieved by using ST with PCA with accuracy 90.96%, the improvement was 6.6%. By comparing DOST and GDOST when both are applied with enhanced MDS, we see that using the GDOST led to improving the accuracy from 96.73% to 97.56%. The significant improvement obtained by these combination (GDOST and enhanced MDS) came from the MDS kernel optimization, so the distances were calculated in a way that actually measure the dissimilarity between

Methods	Accuracy	Reference
TD features set, kNN	85%	[73]
RMS, Median Frequency, Para-consistent artificial neural network	$76\% \pm 9.1\%$	[113]
STFT, SVM, kNN	92%	[114]
ST, PCA	90.96%	Table 4.2
DOST, MDS	87.13%	Table 4.2
DOST, Enhanced MDS	96.73%	this experiment
GDOST, Enhanced MDS	97.56%	this experiment

Table 4.4 The classification accuracy of different feature extraction and dimension reduction combinations done on the same database and same movements. The table shows the significant improvement of using GDOST and enhanced MDS.

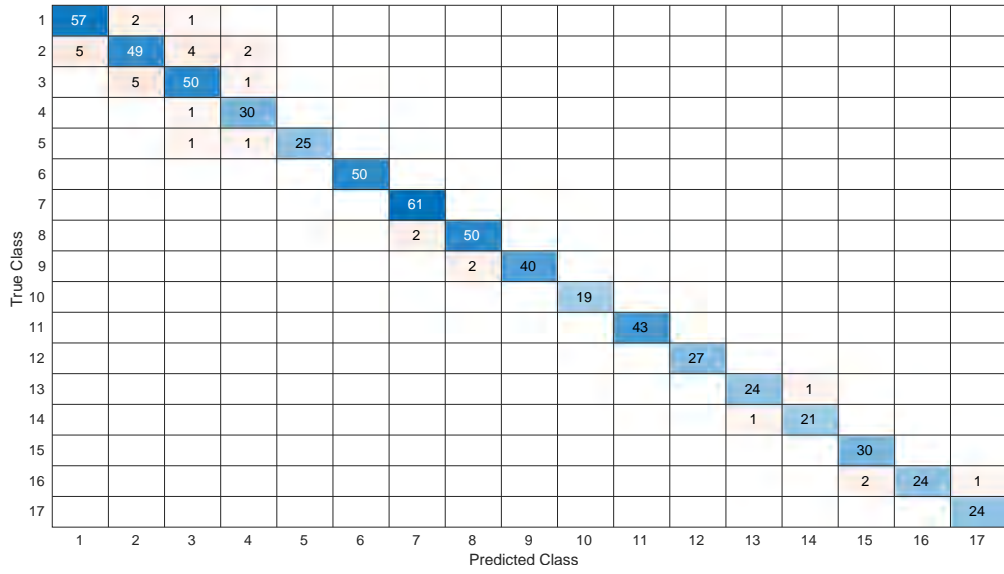


Fig. 4.12 Confusion matrix of 17 hand gestures (shown in figure 4.2) classification.

observations, besides to using Gaussian window instead of rectangle window in DOST, which improved the TF features of the observations. The comparison with TD features which were used by different studies as in [73] or combined with frequency features as in [113] emphasize the superiority of TF features over TD features or TD and FD combined features as we see in Table 4.4.

4.3.7 Confusion Matrix

The confusion matrix of using GDOST with enhanced MDS is shown in figure 4.12, where we can see the classification results of the test set of one of the used subjects. The confusion matrix shows that the miss-classification comes from the first three movements, where the differences are only in a movement of one finger as shown in figure 4.2.

The reason comes from the fact that the four fingers: the index, middle, ring, and

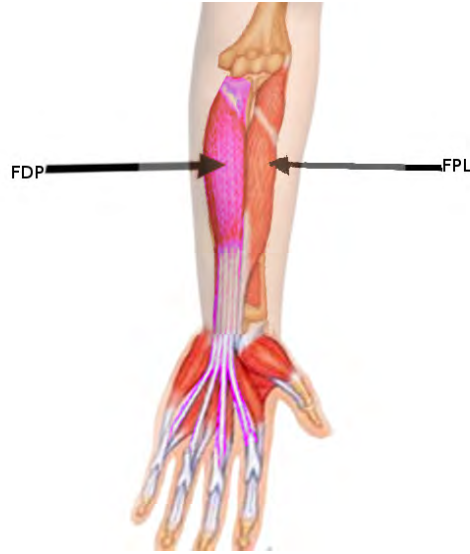


Fig. 4.13 The responsible muscles of the fingers' movements [115] classification.

little fingers are moved by Flexor Digitorum Profundus (FDP) [115], where the thumb is moved by the flexor pollicis longus (FPL) as we see in figure 4.13. These two muscles are responsible for all of fingers' movements and the recorded sEMG signals sometimes fail to address the differences between these movements. However, we see that movements of wrist as rotation, flexion, extension, deviation, hand open and close; all these movements are very well classified due to their differentiated sEMG signals.

The number of movements samples should be balanced on all movements according to the equal movements repetitions number in NinaPro database [84], but here we notice imbalanced number that differs randomly from subject to another. This imbalance could be caused by the experiment's human errors. In this kind of classification, we give equal importance for both true/false classification output, which explains having the accuracy measurement as an evaluation method. In table 4.5, we can see the number of the observations for each movement for all used subjects. The number varies between 927 to 1347 with no large imbalance between the movements' observations overall.

4.3.8 Section Recap

In this section, we proposed using the GDOST, for the sEMG feature extraction, combined with enhanced MDS and k-NN. For the feature extraction stage, the importance of this improvement comes from the fact that GDOST is a time-efficient TF transform. The other significant improvement was made on the performance of the non-linear dimension reduction methods by enhancing their kernel calculations to be more suitable to the TF features. This enhancement promotes these methods as they perform better over smaller training sets, and they also better presents the cross-subject features. At

Movement	Number of observations
1	1319
2	1289
3	1224
4	1305
5	1174
6	1023
7	1347
8	1313
9	1219
10	1023
11	1333
12	1122
13	927
14	1026
15	936
16	997
17	947

Table 4.5 The total number of the movements' observations of the used subjects.

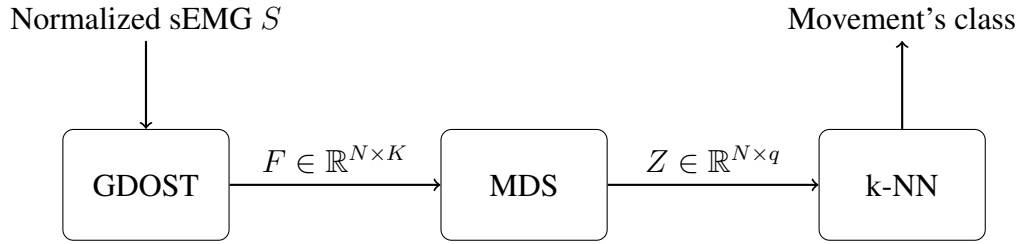


Fig. 4.14 Main algorithm overview of the selected methods.

the end of this chapter, we recommend using GDOST with enhanced MDS and k-NN as shown in Figure 4.14.

4.4 Generalization on Different Datasets

4.4.1 Amputation Impact on Classification Accuracy

4.4.1.1 Clinical Characteristics Effect

The clinical characteristics of the amputation as the remaining percentage of forearm, and the limb sensation have a big effect on the classification accuracy. The relation between the classification and the clinical characteristics of the amputation is not well studied in the literature, while this relation is a very important step in understanding the challenges when building real prostheses.

A study [116] proved that the limb sensation is significant to the classification accuracy, besides to the reasonable dependency between the remaining percentage of the forearm

Subject	Remaining Forearm (%)	Phantom Limb Sensation Intensity	Classification Accuracy (%)
1	30	2	85.36
2	50	2	92.18
5	50	5	93.01
3	70	5	94.08
4	90	5	93.80

Table 4.6 The classification accuracy of amputees' sEMG data.

and the classification accuracy. It also showed that the accuracy increased with the time since amputation, so the subjects are still capable of controlling the muscles despite the cortical reorganization that takes place after amputation.

4.4.1.2 Amputees' Data

The NinaPro DB3 [27, 116] provides a public dataset of sEMG signals collected from a number of amputees with different amputation percentage, phantom limb sensation and years since amputation. For the amputees, the subjects mentally try to repeat several movements represented by movies that are shown on the screen of a laptop. The muscular activity is gathered using 12 active double-differential wireless electrodes with sampling rate 2kHz. In our experiments, we will perform our improved methods as shown Figure 4.14 on the same set of the 17 movements identical to the ones in our previous experiments and shown in Figure 4.2.

4.4.1.3 Experiments And Results

We follow the same work flow as shown in previous section in figure 4.14, and apply these methods on all the available subjects in NinaPro dataset DB3.

The results of classification accuracy using GDOST and enhanced MDS on amputees data are shown in Table 4.6, and we can see that the accuracy ranges between 85.36% and 93.80%. By comparing these results results of tests on intact subjects shown in Table 4.4, we see that, by using same methods, the signals collected from intact subjects will give better classification results. This is consistent with other studies as in [117] shows that the accuracy scores drop by approximately 20% using sEMG signals of amputees compared to intact subjects. One of the reasons is that the amputation causes changes to the muscular anatomy and physiology that may affect also myoelectric control performance.

The remaining forearm percentage has a clear affect on the accuracy as it drops significantly when the percentage is 30%, while it is higher for both 70-90% remaining forearm. This result is reasonable as we see in figure 4.15, the remnant muscles which generates the sEMG signals get smaller with a smaller remaining forearm.

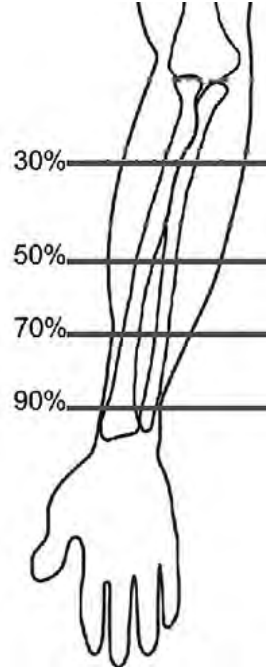


Fig. 4.15 The percentage of remaining forearm.

Another important factor is the phantom limb sensation which is scaled between 0 to 5 (0 = no sensation; 5 = sensation as strong as it could be). The results show that the amputees with higher limb sensation are more able to control the prosthetic.

4.4.2 Number of Movements' Impact on Accuracy

It is known that the number of movements has a significant impact on the classification accuracy, as by the increment on the movements, the discrimination between these movements will be more challenging especially for the movements that are performed by the same muscles. In our previous studies in sections 4.2 and 4.3, we focused on the quality of the features and the methods used 17 movements. In order to understand the limits and accuracy loss with movements number increment, we apply our methods combination on NinaPro DB2 [27] with the full movements list as shown in figure 4.16.

The overall accuracy, using same work flow as shown in figure 4.14 is 90.02% for the all 40 moves. In figure 4.17, we can see the confusion matrix on the classification. In this matrix, it is clear that the moves group: 18,19,20,22 are relatively more misclassified between each others. By looking to their gestures in 4.16, we can see that these move are physically very similar to each other. similarly for moves 27 and 28 which are both holding the ball with a slightly more clenched fist. The classification of this kind of movements could be enhanced by improving the electrodes placement so the small differential patterns of their sEMG signals could be well captured, besides to increasing the training size for these specific movements.

1	161			
2		240		
3			219	3
4	1		2	166
	1	2	3	4

Fig. 4.18 The confusion matrix of classification of the 4 hand gestures.

4.4.3 Data from ZHAW School of Health Sciences

4.4.3.1 Data key characteristics

This data is based on complex movements which require several muscles to be performed, and performed with two hands included, such as opening a can or cutting a bread. In order to extend our experiments on a completely different source of sEMG data. This data is recorded by our partner team from ZHAW School of Health Sciences in Zurich (Switzerland). The recorded sEMG data is a first step of creating wider database with more subjects included. The main goal of experiments on this data was to prove the quality of recorded sEMG and the used protocol in acquisition, and to apply our methods on a dataset that is completely different with regard to:

- The Acquisition kit with different kind of used electrodes.
- The number of electrodes.
- The movements gestures.
- The sampling frequency.
- Acquisition protocol, including the repetitions number and time.

4.4.3.2 Experiments and results

We do the experiments on this dataset in the same way we did in previous ones as shown in 4.14. This means that we use GDOST to extract features from the sEMG time series and enhanced-MDS to reduce its dimension, and we evaluate the performance using cross-folding on k-NN classifier. The classification accuracy of these movements is 99.31%, which is relatively high. This accuracy is also affected by the small number of movements and the type of movements. Figure 4.18 shows the confusion matrix of these 4 movements classification.

The results of this experiments show that our methods performance are not related to the NinaPro data.

Here in this database with different experiment criteria, we proved the protocol of acquisition of our partner's team for there further measurements, and challenged our methods with sEMG signals recorded under different conditions.

4.5 Algorithms and Results Recap

In this chapter, we made an extensive comparative study in section 4.2 for several combinations of sEMG TF features extraction and DR methods. We applied STFT, CWT, ST and DOST as time frequency with linear and non-linear dimension reduction methods which are PCA, Isomap, DM and MDS. Moreover, we applied a DL model with TF features of ST as an input. These methods combinations were tested on a Ninapro dataset of 17 movements and evaluated using known classifiers k-NN, LDA and SVM with 5-Fold cross-validation. The best results were achieved by using ST with PCA and k-NN, while DOST and MDS gave promising results. Based on the comparative study, DOST was selected as a time-efficient method for TF feature extraction, and MDS as a non-linear dimension reduction method. Then we improved the selected methods in section 4.3 by introducing GDOST and enhancing the distance calculations in non-linear DR methods. These improvements increased the classification accuracy to 97.56% for 17 hand movements. After that in section 4.4, we extended our tests on different datasets. First we applied the enhanced selected methods on amputees' sEMG data and observed the classification accuracy with the change of the clinical characteristics of the subjects. Second, more experiments were made on a dataset of 40 hand movements and the classification accuracy was 90.02%. Finally, the selected methods were applied on a different sEMG data source built by a partner team and consists of 4 hand movements as a pilot data, there we achieved 99.31% as a classification accuracy. The next chapter will give an overview about the main findings that could be helpful for the readers who are working in the same field, as well as broader perspectives on the topic.

CHAPTER 5

CONCLUSION AND PERSPECTIVES

5.1 English Version

5.1.1 Thesis Overview

In this thesis, we explored the time-frequency domain in order to classify sEMG signals. Our work was focused on both features extraction and dimension reduction methods of sEMG signals.

Features Extraction Overview: Based on the state of the art studies, we directed our research towards the TF features as the best representative features for the sEMG signals. The methods we used such as STFT, CWT and ST were used in the literature; but there were no concrete comparison between them under the same conditions which significantly affect these studies' impact. We applied these methods and provided more insights about their performance. Based on the conclusions and knowledge obtained from our studies, we introduced a new method to this field which is DOST to overcome the complexity and performance of the previous methods to make solutions more suitable for real prostheses. Finally we improved the performance of DOST by using a generalized version that uses a Gaussian window instead of a rectangular window.

Dimension Reduction Overview: The TF features lead to high dimension feature space, which makes this step very critical in order to avoid classification over-fitting and complexity. The main used method in the literature is PCA which is the base line for dimension reduction, but the requirements of prosthetic controlling systems raise different challenges as the training size and cross-subject features. In order to improve this important stage, we moved to non-linear dimension reduction methods and applied MDS, Isomap and DM. We extended our research about them as they have important advantages. We changed the kernel's calculations of these methods which are based

on the similarity calculations and were able to significantly improve their performance combined with the TF features.

Experiments Overview: We first applied all combination on the same dataset and evaluated their performance regarding the classification accuracy and time consumption. The evaluation was based on three widely used classifiers in this area (k-NN, LDA, SVM) and by following cross-folding validation method. Then we applied our enhanced selected methods on different datasets of amputees subjects to observe the amputation impact on the classification accuracy. Moreover, we repeated our tests on an increased number of the movements.

5.1.2 Experiments Conclusion

The comparative studies we did showed that the TF features are so far the best intrinsic features that could describe the patterns in sEMG signals. The use of these features leads to more robust and accurate classification compared to the TD, FD features, and even better than the deep learning which requires relatively very large training set.

The advantages of TF features come with the price of their complexity and their high dimensional space. This causes over-fitting in classification and higher computation time which is limited in prosthetic applications. The study of different TF methods showed that DOST gives promising results with trade-off between its accuracy and its time efficiency. Furthermore, we applied the generalized version of DOST to improve the results of classification.

Our studies on the dimension reduction methods showed that the non-linear methods could outperform PCA with defining an appropriate similarity measurements between the observations. We changed the distances measurements in the MDS and significantly improved the associated classification accuracy.

The enhanced methods, GDOST, MDS, with the classifier k-NN are according to our study the best combination which lead to better accuracy, and these methods proved to be robust when applied on different database and with increment of the number of movements.

5.1.3 Main Findings

We can summarise the main findings of this thesis in four key points:

Data: For having a proper evaluation, it is very useful to use database that offers various experimental options, as subjects, clinical situations, number of movements, etc... Having these data collected under same conditions regarding the number of channels, sampling rate, acquisition protocol... would help to fairly study the impact of different factors on the overall classification.

Features Engineering: The literature overview showed that both TD and TFD features are sufficient in case of a limited physically-discriminant number of movements as we can see in Table 2.2. By the increment of required movements to be controllable by the prosthetic, the solutions should be based on the TFD features. Even with DL models, the best results were done with TFD features as input for these models [63]. The challenge of complexity of these features is solvable by using DOST or GDOST which we proposed in our research.

Dimension Reduction: We proved the efficiency of the non-linear dimension reduction methods combined with the TFD features, and it is recommended to use these methods based on their needed training size, cross-subject efficiency, accuracy when defining proper similarity measurement. In our research we were able to propose one similarity measurement which significantly improved the classification accuracy.

Classification: We used the well-known classifiers in this field, and we found that the k-NN leads to robust and more accurate classification, besides to the fact that it is proven to perform well in this field. The quality of the features is the core of classification performance, as the good feature engineering will improve the accuracy without the need of more sophisticated classifiers.

5.1.4 Future Works

There are different ideas that deserve further investigation from our point of view:

- **Channels Selection:** the electrodes that are placed on the subjects will record sEMG signals from different muscles based on their position on the subject. This means that the activity on these electrodes will be affected by the muscle that participates in the movement; the electrodes close to the involved muscles will be the ones that record the important sEMG data. The ability to select these channels and ignoring the rest would decrease the required computations which will lead to more accurate and less complex classification. The channel selection is still an open topic in this research field and need more investigation. Some of the channels selection techniques are SVM Recursive Feature (SVM-RFE), Monte Carlo feature selection, and SVD entropy which are tested in study [119].
- Our research focused on the movement classification, and there are still some factors combined with the movements as force and temperature. These kind of data are usually collected by extra sensors and a fusion process should be studied and done in this direction.
- Improving the DL performances by pre-processing of the input in a way to reduce the required training set for the DL. The DL models are usually able to do the features engineering when supplied with the enough training set. The required

size of training set would vary depending on complexity in the patterns that exists in the input, hence choosing processed input (ex: TFD vs raw sEMG) would speed up the training and lead to better results.

- sEMG signals are related to the individual anatomical, biochemical and physiological characteristics of the subjects. This increases the need for an individual training of the prosthesis. Giving amputees the ability to insert their feedback about the correctness of the movements identification while using the prosthetic. This will make the learning process more efficient. One approach that could be studied is the reinforcement learning with fuzzy logic rules as an interface between the prosthesis and the user. Quality of the gesture execution could be evaluated depending on the interpretation of the user.
- More research could be done on the TF representation in order to find features that could be sufficient for the pattern recognition. These features could be based on the energy concentration in the TF. Recently a link between Gaussian Analytic Functions (GAFs) and some time-frequency transforms of white noise has been established in [120]. This work was motivated by earlier study [121] to filter signals based on the zeros of their STFT. More recently, authors in [122] proved the utility of the zeros distribution of the STFT to classify and anonymize the acceleration signals. This approach could be applied on sEMG signals in order to enrich the features extraction process.
- In this thesis, we used DOST as it was a time-efficient version of the ST, because of the time limitation in prosthetic application. Different solution could be considered on the hardware optimization as in [123]. Moreover, we can calculate the TF transform on-the-fly in real time and continuously accumulate the results to generate the time-frequency matrix as proposed in [124].

At the end, we were able to classify 17 movements with sufficient accuracy for the industry especially after we took time-efficiency into consideration. These results are very competitive compared to the state of the art of existing solutions. We proposed solutions that could be extended on more movements and applied for more challenging sEMG pattern recognition. We also contributed to the usage and understanding of TF features and DR for signal classification. This work paved the way for more theoretical studies to be done in the future.

5.2 Version en Français

5.2.1 Aperçu de la thèse

Dans cette thèse, nous avons exploré le domaine temps-fréquence pour classifier les signaux sEMG. Notre travail s'est concentré sur les méthodes d'extraction de caractéristiques et de réduction de dimension des signaux sEMG.

Extraction de caractéristiques. À partir des études de l'état de l'art, nous avons dirigé notre recherche vers les caractéristiques temps-fréquence (TF) en tant que meilleures caractéristiques représentatives des signaux sEMG. Les méthodes que nous avons utilisées telles que STFT, CWT et ST ont été utilisées dans la littérature; mais il n'y avait pas de comparaison concrète entre elles dans les mêmes conditions, ce qui limite considérablement l'impact de ces études. Nous avons appliqué ces méthodes et fourni plus d'informations sur leur performance. Ensuite, nous avons introduit une nouvelle méthode dans ce domaine qui est DOST pour surmonter la complexité calculatoire, et améliorer les performances des méthodes précédentes, afin de rendre les solutions plus adaptées aux prothèses réelles. Enfin, nous avons amélioré les performances de DOST en utilisant une version généralisée qui utilise une fenêtre gaussienne plutôt qu'une fenêtre rectangulaire.

Réduction de dimension. Les caractéristiques TF conduisent à un espace de caractéristiques de dimension élevée, ce qui rend cette étape importante afin d'éviter le surajustement lors de la classification. La méthode principalement utilisée dans la littérature est l'ACP qui est la méthode de base pour la réduction de dimension, mais les exigences des systèmes de commande de prothèse soulèvent différents défis tels que la taille d'apprentissage et les caractéristiques inter-sujets. Pour améliorer cette étape importante, nous avons opté pour des méthodes de réduction de dimension non linéaires et avons appliqué MDS, Isomap et DM. Nous avons étendu notre recherche sur celles-ci car elles présentent des avantages importants. Nous avons modifié les calculs du noyau de ces méthodes qui sont basés sur les calculs de similarité et avons été en mesure d'améliorer significativement leur performance combinée aux caractéristiques TF.

Expériences numériques. Nous avons d'abord appliqué toutes les combinaisons sur le même ensemble de données et avons évalué leur performance en termes d'exactitude de classification et de temps de calcul. L'évaluation était basée sur trois classificateurs largement utilisés dans ce domaine (k-NN, LDA, SVM) et en suivant la méthode de validation croisée. Ensuite, nous avons sélectionné les meilleures méthodes pour les appliquer à différents ensembles de données concernant des sujets amputés pour observer l'impact de l'amputation sur l'exactitude de classification. Nous avons également répété nos tests sur un nombre accru de mouvements.

5.2.2 Conclusions des expériences

Les études comparatives que nous avons menées ont montré que les caractéristiques TF sont jusqu'à présent les meilleures caractéristiques pour décrire les motifs dans les signaux sEMG, dans un contexte de classification. L'utilisation de ces caractéristiques conduit à une classification plus robuste et plus précise par rapport aux caractéristiques TD, FD, et même par rapport à l'apprentissage profond, qui nécessite un ensemble d'entraînement par comparaison très grand. Les avantages des caractéristiques TF viennent avec un prix de complexité et de nombre de dimension. Cela provoque un surajustement dans la classification et un temps de calcul plus élevé, ce qui est limitant dans les applications prothétiques. L'étude de différentes méthodes TF a montré que DOST donne des résultats prometteurs avec un compromis entre sa précision et son efficacité temporelle. De plus, nous avons appliqué la version généralisée de DOST pour améliorer les résultats de classification.

Nos études sur les méthodes de réduction de dimension ont montré que les méthodes non linéaires pourraient surpasser l'ACP en définissant une mesure de similarité appropriée entre les observations. Nous avons changé les mesures de distance dans le MDS et amélioré significativement la précision de classification associée.

Finalement, la méthode combinant GDOST, MDS améliorée, et classificateur k-NN conduit selon notre étude à une meilleure précision. Cette combinaison s'est également avérée robuste lorsqu'elle est appliquée à différentes bases de données et avec l'augmentation du nombre de mouvements.

5.2.3 Principales conclusions

Nous pouvons résumer les principales conclusions de cette thèse en quatre points clés, qui sont détaillés ci-dessous.

Données. Pour avoir une évaluation appropriée, il est très utile d'utiliser une base de données qui offre diverses options expérimentales, comme les sujets, les situations cliniques, le nombre de mouvements, etc. Avoir ces données collectées dans les mêmes conditions en ce qui concerne le nombre de canaux, le taux d'échantillonnage, le protocole d'acquisition... aiderait à étudier équitablement l'impact de différents facteurs sur la classification globale.

Ingénierie des caractéristiques. L'étude de la littérature a montré que les caractéristiques TD et TFD sont suffisantes lorsque l'on travaille sur un nombre limité de mouvements physiquement bien distincts, comme on peut le voir dans le tableau 2.2. Avec l'augmentation du nombre de mouvements requis pour être contrôlés par la prothèse, les solutions devraient être basées sur les caractéristiques TFD. Même avec les modèles de DL, les meilleurs résultats ont été obtenus avec les caractéristiques TFD en tant qu'entrée pour ces modèles [63]. Le défi de la complexité de ces caractéristiques peut

être résolu en utilisant la DOST ou la GDOST, ce que nous avons proposé dans notre recherche.

Réduction de dimension. Nous avons prouvé l'efficacité des méthodes de réduction de dimension non linéaires combinées aux caractéristiques TFD, et il est recommandé d'utiliser ces méthodes en fonction de leur taille d'entraînement nécessaire, de leur efficacité entre sujets, de leur précision lors de la définition de la mesure de similarité appropriée. Dans notre recherche, nous avons ainsi pu proposer une mesure de similarité qui a significativement amélioré la précision de la classification.

Classification. Nous avons utilisé les classificateurs bien connus dans ce domaine, et nous avons constaté que le k-NN mène à une classification robuste et plus précise. Ainsi, la qualité des caractéristiques est au cœur de la performance de la classification, car une bonne ingénierie des caractéristiques améliorera la précision sans avoir besoin de classificateurs plus sophistiqués.

5.2.4 Perspectives

Suite à ces travaux de thèse, nous pouvons évoquer plusieurs idées qui méritent une investigation plus approfondie.

- Sélection de canaux : les électrodes placées sur les sujets enregistreront des signaux sEMG provenant de différents muscles en fonction de leur position sur le sujet. Cela signifie que l'activité de ces électrodes sera affectée par tous les muscles qui participent au mouvement ; les électrodes proches des muscles impliqués enregistreront également un signal sEMG importantes. La capacité à sélectionner ces canaux et à ignorer le reste réduirait les calculs nécessaires, ce qui conduirait à une classification plus précise et surtout moins complexe. La sélection de canaux est encore un sujet ouvert dans ce domaine de recherche et nécessite plus d'investigation. Certaines des techniques de sélection de canaux sont la sélection de caractéristique réursive SVM (SVM-RFE), la sélection de caractéristique par Monte Carlo, et l'entropie SVD, qui ont été testées dans l'étude [119].
- Notre recherche s'est concentrée sur la classification des mouvements, mais il existe encore certains facteurs combinés aux mouvements tels que la force et la température. Ces types de données sont généralement collectés par des capteurs supplémentaires et un processus de fusion devrait être étudié et effectué dans cette direction.
- Les performances du DL pourraient être améliorées par prétraitement de l'entrée de manière à réduire l'ensemble d'entraînement requis. Les modèles DL sont généralement capables de faire de l'ingénierie de caractéristiques lorsqu'ils sont fournis avec suffisamment d'ensemble d'entraînement. La taille requise de l'ensemble

d'entraînement variera en fonction de la complexité des motifs présents dans l'entrée, le choix d'une entrée traitée (par exemple, TFD ou sEMG brut) accélérera l'entraînement et devrait conduire à de meilleurs résultats.

- Les signaux sEMG sont liés aux caractéristiques anatomiques, biochimiques et physiologiques individuelles des sujets. Cela augmente la nécessité d'un entraînement individuel de la prothèse. Cela pourrait aussi donner aux amputés la possibilité d'insérer leur rétroaction pour la correction de l'identification des mouvements lors de l'utilisation de la prothèse. Cela rendra le processus d'apprentissage plus efficace. Une approche qui pourrait être étudiée est l'apprentissage par renforcement avec des règles de logique floue comme interface entre la prothèse et l'utilisateur. La qualité de l'exécution des gestes pourrait être évaluée en fonction de l'interprétation de l'utilisateur.
- Des recherches supplémentaires pourraient être menées sur la représentation TF afin de trouver des caractéristiques suffisantes pour la reconnaissance de motifs. Ces caractéristiques pourraient être basées sur la concentration d'énergie dans le domaine TF. Récemment, un lien entre les fonctions analytiques gaussiennes (GAF) et certaines transformées temps-fréquence du bruit blanc a été établi dans [120]. Ce travail a été motivé par une étude antérieure [121] visant à filtrer les signaux en fonction des zéros de leur STFT. Plus récemment, les auteurs de [122] ont prouvé l'utilité de la distribution des zéros de la STFT pour classer et anonymiser les signaux d'accélération. Cette approche pourrait être appliquée aux signaux sEMG afin d'enrichir le processus d'extraction de caractéristiques.
- Dans cette thèse, nous avons utilisé la DOST car c'était une version plus rapide que la ST, en raison des limites de temps dans l'application prothétique. Différentes solutions pourraient être envisagées pour l'optimisation matérielle, comme décrit dans [123]. De plus, nous pourrions calculer la transformée TF en temps réel et accumuler continuellement les résultats pour générer la matrice temps-fréquence, comme proposé dans [124].

Finalement, nous avons pu classer 17 mouvements avec une précision suffisante pour l'industrie, notamment après avoir pris en compte les temps de calculs. Ces résultats sont très compétitifs par rapport à l'état de l'art des solutions existantes. Nous avons proposé des solutions qui pourraient être étendues à davantage de mouvements et appliquées à une reconnaissance de motifs sEMG plus complexes. Nous avons également contribué à l'utilisation et à la compréhension des caractéristiques de TF et de la RD pour la classification des signaux. Ce travail a ouvert la voie à des études théoriques supplémentaires à l'avenir.

Appendices

APPENDIX A

SEMG DATABASE FROM ZHAW SCHOOL OF HEALTH SCIENCES IN ZURICH (SWITZERLAND)

A.1 Background Information

Measuring system and information on electrodes: Bipolar electrodes (Blue Sensor, Ambu, Denmark, Type P-00, interelectrode distance: 20.148 mm) were used with a wireless myon sEMG system (myon AG, Baar Switzerland; Type 142 RFTD-A01, D02-RFTD) and placed according to the photos in Table A.1. All data was collected using a sampling rate of 1200 Hz and 12-bit resolution. Additionally, the signal from the sEMG system was amplified by 1000 or 2000 Hz (which channel has which amplification can be seen in the mat-file of the data). Data was recorded with a camera-based motion capture system (Vicon, Oxford. UK, Version 2.11).

A.2 Tasks

First task: Open bottle (0.5l water plastic bottle fully filled):

- Starting position: sitting with a 90° angle of elbows, hip, and knees; wrists are on the desk at marked points at shoulder width, bottle is on a marked point (between wrist marks and 15cm from desk).
- Mark on bottle neck and on its lid.
- Task instructions: Open the bottle until there is no resistance (the lid is on the last crease) and close it until the marks align. Then return to the starting position.

Second task: Pour water from a jug into a glass:

- Starting position: sitting with a 90° angle of elbows, hip, and knees, wrists are on the desk at marked points at shoulder width, jug and glass are at two marked points (1/3 and 2/3 of the distance between the two wrist markings).
- The jug was filled with 1l of water.
- Task instructions: Lift the glass approximately 10cm from the table, pour water from the jug into the glass until a mark on the glass is reached. Then put everything down on the marked points and return to the starting position.

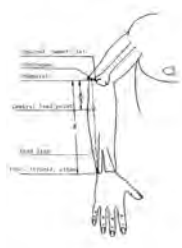

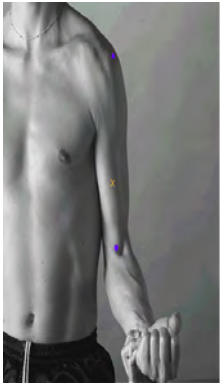
Third task: Cut bread:

- Starting position: standing with feet hip-width apart, arms hang loosely by the side and the upper body is in an upright position.
- Baguette (300g) on a board, knife next to it.
- Task instruction: Take the knife with one hand, hold the bread with the other hand and cut a piece of 1cm width from it. Then lay down the knife and return to the starting position
- After cutting two pieces, the bread slices were taken from the board.

Fourth task: Cut and eat meat imitate:


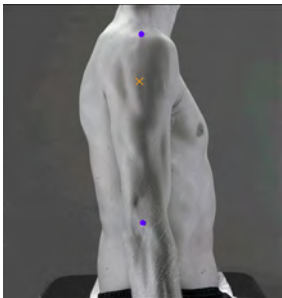
- Starting position: sitting with a 90° angle of elbows, hip, and knees; wrists are on the desk at marked points at shoulder width.
- A piece of clay (approx. 1cm thickness) is placed on a plate, the fork and knife are placed next to it.
- Task instructions: Take the knife and fork into your hands, cut a piece of clay and bring the cut piece to the mouth. Then lay everything down and return to the starting position.
- After each repetition the clay is attached again in order to achieve a similar starting point again.

Table A.1: The electrodes placement in ZHAW database.

Muscle		Function	EMG Channel
Extensor carpi ulnaris (amplification 1000)		Wrist extension Radial adduction of the wrist	<ul style="list-style-type: none"> • Right: 10 • Left: 13
Flexor carpi radialis (amplification 1000)		Palmarflexion Radialabduction Assisting pronation when the elbow is stretched	<ul style="list-style-type: none"> • Right: 9 • Left: 12
Biceps brachii (amplification 1000)		Elbow flexion	<ul style="list-style-type: none"> • Right: 11 • Left: 14

Continued on next page

Table A.1: The electrodes placement in ZHAW database. (Continued)

Muscle		Function	EMG Channel
Biceps brachii (amplification 2000)		Elbow extension	<ul style="list-style-type: none"> • Right: 3 • Left: 5
Deltoideus Medius (amplification 2000)		Abduction of the shoulder joint	<ul style="list-style-type: none"> • Right: 4 • Left: 6

LIST OF PUBLICATIONS

Un Journal international (Impact Factor 8.665) :

- Somar Karheily, Ali Moukadem, Jean-Baptiste Courbot, Djaffar Ould Abdeslam, sEMG Time-Frequency Features For Hand Movements Classification, Elsevier: Expert Systems With Applications journal, Vol. 210, 118282, <https://doi.org/10.1016/j.eswa.2022.118282>, 30 December 2022,

Deux Communications dans des congrès internationaux avec actes et comité de lecture:

- Somar Karheily, Ali Moukadem, Jean-Baptiste Courbot, Djaffar Ould Abdeslam, sEMG Features Extraction Using Generalized Discrete Orthonormal Stockwell Transform and Modified Multi-Dimensional Scaling, 30th European Signal Processing Conference (EUSIPCO 2022), Belgrade, Serbia, 29 August-2 September 2022,
- Somar Karheily, Ali Moukadem, Jean-Baptiste Courbot, Djaffar Ould Abdeslam, Time-Frequency Features For sEMG Signals Classification, 13th International Conference on Bio-inspired Systems and Signal Processing (BIOSIGNALS 2020), pp. 244-249, Valletta, Malta, February 24-26, 2020,

Une communication dans un congrès international francophone:

- Somar Karheily, Ali Moukadem, Jean-Baptiste Courbot, Djaffar Ould Abdeslam, Extraction de caractéristique améliorée pour les signaux sEMG par transformées temps-fréquence et réduction de dimension, XXVIIIème Colloque Francophone

de Traitement du Signal et des Images GRETSI'22, Nancy, 06 – 09 Septembre
2022,

REFERENCES

- [1] Kathryn Ziegler-Graham, Ellen J MacKenzie, Patti L Ephraim, Thomas G Travison, and Ron Brookmeyer. Estimating the prevalence of limb loss in the united states: 2005 to 2050. *Archives of physical medicine and rehabilitation*, 89(3):422–429, 2008.
- [2] NHS England. Hand and upper limb reconstruction using vascularised composite allotransplantation (haul-vca). <https://www.england.nhs.uk/commissioning/wp-content/uploads/sites/12/2015/07/d00pa-hand-transplnt-forearm-loss.pdf>, 2015.
- [3] NHS England. Complex disability equipment – prosthetic specialised services for people of all ages with limb loss. <https://www.england.nhs.uk/commissioning/wp-content/uploads/sites/12/2015/01/d01-serv-spec-dis-equ-prosth.pdf>, 2015.
- [4] SR Whiteside, J Alaimo, WJ Barringer, WD Beiswenger, T Bulgarelli, CJ Hentges, RS Lin, TE Miller, RG Parr, JH Reynolds, et al. Practice analysis task force. alexandria: American board for certification in orthotics and prosthetics, 2000.
- [5] Stefan Salminger, Heiko Stino, Lukas H Pichler, Clemens Gstoettner, Agnes Sturma, Johannes A Mayer, Michael Szivak, and Oskar C Aszmann. Current rates of prosthetic usage in upper-limb amputees—have innovations had an impact on device acceptance? *Disability and Rehabilitation*, pages 1–12, 2020.
- [6] Peter J Kyberd and Wendy Hill. Survey of upper limb prosthesis users in sweden, the united kingdom and canada. *Prosthetics and orthotics international*, 35(2):234–241, 2011.

- [7] Elaine Biddiss, Dorcas Beaton, and Tom Chau. Consumer design priorities for upper limb prosthetics. *Disability and rehabilitation: Assistive technology*, 2(6):346–357, 2007.
- [8] Jacob Segil. *Handbook of Biomechatronics*. Academic Press, 2018.
- [9] Nisheena V Iqbal and Kamalraj Subramaniam. A review on upper-limb myoelectric prosthetic control. *IETE Journal of Research*, 64(6):740–752, 2018.
- [10] Marco Gazzoni, Nicolò Celadon, Davide Mastrapasqua, Marco Paleari, Valentina Margaria, and Paolo Ariano. Quantifying forearm muscle activity during wrist and finger movements by means of multi-channel electromyography. *PloS one*, 9(10):e109943, 2014.
- [11] Wei Li, Ping Shi, and Hongliu Yu. Gesture recognition using surface electromyography and deep learning for prostheses hand: State-of-the-art, challenges, and future. *Frontiers in Neuroscience*, 15, 2021.
- [12] Rubana H Chowdhury, Mamun BI Reaz, Mohd Alauddin Bin Mohd Ali, Ashrif AA Bakar, Kalaivani Chellappan, and Tae G Chang. Surface electromyography signal processing and classification techniques. *Sensors*, 13(9):12431–12466, 2013.
- [13] Jiajia Wu, Xiaou Li, Wanyang Liu, and Z Jane Wang. Semg signal processing methods: A review. 1237(3):032008, 2019.
- [14] Rubana H Chowdhury, Mamun BI Reaz, Mohd Alauddin Bin Mohd Ali, Ashrif AA Bakar, Kalaivani Chellappan, and Tae G Chang. Surface electromyography signal processing and classification techniques. *Sensors*, 13(9):12431–12466, 2013.
- [15] AW Preece, HS Wimalaratna, JL Green, E Churchill, and HM Morgan. Non-invasive quantitative emg. *Electromyography and clinical neurophysiology*, 34(2):81–86, 1994.
- [16] Yves Blanc and Ugo Dimanico. Electrode placement in surface electromyography (semg)” minimal crosstalk area “(mca). *The Open Rehabilitation Journal*, 3(1), 2010.
- [17] JF Alonso, MA Mañanas, and M Rojas. High-density surface emg maps from upper-arm and forearm muscles. 2012.
- [18] Hermie Hermens and B Freriks. *The state of the art on sensors and sensor placement procedures for surface electromyography: a proposal for sensor placement procedures*. Roessingh Research and Development Enschede, 1997.

- [19] Andrea Merlo and Isabella Campanini. Technical aspects of surface electromyography for clinicians. *The open rehabilitation journal*, 3(1), 2010.
- [20] Xavier Navarro, Thilo B Krueger, Natalia Lago, Silvestro Micera, Thomas Stieglitz, and Paolo Dario. A critical review of interfaces with the peripheral nervous system for the control of neuroprostheses and hybrid bionic systems. *Journal of the Peripheral Nervous System*, 10(3):229–258, 2005.
- [21] DA Winter, Andrew J Fuglevand, and SE Archer. Crosstalk in surface electromyography: theoretical and practical estimates. *Journal of Electromyography and Kinesiology*, 4(1):15–26, 1994.
- [22] Mohammadreza Asghari Oskoei and Huosheng Hu. Myoelectric control systems—a survey. *Biomedical Signal Processing and Control*, 2(4):275–294, 2007.
- [23] HA Romo, JC Realpe, PE Jojoa, and U Cauca. Surface emg signals analysis and its applications in hand prosthesis control. *Av. en Sist. e Informática*, 4(1):127–136, 2007.
- [24] K. Englehart, B. Hudgin, and P.A. Parker. A wavelet-based continuous classification scheme for multifunction myoelectric control. *IEEE Transactions on Biomedical Engineering*, 48(3):302–311, 2001.
- [25] Dapeng Yang, Jingdong Zhao, Li Jiang, and Hong Liu. Dynamic hand motion recognition based on transient and steady-state emg signals. *International Journal of Humanoid Robotics*, 9(01):1250007, 2012.
- [26] Ahmet Alkan and Mücahid Günay. Identification of emg signals using discriminant analysis and svm classifier. *Expert systems with Applications*, 39(1):44–47, 2012.
- [27] Manfredo Atzori, Arjan Gijsberts, Claudio Castellini, Barbara Caputo, Anne-Gabrielle Mittaz Hager, Simone Elsig, Giorgio Giatsidis, Franco Bassetto, and Henning Müller. Electromyography data for non-invasive naturally-controlled robotic hand prostheses. *Scientific data*, 1(1):1–13, 2014.
- [28] Somar Karheily, Ali Moukadem, Jean-Baptiste Courbot, and Djaffar Ould Abdeslam. semg time–frequency features for hand movements classification. *Expert Systems with Applications*, 210:118282, 2022.
- [29] Somar Karheily, Ali Moukadem, Jean-Baptiste Courbot, and Djaffar Ould Abdeslam. Time-frequency features for semg signals classification. pages 244–249, 2020.

- [30] Somar Karheily, Ali Moukadem, Jean-Baptiste Courbot, and Djaffar Ould Abdeslam. semg feature extraction using generalized discrete orthonormal stockwell transform and modified multi-dimensional scaling. In *2022 30th European Signal Processing Conference (EUSIPCO)*, pages 1198–1202. IEEE, 2022.
- [31] Somar KARHEILY, Ali MOUKADEM, Jean-Baptiste COURBOT, and Djaffar OULD ABDESLAM. Extraction de caractéristique améliorée pour les signaux semg par transformées temps-fréquence et réduction de dimension.
- [32] Francesca Cordella, Anna Lisa Ciano, Rinaldo Sacchetti, Angelo Davalli, Andrea Giovanni Cutti, Eugenio Guglielmelli, and Loredana Zollo. Literature review on needs of upper limb prosthesis users. *Frontiers in neuroscience*, 10:209, 2016.
- [33] Martin Vilarino. Enhancing the control of upper limb myoelectric prostheses using radio frequency identification. 2013.
- [34] Alexandre Calado, Filomena Soares, and Demétrio Matos. A review on commercially available anthropomorphic myoelectric prosthetic hands, pattern-recognition-based microcontrollers and semg sensors used for prosthetic control. In *2019 IEEE International Conference on Autonomous Robot Systems and Competitions (ICARSC)*, pages 1–6. IEEE, 2019.
- [35] Kexiang Li, Jianhua Zhang, Lingfeng Wang, Minglu Zhang, Jiayi Li, and Shancheng Bao. A review of the key technologies for semg-based human-robot interaction systems. *Biomedical Signal Processing and Control*, 62:102074, 2020.
- [36] Muhammad Zahak Jamal. Signal acquisition using surface emg and circuit design considerations for robotic prosthesis. *Computational Intelligence in Electromyography Analysis-A Perspective on Current Applications and Future Challenges*, 18:427–448, 2012.
- [37] Yves Blanc and Ugo Dimanico. Electrode placement in surface electromyography (semg)” minimal crosstalk area “(mca). *The Open Rehabilitation Journal*, 3(1), 2010.
- [38] Scott Day. Important factors in surface emg measurement. *Bortec Biomedical Ltd publishers*, pages 1–17, 2002.
- [39] Xu Zhang, Xiang Chen, Zhang-yan Zhao, You-qiang Tu, Ji-hai Yang, Vuokko Lantz, and Kong-qiao Wang. Research on gesture definition and electrode placement in pattern recognition of hand gesture action semg. In *Medical Biometrics*:

First International Conference, ICMB 2008, Hong Kong, China, January 4-5, 2008. Proceedings 1, pages 33–40. Springer, 2007.

- [40] Xueyan Tang, Yunhui Liu, Congyi Lv, and Dong Sun. Hand motion classification using a multi-channel surface electromyography sensor. *Sensors*, 12(2):1130–1147, 2012.
- [41] Bernabe Rodríguez-Tapia, Israel Soto, Daniela M Martínez, and Norma Candolfi Arballo. Myoelectric interfaces and related applications: current state of emg signal processing—a systematic review. *IEEE Access*, 8:7792–7805, 2020.
- [42] Heather Daley, Kevin Englehart, Levi Hargrove, and Usha Kuruganti. High density electromyography data of normally limbed and transradial amputee subjects for multifunction prosthetic control. *Journal of Electromyography and Kinesiology*, 22(3):478–484, 2012.
- [43] Alex Andrews, Evelyn Morin, and Linda McLean. Optimal electrode configurations for finger movement classification using emg. In *2009 Annual International Conference of the IEEE Engineering in Medicine and Biology Society*, pages 2987–2990. IEEE, 2009.
- [44] Gianluca De Luca. Fundamental concepts in emg signal acquisition, 2003.
- [45] Alexandre Balbinot and Gabriela Favieiro. A neuro-fuzzy system for characterization of arm movements. *Sensors*, 13(2):2613–2630, 2013.
- [46] Yinfeng Fang, Xiangyang Zhu, and Honghai Liu. Development of a surface emg acquisition system with novel electrodes configuration and signal representation. In *International Conference on Intelligent Robotics and Applications*, pages 405–414. Springer, 2013.
- [47] Maria Hakonen, Harri Piitulainen, and Arto Visala. Current state of digital signal processing in myoelectric interfaces and related applications. *Biomedical Signal Processing and Control*, 18:334–359, 2015.
- [48] DC Toledo-Perez, Juvenal Rodríguez-Reséndiz, and Roberto A Gómez-Loenzo. A study of computing zero crossing methods and an improved proposal for emg signals. *IEEE Access*, 8:8783–8790, 2020.
- [49] Daniel Ramírez-Martínez, Mariel Alfaro-Ponce, Oleksiy Pogrebnyak, Mario Aldape-Pérez, and Amadeo-José Argüelles-Cruz. Hand movement classification using burg reflection coefficients. *Sensors*, 19(3):475, 2019.

- [50] B. Hudgins, P. Parker, and R. N. Scott. A new strategy for multifunction myoelectric control. *IEEE Transactions on Biomedical Engineering*, 40(1):82–94, 1993.
- [51] K. Englehart and B. Hudgins. A robust, real-time control scheme for multifunction myoelectric control. *IEEE Transactions on Biomedical Engineering*, 50(7):848–854, 2003.
- [52] Mohammadreza Asghari Oskoei and Huosheng Hu. Support vector machine-based classification scheme for myoelectric control applied to upper limb. *IEEE Transactions on Biomedical Engineering*, 55(8):1956–1965, 2008.
- [53] Dennis C Tkach, Aaron J Young, Lauren H Smith, Elliott J Rouse, and Levi J Hargrove. Real-time and offline performance of pattern recognition myoelectric control using a generic electrode grid with targeted muscle reinnervation patients. *IEEE Transactions on Neural Systems and Rehabilitation Engineering*, 22(4):727–734, 2014.
- [54] M. Rojas-Martínez, M. A. Mañanas, and J. Alonso. High-density surface EMG maps from upper-arm and forearm muscles. *Journal of NeuroEngineering and Rehabilitation*, 9:85 – 85, 2011.
- [55] Kyung Hyun Lee, Ji Young Min, and Sangwon Byun. Electromyogram-based classification of hand and finger gestures using artificial neural networks. *Sensors*, 22(1):225, 2022.
- [56] A. Phinyomark, P. Phukpattaranont, and C. Limsakul. Feature reduction and selection for EMG signal classification. *Expert Syst. Appl.*, 39:7420–7431, 2012.
- [57] Angkoon Phinyomark, Sirinee Thongpanja, Huosheng Hu, Pornchai Phukpattaranont, and Chusak Limsakul. The usefulness of mean and median frequencies in electromyography analysis. In Ganesh R. Naik, editor, *Computational Intelligence in Electromyography Analysis*, chapter 8. IntechOpen, Rijeka, 2012.
- [58] Angkoon Phinyomark, Chusak Limsakul, and P. Phukpattaranont. A novel feature extraction for robust EMG pattern recognition. *Journal of Computing*, 1:71–80, 12 2009.
- [59] Maria V Arteaga, Jenny C Castiblanco, Ivan F Mondragon, Julian D Colorado, and Catalina Alvarado-Rojas. Emg-driven hand model based on the classification of individual finger movements. *Biomedical Signal Processing and Control*, 58:101834, 2020.

- [60] Jinxian Qi, Guozhang Jiang, Gongfa Li, Ying Sun, and Bo Tao. Surface emg hand gesture recognition system based on pca and grnn. *Neural Computing and Applications*, 32(10):6343–6351, 2020.
- [61] Ervin Sejdic, Igor Djurovic, and Jin Jiang. Time–frequency feature representation using energy concentration: An overview of recent advances. *Digital Signal Processing*, 19:153–183, 01 2009.
- [62] N. Rabin, Maayan Kahlon, Sarit Malayev, and A. Ratnovsky. Classification of human hand movements based on EMG signals using nonlinear dimensionality reduction and data fusion techniques. *Expert Syst. Appl.*, 149:113281, 2020.
- [63] Lin Chen, Jianting Fu, Yuheng Wu, Haochen Li, and Bin Zheng. Hand gesture recognition using compact cnn via surface electromyography signals. *Sensors*, 20(3):672, 2020.
- [64] K. Englehart and B. Hudgins. A robust, real-time control scheme for multi-function myoelectric control. *IEEE Transactions on Biomedical Engineering*, 50(7):848–854, 2003.
- [65] Karan Veer and Ravinder Agarwal. Wavelet and short-time fourier transform comparison-based analysis of myoelectric signals. *Journal of Applied Statistics*, 42(7):1591–1601, 2015.
- [66] Turker Tuncer, Sengul Dogan, and Abdulhamit Subasi. Surface emg signal classification using ternary pattern and discrete wavelet transform based feature extraction for hand movement recognition. *Biomedical Signal Processing and Control*, 58:101872, 2020.
- [67] Ali Moukadem, Bouguila Zied, Djaffar Ould-Abdeslamb, and Alain Dieterlen. A new optimized Stockwell transform applied on synthetic and real non-stationary signals. *Digital Signal Processing*, (46):226–238, 2015.
- [68] Haotian She, Jinying Zhu, Ye Tian, Yanchao Wang, Hiroshi Yokoi, and Qiang Huang. Semg feature extraction based on stockwell transform improves hand movement recognition accuracy. *sensors*, 19(20):4457, 2019.
- [69] Mehmet Rahmi Canal. Comparison of wavelet and short time fourier transform methods in the analysis of emg signals. *Journal of medical systems*, 34(1):91–94, 2010.
- [70] I.T. Jolliffe and Springer-Verlag. *Principal Component Analysis*. Springer Series in Statistics. Springer, 2002.

- [71] J. . Chu, I. Moon, and M. . Mun. A real-time EMG pattern recognition system based on linear-nonlinear feature projection for a multifunction myoelectric hand. *IEEE Transactions on Engineering*, 53(11):2232–2239, 2006.
- [72] José Jair A. Mendes Junior, Melissa L.B. Freitas, Hugo V. Siqueira, André E. Lazzaretti, Sergio F. Pichorim, and Sergio L. Stevan. Feature selection and dimensionality reduction: An extensive comparison in hand gesture classification by sEMG in eight channels armband approach. *Signal Processing and Control*, 59:101920, 2020.
- [73] Carl Peter Robinson, Baihua Li, Qinggang Meng, and Matthew TG Pain. Pattern classification of hand movements using time domain features of electromyography. pages 1–6, 2017.
- [74] Kang Soo Kim, Heung Ho Choi, Chang Soo Moon, and Chi Woong Mun. Comparison of k-nearest neighbor, quadratic discriminant and linear discriminant analysis in classification of electromyogram signals based on the wrist-motion directions. *Current applied physics*, 11(3):740–745, 2011.
- [75] Ali Raza Asif, Asim Waris, Syed Omer Gilani, Mohsin Jamil, Hassan Ashraf, Muhammad Shafique, and Imran Khan Niazi. Performance evaluation of convolutional neural network for hand gesture recognition using emg. *Sensors*, 20(6):1642, 2020.
- [76] Jinxian Qi, Guozhang Jiang, Gongfa Li, Ying Sun, and Bo Tao. Surface emg hand gesture recognition system based on pca and grnn. *Neural Computing and Applications*, 32(10):6343–6351, 2020.
- [77] Smita Bhagwat and Prachi Mukherji. Electromyogram (emg) based fingers movement recognition using sparse filtering of wavelet packet coefficients. *Sādhanā*, 45(1):1–11, 2020.
- [78] Angkoon Phinyomark and Erik Scheme. Emg pattern recognition in the era of big data and deep learning. *Big Data and Cognitive Computing*, 2(3):21, 2018.
- [79] Hyeon-min Shim and Sangmin Lee. Multi-channel electromyography pattern classification using deep belief networks for enhanced user experience. *Journal of Central South University*, 22(5):1801–1808, 2015.
- [80] Wenguo Li, Zhizeng Luo, Yan Jin, and Xugang Xi. Gesture recognition based on multiscale singular value entropy and deep belief network. *Sensors*, 21(1):119, 2021.

- [81] Ryohei Shioji, Shin-ichi Ito, Momoyo Ito, and Minoru Fukumi. Personal authentication and hand motion recognition based on wrist emg analysis by a convolutional neural network. In *2018 IEEE International Conference on Internet of Things and Intelligence System (IOTAIS)*, pages 184–188. IEEE, 2018.
- [82] Kai Xing, Zhen Ding, Shuai Jiang, Xueyan Ma, Kai Yang, Chifu Yang, Xiang Li, and Feng Jiang. Hand gesture recognition based on deep learning method. In *2018 IEEE Third International Conference on Data Science in Cyberspace (DSC)*, pages 542–546. IEEE, 2018.
- [83] Panagiotis Tsinganos, Bruno Cornelis, Jan Cornelis, Bart Jansen, and Athanasios Skodras. Hilbert semg data scanning for hand gesture recognition based on deep learning. *Neural Computing and Applications*, 33(7):2645–2666, 2021.
- [84] Manfredo Atzori, Arjan Gijsberts, Claudio Castellini, Barbara Caputo, Anne-Gabrielle Mittaz Hager, Simone Elsig, Giorgio Giatsidis, Franco Bassetto, and Henning Müller. Electromyography data for non-invasive naturally-controlled robotic hand prostheses. *Scientific data*, 1(1):1–13, 2014.
- [85] Stefano Pizzolato, Luca Tagliapietra, Matteo Cognolato, Monica Reggiani, Henning Müller, and Manfredo Atzori. Comparison of six electromyography acquisition setups on hand movement classification tasks. *PloS one*, 12(10):e0186132, 2017.
- [86] Yunan He, Osamu Fukuda, Nan Bu, Hiroshi Okumura, and Nobuhiko Yamaguchi. Surface emg pattern recognition using long short-term memory combined with multilayer perceptron. In *2018 40th Annual International Conference of the IEEE Engineering in Medicine and Biology Society (EMBC)*, pages 5636–5639. IEEE, 2018.
- [87] Ulysse Côté-Allard, Cheikh Latyr Fall, Alexandre Drouin, Alexandre Campeau-Lecours, Clément Gosselin, Kyrre Glette, François Laviolette, and Benoit Gosselin. Deep learning for electromyographic hand gesture signal classification using transfer learning. *IEEE transactions on neural systems and rehabilitation engineering*, 27(4):760–771, 2019.
- [88] Dheeru Dua and Casey Graff. UCI machine learning repository, 2017.
- [89] Susanna Rampichini, Taian Martins Vieira, Paolo Castiglioni, and Giampiero Merati. Complexity analysis of surface electromyography for assessing the myoelectric manifestation of muscle fatigue: A review. *Entropy*, 22(5):529, 2020.

- [90] KC McGill. Surface electromyogram signal modelling. *Medical and Biological Engineering and Computing*, 42(4):446–454, 2004.
- [91] Necille Hogan and Robert W Mann. Myoelectric signal processing: Optimal estimation applied to electromyography-part i: Derivation of the optimal myoprocessor. *IEEE Transactions on Biomedical Engineering*, (7):382–395, 1980.
- [92] Van Der Bilt and Van Der Glas. Detection of onset and termination of muscle activity in surface electromyograms. *Journal of oral rehabilitation*, 25(5):365–369, 1998.
- [93] HS Milner-Brown and RB Stein. The relation between the surface electromyogram and muscular force. *The Journal of physiology*, 246(3):549–569, 1975.
- [94] Kianoush Nazarpour, Ali H Al-Timemy, Guido Bugmann, and Andrew Jackson. A note on the probability distribution function of the surface electromyogram signal. *Brain research bulletin*, 90:88–91, 2013.
- [95] Edward A Clancy and Neville Hogan. Probability density of the surface electromyogram and its relation to amplitude detectors. *IEEE Transactions on Biomedical Engineering*, 46(6):730–739, 1999.
- [96] Manfredo Atzori, Arjan Gijsberts, Claudio Castellini, Barbara Caputo, Anne-Gabrielle Mittaz Hager, Simone Elsig, Giorgio Giatsidis, Franco Bassetto, and Henning Müller. Electromyography data for non-invasive naturally-controlled robotic hand prostheses. *Scientific data*, 1(1):1–13, 2014.
- [97] J. Allen. Short term spectral analysis, synthesis, and modification by discrete fourier transform. *IEEE Transactions on Acoustics, Speech, and Signal Processing*, 25(3):235–238, 1977.
- [98] Hohyub Jeon, Yongchul Jung, Seongjoo Lee, and Yunho Jung. Area-efficient short-time fourier transform processor for time–frequency analysis of non-stationary signals. *Applied Sciences*, 10(20):7208, 2020.
- [99] W Christopher Lang and Kyle Forinash. Time-frequency analysis with the continuous wavelet transform. *American journal of physics*, 66(9):794–797, 1998.
- [100] Alexander Grossmann and Jean Morlet. Decomposition of hardy functions into square integrable wavelets of constant shape. *SIAM journal on mathematical analysis*, 15(4):723–736, 1984.
- [101] Ali Moukadem, Bouguila Zied, Djaffar Ould-Abdeslamb, and Alain Dieterlen. A new optimized Stockwell transform applied on synthetic and real non-stationary signals. *Digital Signal Processing*, (46):226–238, 2015.

- [102] R. G. Stockwell, L. Mansinha, and R. P. Lowe. Localization of the complex spectrum: the s transform. *IEEE Transactions on Signal Processing*, 44(4):998–1001, 1996.
- [103] M. Jaya Bharata Reddy, Rama Krishnan Raghupathy, K.P. Venkatesh, and D.K. Mohanta. Power quality analysis using discrete orthogonal s-transform (dost). *Digital Signal Processing*, 23(2):616–626, 2013.
- [104] R.G. Stockwell. A basis for efficient representation of the s-transform. *Digital Signal Processing*, 17(1):371 – 393, 2007.
- [105] Joshua Tenenbaum, Vin Silva, and John Langford. A global geometric framework for nonlinear dimensionality reduction. *Science*, 290:2319–2323, 01 2000.
- [106] J De la Porte, BM Herbst, W Hereman, and SJ Van Der Walt. An introduction to diffusion maps. pages 15–25, 2008.
- [107] Trevor Cox and Mike Cox. *Multidimensional Scaling, Second Edition*. 09 2000.
- [108] Jerome Friedman, Trevor Hastie, Robert Tibshirani, et al. *The elements of statistical learning*, volume 1. Springer series in statistics New York, 2001.
- [109] Michael AA Cox and Trevor F Cox. Multidimensional scaling. In *Handbook of data visualization*, pages 315–347. Springer, 2008.
- [110] Sumit Raurale, John McAllister, and Jesus Martinez del Rincon. Real-time embedded EMG signal analysis for wrist-hand pose identification. *IEEE Transactions on Signal Processing*, 68:2713–2723, April 2020.
- [111] Ubertino Battisti and Luigi Riba. Window-dependent bases for efficient representations of the stockwell transform. *Applied and Computational Harmonic Analysis*, 40(2):292–320, 2016.
- [112] Somar Karheily, Ali Moukadem, Jean-Baptiste Courbot, and Djaffar Ould Abdeslam. Time-frequency features for semg signals classification. pages 244–249, 2020.
- [113] Gabriela W Favieiro, Karina OA Moura, and Alexandre Balbinot. Novel method to characterize upper-limb movements based on paraconsistent logic and myoelectric signals. pages 395–398, 2016.
- [114] Jingwei Too, AR Abdullah, N Mohd Saad, N Mohd Ali, and TNS Tengku Zawawi. Application of gabor transform in the classification of myoelectric signal. *TELKOMNIKA (Telecommunication Computing Electronics and Control)*, 17(2):873–881, 2019.

- [115] Brandon E Lung and Bracken Burns. Anatomy, shoulder and upper limb, hand flexor digitorum profundus muscle. 2020.
- [116] Manfredo Atzori, Arjan Gijsberts, Claudio Castellini, Barbara Caputo, Anne-Gabrielle Mittaz Hager, Simone Elsig, Giorgio Giatsidis, Franco Bassetto, and Henning Müller. Clinical parameter effect on the capability to control myoelectric robotic prosthetic hands. *Journal of rehabilitation research and development*, 53(3):345–358, 2016.
- [117] Manfredo Atzori, Arjan Gijsberts, Henning Müller, and Barbara Caputo. Classification of hand movements in amputated subjects by semg and accelerometers. pages 3545–3549, 2014.
- [118] Manfredo Atzori, Arjan Gijsberts, Simone Heynen, Anne-Gabrielle Mittaz Hager, Olivier Deriaz, Patrick Van Der Smagt, Claudio Castellini, Barbara Caputo, and Henning Müller. Building the ninapro database: A resource for the biorobotics community. pages 1258–1265, 2012.
- [119] Maurício Cagliari Tosin, Vinícius Horn Cene, and Alexandre Balbinot. Statistical feature and channel selection for upper limb classification using semg signal processing. *Research on Biomedical Engineering*, 36(4):411–427, 2020.
- [120] Rémi Bardenet and Adrien Hardy. Time-frequency transforms of white noises and gaussian analytic functions. *Applied and computational harmonic analysis*, 50:73–104, 2021.
- [121] Patrick Flandrin. Time–frequency filtering based on spectrogram zeros. *IEEE Signal Processing Letters*, 22(11):2137–2141, 2015.
- [122] Pierre Rougé, Ali Moukadem, Alain Dieterlen, Antoine Boutet, and Carole Frindel. Generalizable features for anonymizing motion signals based on the zeros of the short-time fourier transform. *Journal of Signal Processing Systems*, pages 1–11, 2022.
- [123] Nevena Radović, Veselin N Ivanović, Igor Djurović, Marko Simeunović, and Ervin Sejdić. A step toward real-time time–frequency analyses with varying time–frequency resolutions: Hardware implementation of an adaptive s-transform. *Circuits, Systems, and Signal Processing*, pages 1–22, 2022.
- [124] Mahfoud Drouaz. Les transformées temps-fréquence appliquées au non-intrusive load monitoring. 2018.